VISUALIZATION, MANIPULATION AND FORCE SPECTROSCOPY OF CYLINDRICAL POLYMER BRUSHES

Dissertation

For attaining the degree of

Doctor of Natural Sciences

At the Faculty of Chemistry

Of Johannes Gutenberg University

Nikhil Arun Gunari

Born in Pune, India

Mainz, 2005

CONTENTS

CHAPTER 1

CHAPTER 2

CHAPTER 3

CHAPTER 4

CHAPTER 5

CHAPTER 6

CHAPTER 7

CHAPTER 8

CHAPTER 9

CHAPTER 10

1 INTRODUCTION

The numerous imaging and manipulation techniques established in the past two decades have brought about a significant number of breakthroughs in the field of polymers and biopolymers, which include monitoring motions of individual molecules,[1] progress of reactions,[2] and processes such as polymer crystallization[3,4] without loss of spatial resolution. Also mechanical properties[5,6] and molecular conformations[7,8] of individual molecules have been studied.

Molecular machines based on natural and synthetic polymers[9] are examples of sophisticated nanoscale devices designed to perform mechanical work when an external stimulus is applied. With the availability of probe microscopes research on artificial molecular machines has achieved new dimensions. Recently a model system for light-powered molecular machines was shown using polyazopeptides.[10] Individual polyazopeptide molecules were investigated by single molecule force spectroscopy in combination with optical excitation.

The examples of biomacromolecules reveal how single polymer molecules and their ensembles serve as functional nanoobjects. While functional properties such as catalytic activity, directed motion and the energy transport are well established in case of biomolecules, the ability to develop synthetic molecular devices is in its infancy. Among the vast research on nanoobjects significant efforts are directed towards shape control and directed motion.

1.1 Cylindrical Polymer Brushes

Cylindrical polymer brushes are molecules possessing densely grafted side chains on a linear polymer main chain. This type of structure has also been given the name *molecular bottlebrush* (as shown in the **Figure 1-1)**. To render a cylindrical shape, the main chain of a polymer brush should be much longer than the side chains. Although most of the cylindrical polymer brushes synthesized so far have linear side chains, polymer brushes with branched grafts are also cylindrical. A typical example is a dendronized polymer with high-generation dendritic side chains.[11]

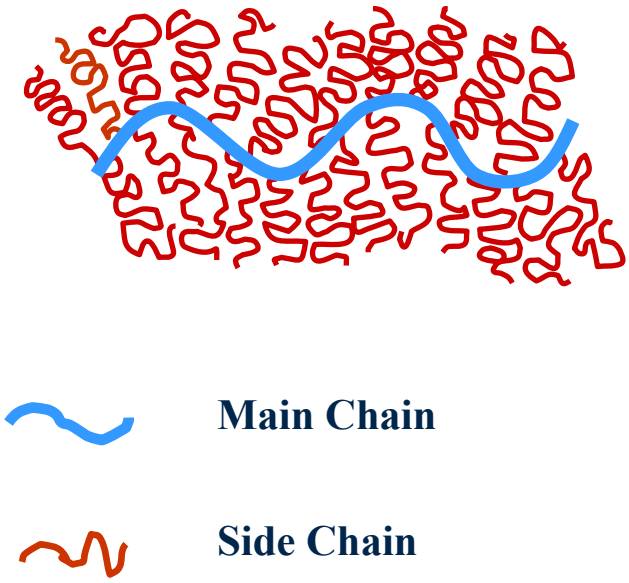

Figure 1-1 Schematics of a cylindrical polymer brush also known as molecular bottlebrush

1.2 Properties of Cylindrical Polymer Brushes

The shape persistent property of cylindrical brush polymers with high grafting density was revealed about 10 years ago.[12] Because of the regular comblike structure, they have the following characteristics in comparison with the corresponding linear polymers of the same molecular weight: (1) a small and compact molecular dimension, (2) an extended wormlike conformation resulting from steric repulsion between densely grafted side chains.

1.2.1 Solution Properties

So, far experimental and theoretical studies on dilute solutions of cylindrical polymer brushes has proved that the densely grafted side chains force the main chain into an extended wormlike conformation. This conformational effect is caused by competition of the entropic restoring force of the extended backbone and the repulsive, steric interaction forces between the side chains. The length of the cylinder per main-chain monomer unit increases with increasing solvent quality for the side chain. By combining Gel Permeation Chromatography (GPC) with multi-angle light scattering and viscosity detectors, it was shown that cylindrical polymer brushes with a polymethacrylate main chain and polystyrene side chains in a dilute solution with a fixed side-chain length but variable main-chain length, the relation of molar mass versus radius of gyration (R_g) can be excellently described by the Kratky-Porod wormlike chain model. By studying the same sample in a dilute toluene solution, it was shown that these polymers exhibit a bottle brush structure, in which the main chain adopts a stiff conformation surrounded by the expanded but still flexible side chains.

If the size of the backbone is significantly smaller than the side chain, the bottle brush molecule effectively represents a star, in which the number of arms is equal to the total number of grafted chains.[13] As the length of the backbone grows beyond some limiting value a conformational change from a star to a cylinder takes place. The radius of the cylinder is determined by the size of the side chain, while the length of the cylinder grows proportional to the backbone molecular weight.[14]

1.2.2 Bulk Properties

Cylindrical polymer brushes are expected to have significantly different bulk properties from those of the corresponding linear polymers due to their peculiar structure. So far the studies on the bulk properties of the cylindrical polymer brushes have focused on the film-forming properties[15] and the presence of liquid-crystalline mesophases. The solution-casting films of PS brushes were observed to have cracks and the resulting films were found to be brittle. The same conclusions were drawn from rheological measurements.[16] This behavior was explained by the absence of intermolecular chain

entanglements. Such a kind of behavior was also confirmed directly by STM[17] and AFM[15] measurements.

Lyotropic main-chain liquid crystals were observed in solvent-cast films of PS brushes possessing a large branch number and a significant branch length.[18] The formation of a liquid-crystalline phase indicates that these cylindrical molecules behave as rodlike molecules in which the effective stiffness of the cylindrical brush molecule can be much larger than that of the backbone. Direct observation of lyotropic behavior of cylindrical brushes has been reported in which the polymers were found to have an effective Kuhn length of 89 nm and it was observed that the Kuhn length increased with increase in side chain length from 89 nm to 207 nm if the side chain molar mass increases from 2780 g/mol up to 4940 g/mol.[19]

1.2.3 Mechanical properties of cylindrical brushes

Semiflexible chains are of great interest due their prevalence in nature. The interest in cylindrical brushes is due to conformational effects caused by competition of the entropic restoring force of the extended backbone and the repulsive, steric interaction forces between the side chains. The force-extension behavior of such molecules would provide deeper insight into the local properties of the molecule. Till date there is not much information on the mechanical properties of cylindrical brushes on a single molecule level.

1.2.4 Responsive molecules

The main chain can be considered as a statistical coil or, in other words, an entropic spring, which resists stretching. On the other hand, the repulsion between the side chains in good solvent condition makes such stretching favorable. This ultimately should lead to length variation of cylindrical brushes upon a change in solvent quality for the side chains. Thus, we can manipulate the properties of a single molecule. It has been reported that rod-like molecule (polymacromonomers- PS with a methacrylol end group)

exhibit variation in length which was investigated by static and dynamic light scattering in THF and cyclohexane.[20] Such polymers seem to be suitable as responsive materials for sensors or actuators if a directional orientation of the cylinders is achieved. Statistical copolymers of two different macromonomers were observed to exhibit conformational transition from cylindrical brushes to curved structures, such as the horseshoe shape, when the side chains were made incompatible by chemical transformations.[21] More recently cylindrical polymer brushes with temperature responsive side chains, poly-isopropylacrylamide (PNIPAM) were synthesized which exhibited a cylinder to globule transition at the lower critical solution temperature (LCST) of PNIPAM.[22] It was shown that the cylinder to sphere transition was a single molecule phenomenon. Thus such a single macromolecule cylinder to a sphere for a synthetic system within an extremely small temperature range can form the basis for experiments towards realization of soft nanomachines, in which mechanical action is triggered by variation of the temperature.

1.3 Conformation of 2D Confined Cylindrical Polymer Brushes

So far, high-resolution microscopy can depict the contour of a macromolecule but does not resolve the individual atoms of a macromolecule. The information on the molecular structure obtained from such an image includes contour length, the curvature and the end-to-end distance. This enables quantitative analysis of local properties (flexibility). In order to understand the conformation of the cylindrical brush molecule we need to define some parameters. **Figure 1-2** shows a model of the bottle brush with L being the contour length, d the cross-sectional dimension of the cylindrical polymer brush, $\left\langle R^2 \right\rangle$ is the end-to-end distance and finally the stiffness of the cylindrical polymer brush is traditionally described by its persistence length l_p.

1.4 Applications of Cylindrical Polymer Brushes

During the last decades the fast technological developments promoted mainly ba the microelectronics industry have lead to a progressive miniaturization of electronic

devices. Thus in the past few years the synthesis of metal and semiconductor nanowires, due to the wide range of applications, has been a prime focus of research.[23-25]

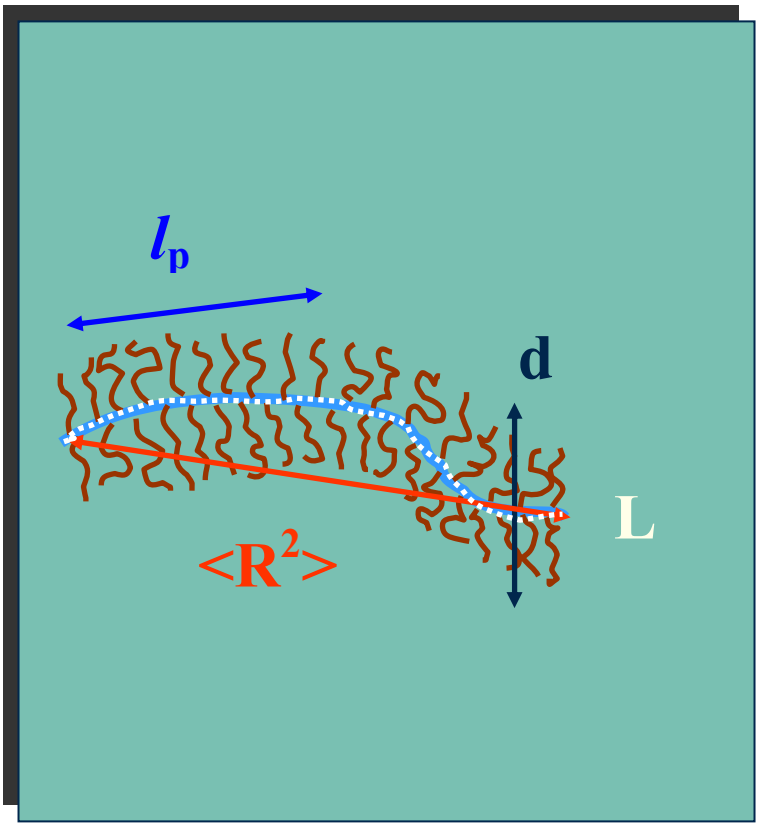

Figure 1-2 Model of the cylindrical polymer brush showing the contour length *L*, cross-sectional dimension *d*, end-to-end distance $\langle R^2 \rangle$ and stiffness of the molecule described by its persistence length l_p.

Cylindrical polymer brushes with linear or dendriticlly branched side chains may exhibit a block structure leading to a amphipolar core-shell structure, which may be used as templates to synthesize nanoparticles and nanowires. Amphipolar core-shell cylindrical brushes with a vinylpyridine core and a polystyrene shell were used as templates to synthesize gold nanowires.[26] Recently semiconducting cadmium sulfide (CdS) nanowires[27] and supermagnetic (iron oxide) nanoparticles[28] were synthesized using core-shell cylindrical polymer brushes with a polyacrylic acid (PAA) core and a poly(*n*-butyl acrylate) (P*n*BA) shell as a template.

An interesting example of cylindrical polymer brushes in nature is found in proteoglycans. This macromolecule appears to provide energy-absorbing, cushioning

properties and determine the viscoelastic properties of connective tissues. This provides an opportunity to apply cylindrical polymer brushes as additives in materials to enhance energy absorbing and other mechanical properties. Hence it would be interesting to study the mechanical properties of individual cylindrical brush molecules.

Nanomanipulation of single macromolecular objects and responsive polymers[22] constitutes an exciting challenge in polymer research. Recently, dendronized cylindrical brush molecules were visualized and manipulated on a HOPG surface by an AFM tip.[11] Compared to linear polymers, cylindrical polymer brushes have a significantly high stiffness, and are easily manipulated on a single molecule level. Thus cylindrical brush molecules can be ideal contenders for nano sensors, actuators or soft machines if directed motion can be achieved.

1.5 Objectives

- Visualization and conformational analysis of cylindrical polymer brushes on surfaces.
- Studying of the mechanical properties of individual cylindrical polymer brushes by single molecule force spectroscopy.
- Visualization of the conformational change from cylinder to globule on the surface.
- Quantification of the unfolding-folding transitions in collapsed cylindrical brushes.
- Studying force induced conformational transitions from a globule to cylinder and the development of a protocol for controlled manipulation of individual cylindrical brush molecules.
- Studying the elasticity and desorption of polyelectrolyte cylindrical brushes.
- Formation and characterization of polyelectrolyte cylindrical brush-surfactant complexes.

1.6 Research Impact and Significance

Cylindrical polymer brushes with thermally sensitive side chains may form one of the basis of nano actuation devices. The proposed research will lead to a better understanding of the mechanical properties of single cylindrical polymer brushes. Studying the force induced conformational changes of a collapsed globule to a cylinder might lead to the understanding of the collapse forces, which may further be extended to a quantitative determination of the collapse forces of the responsive cylindrical brush molecules.

1.7 References

(1) Argaman, M.; Golan, R.; Thomson, N. H.; Hansma, H. G. *Nucleic Acids Res.* **1997**, *25(21)*, 4379.

(2) Häring, P.; Kötz, R.; Repphun, G.; Haas, O.; Siegenthaler, H. *Appl. Phys. A* **1998**, *66*, S481.

(3) Hobbs, J. K.; Miles, M. J. *Macromolecules* **2001**, *34*, 353.

(4) Zhou, W.; Cheng, S. Z. D.; Putthanarat, S.; Eby, R. K.; Reneker, D. H.; Lotz, B.; Magonov, S. N.; Hsieh, E. T.; Palackal, S. J.; Hawley, G. R.; Welch, M. B. *Macromolecules* **2000**, *33*, 6861.

(5) Janshoff, A.; Neitzert, M.; Oberdörfer, Y.; Fuchs, H. *Angew. Chem. Int. Ed.* **2000**, *39*, 3212.

(6) Hugel, T.; Seitz, M. *Macromol. Rapid Commun.* **2001**, *22*, 989.

(7) Rief, M.; Clausen-Schaumann, H.; Gaub, H. E. *Nat. Struct. Biol.* **1999**, *6(4)*, 346.

(8) Marszalek, P. E.; Oberhauser, A. F.; Pang, Y. P.; Fernandez, J. M. *Nature* **1998**, *396*, 661.

(9) Balzani, V.; Credi, A.; Raymo, F.; Stoddart, J. *Angew. Chem. Int. Ed.* **2000**, *39*, 3348.

(10) Hugel, T.; Holland, N. B.; Cattani, A.; Seitz, M.; Gaub, H. E. *Science* **2002**, *296*, 1103.

(11) Shu, L.; Schlüter, A. D.; Ecker, C.; Severin, N.; Rabe, J. P. *Angew. Chem. Int. Ed.* **2001**, *40*, 4666.

(12) Wintermantel, M.; Schmidt, M.; Tsukahara, Y.; Kajiwara, K.; Kohjiya, S. *Macromol. Rapid Commun.* **1994**, *15*, 279.

(13) Heerbeek van, R.; Kamer, P. C. J.; van Leeuwen, P. W. N. M.; Reek, J. N. H. *Chem. Rev.* **2002**, *102*, 3717.

(14) Fang, J.; Kita, H.; Okamoto, K. *Macromolecules* **2000**, *33*, 4639.

(15) Sheiko, S. S.; Gerle, M.; Möller, M. *Langmuir* **1997**, *13*, 5368.

(16) Namba, S.; Tsukahara, Y.; Tsutsumi, K.; Okamoto, Y. *Polymer* **2000**, *41*, 5165.

(17) Unayama, S.-I.; Nakajima, K.; Ikehara, T.; Nishi, T.; Tsukahara, Y. *J. Appl. Phys.* **1996**, *35*, 2280.

(18) Tsukahara, Y.; Miyata, M.; Senoo, K.; Yoshimoto, N.; Kaeriyama, K. *Polm Adv Technol* **2000**, *11*, 210.

(19) Wintermantel, M.; Fischer, K.; Gerle, M.; Ries, E.; Schmidt, M.; Kajiwara, K.; Urakawa, H.; Wataoka, I. *Angew. Chem. Int. Ed.* **1995**, *34*, 1472.

(20) Fischer, K.; Schmidt, M. *Macromol. Rapid Commun.* **2001**, *22*, 787.

(21) Stephan, T.; Muth, S.; Schmidt, M. *Macromolecules* **2002**, *35*, 9857.

(22) Li, C.; Gunari, N.; Fischer, K.; Janshoff, A.; Schmidt, M. *Angew. Chem. Int. Ed.* **2004**, *43*, 1101.

(23) Govindraj, A.; Satishkumar, B. C.; Nath, M.; Rao, C. N. R. *Chem.Mater.* **2000**, *12*, 202.

(24) Rao, C. N. R.; Govindraj, A.; Deepak, F. L.; Gunari, N.; Nath, M. *Appl. Phys. Lett.* **2001**, *78*, 1853.

(25) Liu, S.; Yue, J.; Gedanken, A. *Adv. Mater.* **2001**, *9*, 13.

(26) Djalali, R.; Li, S.-Y.; Schmidt, M. *Macromolecules* **2002**, *35*, 4282.

(27) Zhang, M.; Drechsler, M.; Müller, A. X. E. *Chem. Mater.* **2004**, *16*, 537.

(28) Zhang, M.; Estournes, C.; Bietsch, W.; Müller, A. X. E. *Adv. Funct. Mater.* **2004**, *14*.

2 SCANNING PROBE MICROSCOPY

2.1 Introduction

The enormous importance of microscopic imaging in the natural sciences, medicine and various engineering disciplines is well known. The demand for high spatial resolution and surface characterization of nano and microstructures has lead to several discoveries in the field of microscopy. Among the vast number of instrumental techniques one of the most powerful one is the Scanning Probe Microscope (SPM), which not only enables visualization of single molecules but also allows the probing of their properties.[1]

The starting point of scanning probe microscope was the invention of the scanning tunneling microscopy in 1982 by Gerd Binnig and Heinrich Rohrer at the IBM laboratory in Zurich.[2] Since that time, a vast family of scanning probe microscopes has been spawned, a few of which are shown in the "family tree" in **Figure 2-1**.

Among the various family of scanning probe microscopes, scanning force microscopy (SFM)[3] became a versatile method for characterization of the microstructure of polymeric materials at the nanometer scale.

2.2 Scanning Force Microscopy

The basic concept of force microscopy is the measurement of forces between a sharp tip and a sample surface**.** The principle set-up is shown in the **Figure 2-2**: a sharp tip with a radius of curvature ~ 30-50 nm attached to a microfabricated cantilever with nominal spring constants are 0.001-50 N/m and with typical resonance frequencies ranging from 10-400 kHz. While scanning, the vertical and lateral position of the cantilever with respect to the substrate is varied by the movement of a piezoelectric crystal supporting either the sample or the cantilever.

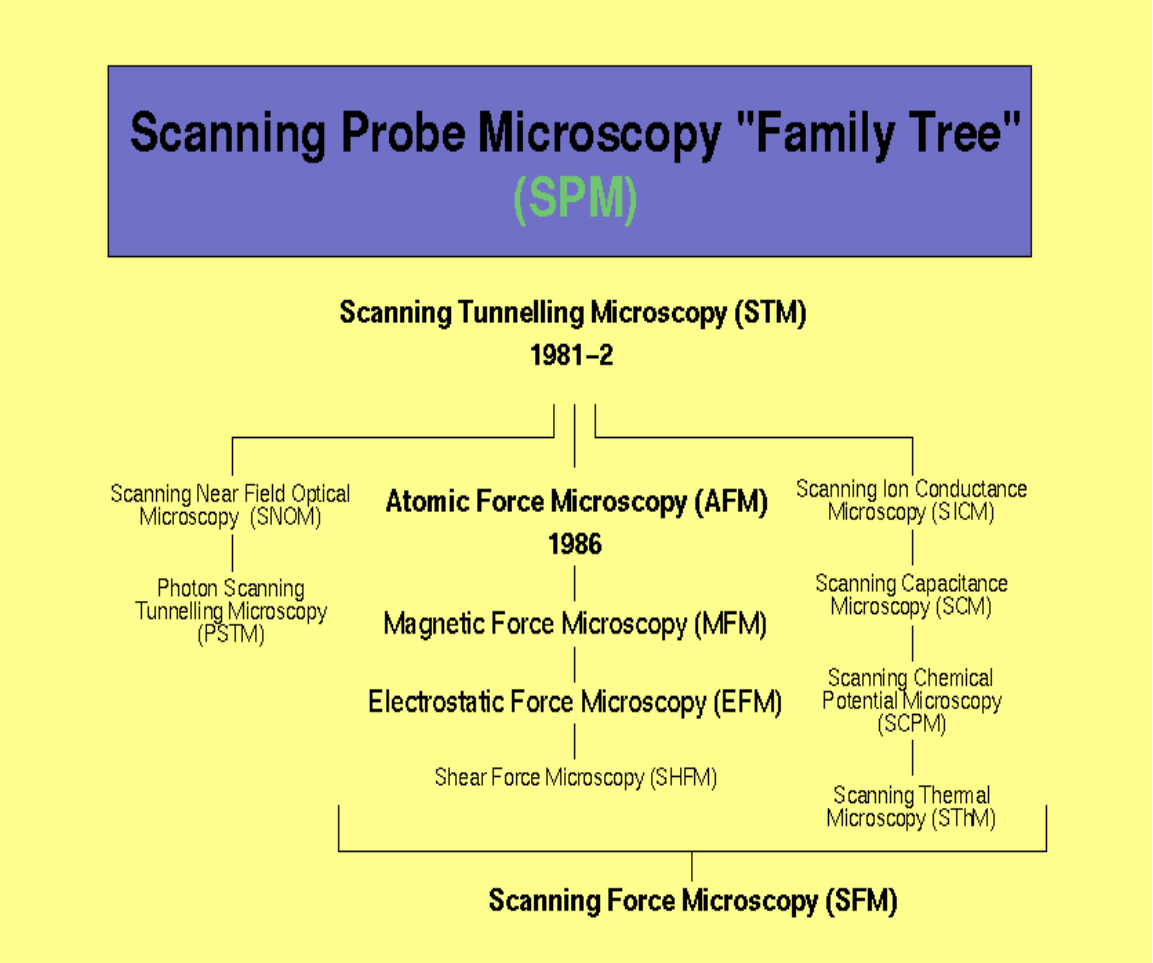

Figure 2-1 A "family tree" showing the development of instrumentation in the field of scanning probe microscopy.

When the tip encounters the sample the tip experiences a force due to which the cantilever bends. There are several techniques to detect the small deflection of the cantilever. Most instruments today use the optical lever method[4,5] to measure the cantilever deflection with high resolution; a laser beam is focused on the free end of the cantilever, and the position of the reflected beam is detected by a position-sensitive detector (photodiode). AFM cantilevers and probes are typically made of silicon or silicon nitride by microfabrication techniques.

2-2 a)

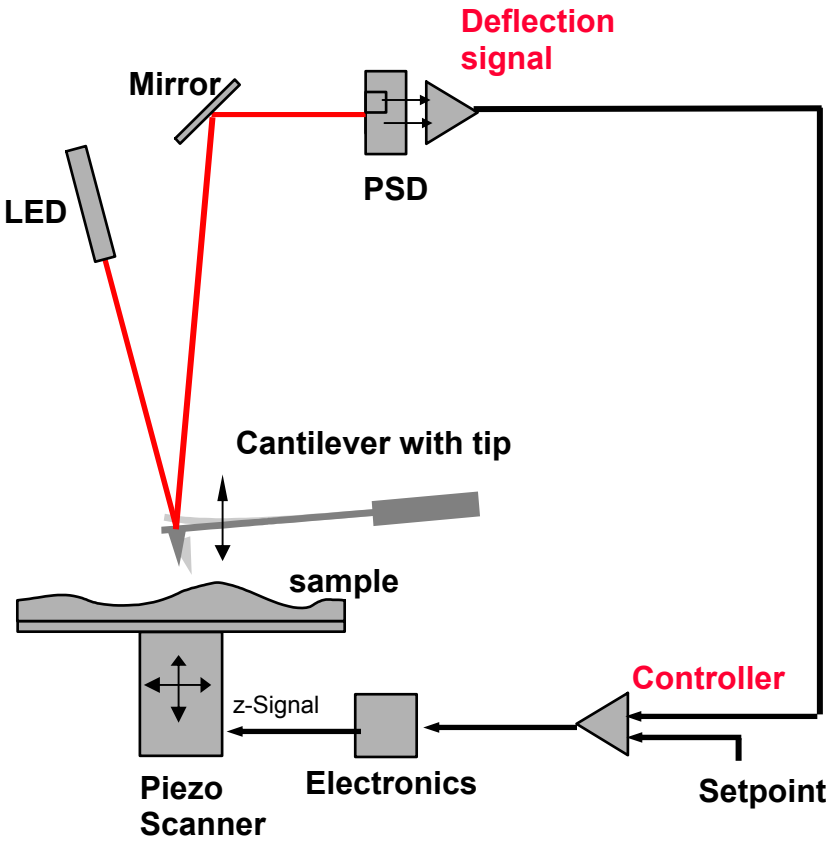

b)

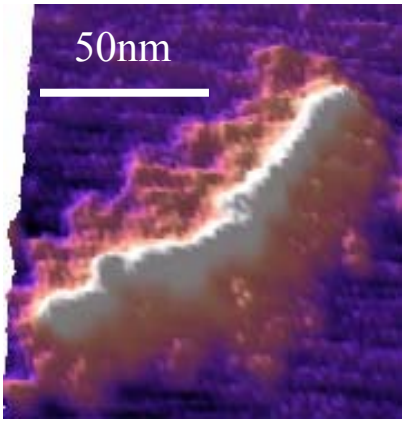

Figure 2-2 a) Principle set of the atomic force microscope (AFM). b) A typical topography image generated modified by the image processing software to obtain a 3D image.

Depending on the separation of tip and sample a variety of tip-sample interactions may be measured by an AFM. The force is inversely proportional to the tip-sample distance. When the tip is lifted off the sample surface, long-range interactions, viz. electric or magnetic forces and thermal noise, influence the cantilever deflection. During sample contact the tip primarily experiences repulsive *van-der-Waals* forces, which are essential for short-distance interactions in the nanometer scale. Beside *van-der-Waals* and Coulomb interactions, hydration interactions also appear in aqueous solutions. At distances of a few nanometers, attractive *van-der-Waals forces* ($\Delta F \sim$ 5-10 pN) are sufficiently strong to deflect the AFM cantilever, which are detected by the photo diode with high precision. The complete interaction comprises the sum of repulsive as well as attractive contributions in a range of 10^{-6} to 10^{-12} N. **Figure 2-3** shows the tip-sample interaction.

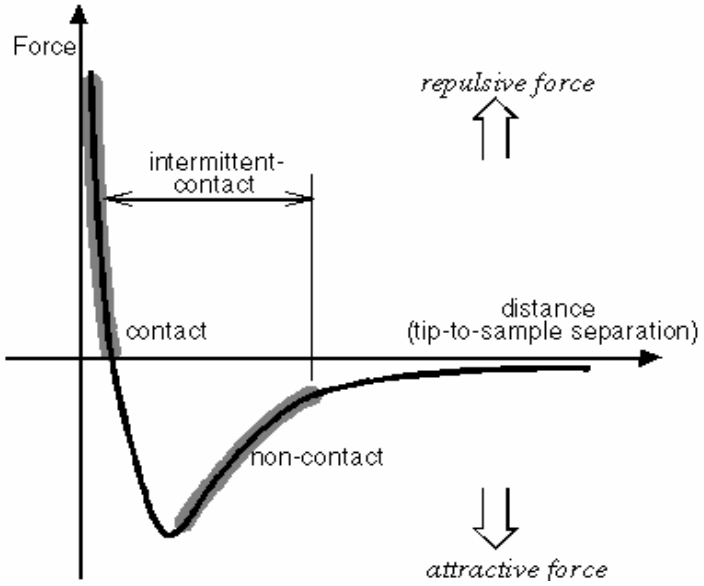

Figure 2-3 Plot of force-distance showing the tip sample interaction as the tip approaches the surface.

2.3 Resolution of AFM

The resolution of the AFM depends on two main components: (1) Sharpness of the tip. Sharper the cantilever higher is the resolution, this can be realized the cartoon shown in **Figure2-4** where two tips one blunt (left) and one sharp (right) scans the surface containing two spheres. The theoretical line scans shown below clearly depicts that the sharper tip has a better resolution. And the second component is the scanner that controls the x-y-z position. Atomic resolution can be achieved for robust and uniform samples in contrast to soft samples such as biological samples, which are more difficult to image because the forces exerted by the tip during imaging may cause deformation of the sample. Usually the width of a DNA molecule is roughly used as a measure of resolution, because it has a known diameter of 2.0 nm in the B form. Some of the best values for AFM imaging are 3.0 nm quoted form DNA in propanol.

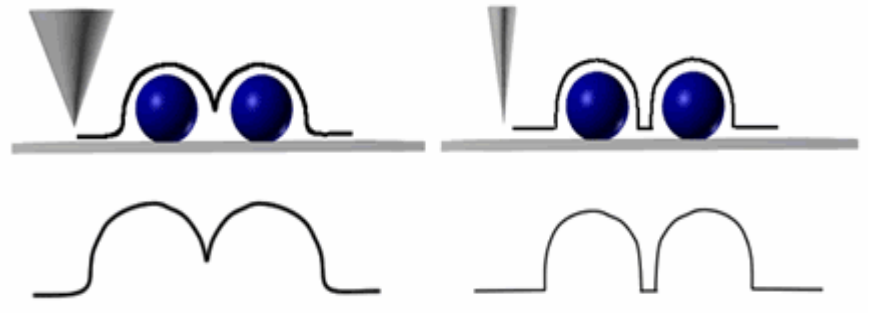

Figure 2-4 Cartoon showing the scanning of two tips, one blunt (left) and a sharp tip (right) that depicts the later resolution is limited by the apical probe geometry.

2.4 Imaging Modes

There are several modes of operation in AFM that can be divided into static and dynamic modes, wherein the static bending of the cantilever or its dynamic properties are measured, respectively.

2.4.1 Contact Mode

The most important static mode is the contact mode is the most common method of operation where the tip scans the sample in close contact with the surface. The force exerted by the tip is repulsive as shown in **Figure 2-3** and is in the range of 100 pN to 10 nN. This force is set by pushing the cantilever against the sample surface with a piezoelectric positioning element. The tip scans the sample and the feedback loop maintains a constant cantilever deflection (force).

The advantages of contact mode imaging are that images can be taken at high scan speeds and atomic resolution can be achieved. Si (111) surface has been imaged in contact mode with atomic periodicity.[6] However single point defects have not been observed so far. This lack of true atomic resolution in contact mode is explained by the fact that the area of the tip-sample contact is larger than atomic dimensions. Even if contact of atomic dimensions is achieved, the attractive forces would cause a pressure of the order of GPa. Thus, tip and sample would be elastically deformed to increase contact area and reduce pressure. One way to obtain higher resolution is to operate in liquids, wherein the attractive forces can be reduced to 10 pN and true atomic resolution can be achieved.[7] However, the disadvantage of this mode is that the lateral forces can damage the sample thereby distorted images may be obtained. This mode is more suitable for robust samples than soft samples such as polymers and biological.

2.4.2 Non-Contact mode

As discussed above soft samples can be easily damaged when imaged in contact mode due to strong tip-sample interactions. This drawback can be overcome by imaging

in the non-contact mode. In this mode, the probe operates in attractive force region and tip-sample interaction is minimized. The force on the tip in this mode is attractive as shown in **Figure 2-3.** In non-contact mode a stiff cantilever (spring constants in the range 20-100 nN) is made to vibrate near its resonant frequency (50-200 kHz) with amplitude of a few tens of nanometers. The tip-sample interaction forces change in both the effective resonant frequency and the amplitude of oscillations. When scanning, the feedback loop keeps constant tip-sample distance by maintaining the resonant frequency of oscillation (frequency-modulation mode) or the amplitude of oscillation (amplitude-modulation mode).

2.4.3 Intermittent Contact Mode or Tapping Mode AFM

In tapping mode AFM,[8] first realized in 1993, the cantilever is oscillated at its resonance frequency and scanned across the sample. The amplitude of the oscillation is reduced and the change in amplitude is used to measure the surface topography. As the name suggests the tip is not in contact with the surface for most of the oscillation cycle. Hence lateral forces in this mode are much lower than in contact mode. Tapping mode AFM is ideal for polymer and biological samples, providing a high lateral resolution up to 1.5 nm and a vertical resolution of ~0.1 nm.[9]

As the changes in amplitude are used for topographic imaging, the phase signal changes may be used to image regions of different composition. The phase lag between the drive signal and actual cantilever oscillation is monitored as shown in **Figure 2-5**. Basically the phase shifts are registered as bright and dark regions. Thus variations in the surface properties, such as viscoelasticity or mechanical properties may be studied using phase imaging.

2-5)

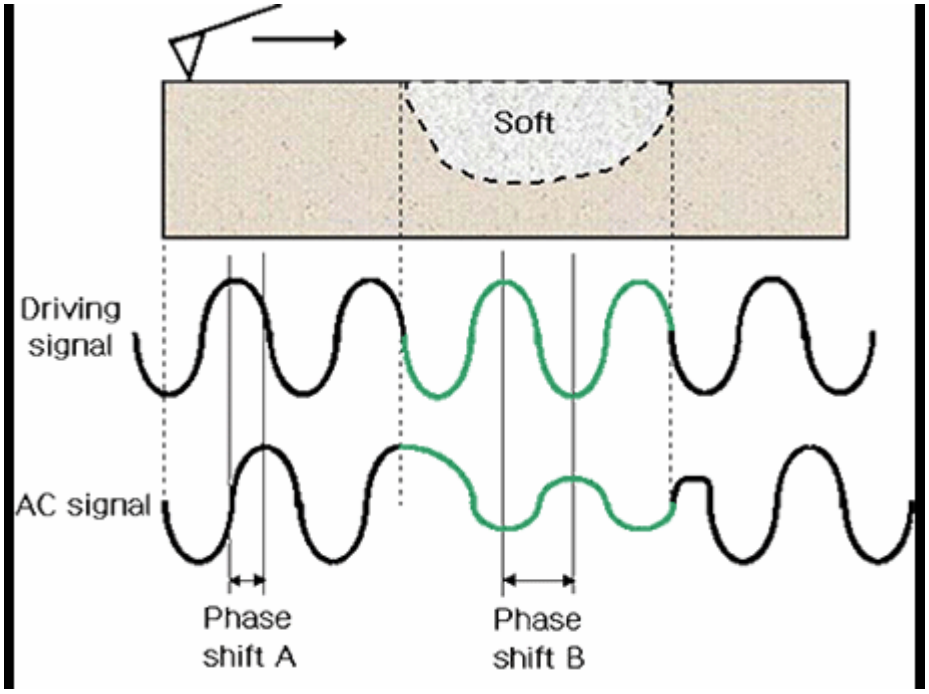

Figure 2-5 Phase changes as the tip scans the sample surface with different mechanical properties.

2.5 Lateral Force Microscopy (LFM)

When scanned in contact mode force microscopy the tip is moved over the surface, friction on the tip-sample contact produces a lateral force on the tip apex that bends the cantilever not only normal to the surface but also the cantilever torsional (lateral) deformation occurs. Thus LFM measures the torsional deformation of the cantilever during scanning in contact mode as shown in **Figure 2-6**.

The cantilever deflections are registered by beam-deflection-type force microscopes. In this way the local variation of friction can be studied with high resolution.

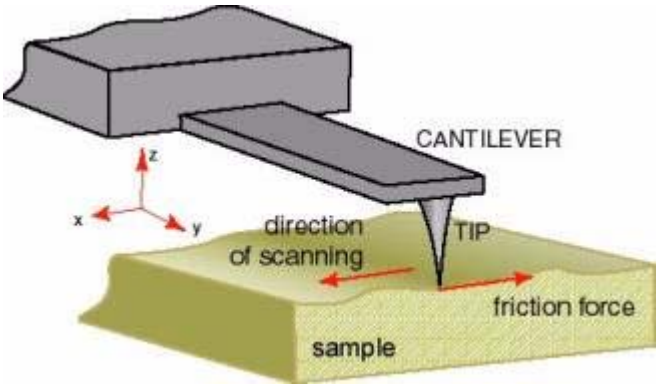

Figure 2-6 Contact mode imaging measuring the torsional deformation.

2.5 References

(1) Meyer, E.; Hug, H. J.; Bennewitz, R. *Scanning Probe Microscopy*; Springer-Verlag Berlin Heidelberg New York, 2003.

(2) Binnig, G.; Rohrer, H.; Gerber, C.; Weibel, E. *Phys. Rev. Lett.* **1982**, *49*, 57.

(3) Binnig, G.; Quate, C. F.; Gerber, C. *Phys. Rev. Lett.* **1986**, *56*, 930.

(4) Meyer, G.; Amer, N. M. *Appl. Phys. Lett.* **1988**, *53(12)*, 1045.

(5) Alexander, S.; Hellemans, L.; Marti, O.; Schneir, J.; Elings, V.; Hansma, P. K.; Longmiro, M.; Gurley, J. *J. Appl. Phys.* **1989**, *65(1)*, 164.

(6) Howald, L.; Lüthi, R.; Meyer, E.; Güthner, P.; Güntherodt, H.-J. *Phys. B* **1994**, *93*, 267.

(7) Ohnesorge, F.; Binnig, G. *Science* **1993**, *260*, 1451.

(8) Zhong, Q.; Inniss, D.; Kjoller, K.; Elings, V. *Surface Science* **1993**, *290*, L688.

(9) Möller, C.; Alln, M.; Elings, V.; Engel, A.; Müller, D. J. *Biophys. J.* **1999**, *77*, 1150.

3 SINGLE MOLECULE FORCE SPECTROSCOPY AND POLYMER MODELS

Mechanical properties of single biological and polymer molecules is stimulating new fields of research such as receptor-ligand interactions,[1] protein unfolding[2] and molecular motor mechanics.[3] There are several techniques used for manipulating single molecules. Basically single molecule manipulation may be classified into two main groups: mechanical transducers and external field manipulators. Mechanical transducers directly contact the molecule under investigation. Mechanical transducers include glass micropipettes, microfabricated cantilevers and single molecule force microscopy (SMFS) by atomic force microscope (AFM). External field manipulators act from a distance and usually do not directly probe the molecule under investigation. External field manipulators include optical, magnetic tweezers and flow fields. The techniques can be summarized as shown in **Figure 3-1**.[4] In this chapter, SMFS is described in detail as this method has been used for the single molecule manipulation of the cylindrical polymer brush molecules.

3.1 Introduction to Single Molecule Force Spectroscopy (SMFS)

Force spectroscopy is an analytical technique that provides an opportunity to study mechanical properties and molecular conformations of individual polymer molecules. The name “force spectroscopy”, although widely used, is misleading, as there is no true matter-radiation interaction. Force spectroscopy measures the behavior of a molecule when stretched between a tip and the substrate. Basically, the cantilever of the microscope acts as a sensor for local interaction between the tip and the sample. In this way a great deal has been learned in recent years about the mechanocoupling in the enzymes responsible for muscle contraction, DNA mechanics, protein unfolding, ligand-receptor interactions, elasticity of polysaccharides and also synthetic polymers.

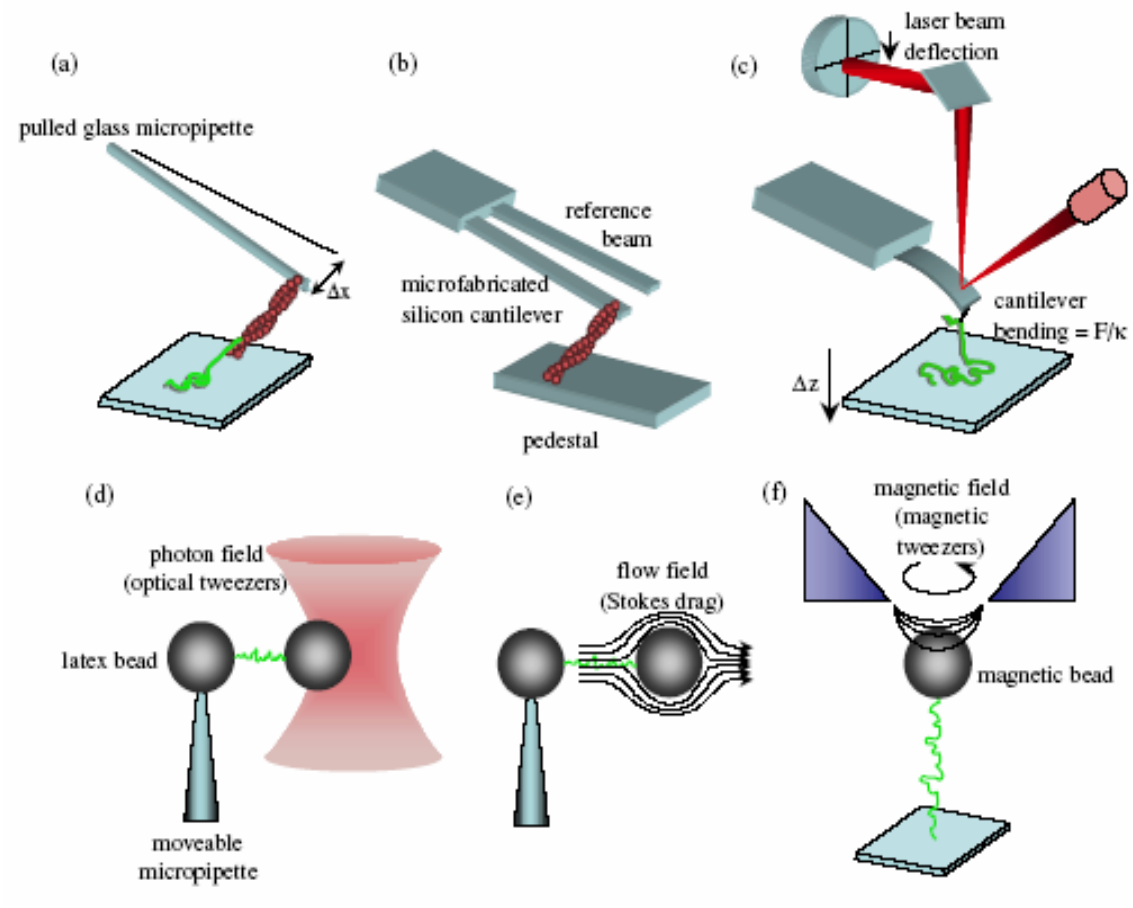

Figure 3-1 Single molecule manipulation methods. (a)-(c) are cantilever methods including (a) pulled glass micropipette, (b) microfabricated cantilevers and (c) single molecule force spectroscopy using the AFM. Methods (d)-(f) are force field methods which include (d) optical tweezer method, (e) flow field method and (f) magnetic tweezer method.

With the accessible force range of several fN to a few nN the whole force spectrum from entropic forces to rupture of covalent bonds has now been investigated at the molecular level.

3.2 SMFS: The Technique

The general set-up of the AFM has been described in chapter 2 (see **Figure 2-1**). Single molecule force spectroscopy is a simple technique in which, the AFM tip is initially at a certain height h (the z coordinate, imposed by the piezo actuator, is the distance between the sample and the rest position of the cantilever); subsequently, the sample approaches the cantilever, acquiring deflection values at each pre-assigned step. This process stops at the height $z(F_{max})$, when the force exerted on the tip reaches the pre-assigned load F_{max}. The height $z(F_{max})$ and the deflections in the last N_z approaching points, whose mutual distance is δ_z, are stored. Then the sample is retracted step by step for a distance $\Delta z = N_z\delta_z$ and the deflections in the next N_z withdrawal points are acquired and stored. In this way the tip is finally retracted to its initial height h acquiring a force-distance curve.

A force curve is a plot of the measured cantilever deflection, Δz versus the displacement of the z-piezo device. The spring constant has to be determined accurately for quantitative evaluation of the force. We can realize the meaning of spring constant as applied to cantilevers in the schematic illustration in **Figure 3-2**. Visualizing the cantilever as a coil spring, its spring constant directly affects the downward force exerted on the sample. One of the methods for calibrating the cantilever is to monitor the thermal noise of the cantilever. Determination of the average amplitude of the vibrational resonance allows calculation of the spring constant, which is described in chapter 4.

From Hooke's law:

$$F = k\Delta z \qquad \text{Equation (1)}$$

where the applied force F is deduced from the cantilever deflection Δz and the spring constant k.

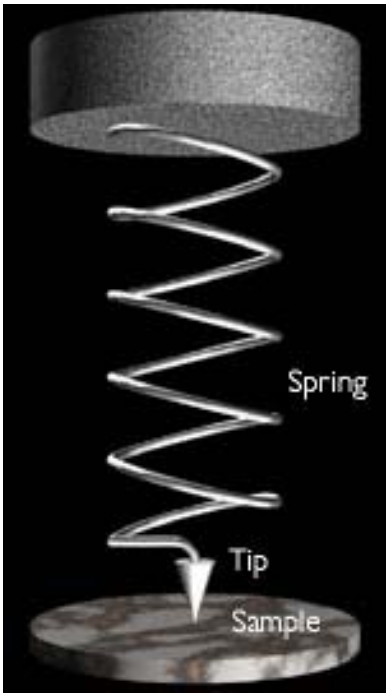

Figure 3-2 Schematic representation of a cantilever to apprehend the meaning of spring constant as applied to AFM cantilevers.

3.3 Force-Distance Curves

The cantilever deflection is a measure of the interaction force. Relationship between the cantilever deflection and the distance between the tip and sample is shown in **Figure 3-3b**. When the tip is far away from the surface, forces are absent and the cantilever is not deflected as shown in the **Figure 3-3b** (1). As inferred from equation (1), attractive forces ($F < 0$) lead to a negative cantilever deflection, while repulsive forces ($F > 0$) lead to positive cantilever deflection. When then tip approaches the substrate, attractive forces set in: if the value of the positive force gradient is the same as the spring constant ($F'(d) = k$) a mechanical instability occurs, called the "snap-on" (2). At this point, the tip jumps into a close repulsive contact with the sample ($2 \rightarrow 3$), and hence the surface may experiences deformation. The cantilever presses onto the substrate thus repulsive forces act on the cantilever ($3 \rightarrow 4$), which is determined by the viscoelasticity

of the substrate. The pressure exerted by the tip on the surface increases as the sample displacement increases.

a)

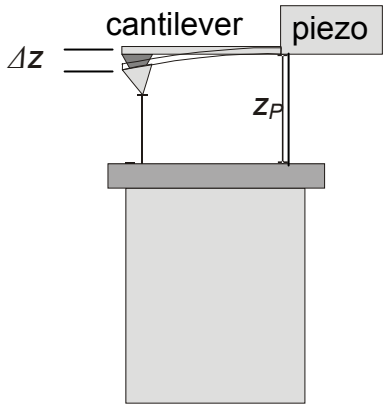

b)

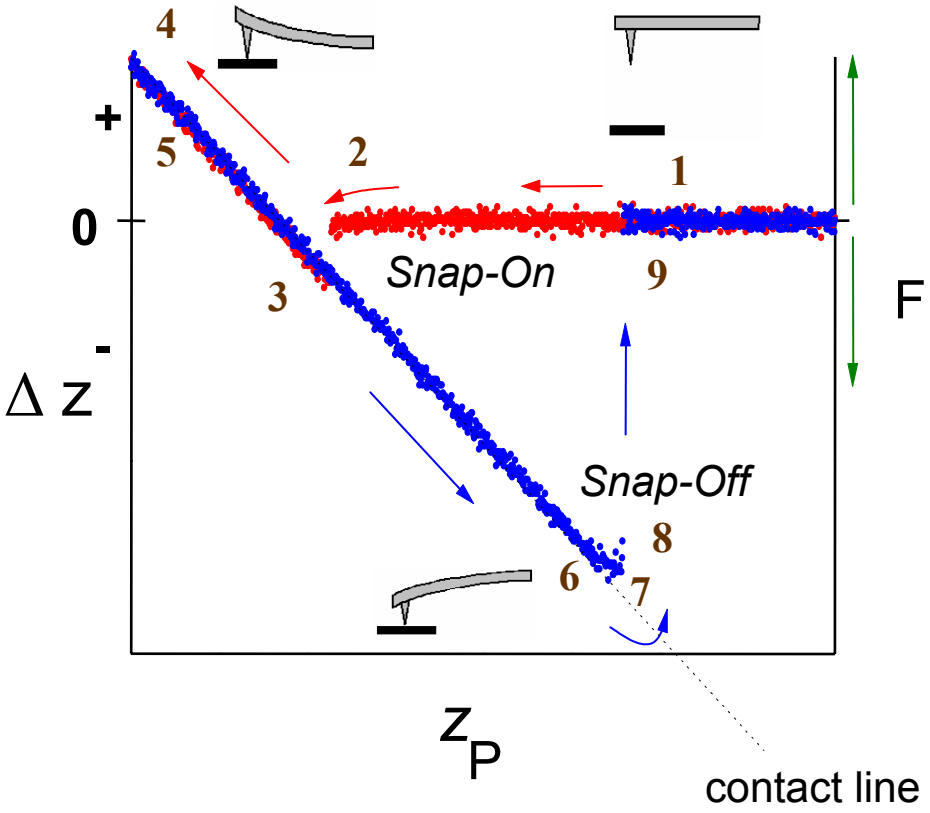

Figure 3-3 a) Parameters relevant for calculating the transfer function between z-piezo displacement (z_P) and cantilever deflection (Δz). b) Simple force curve (red is the approach curve and blue is the retraction); the numbers and arrows illustrate the course of the measurement. (Figure adopted from Janshoff et. al. [1])

And finally the forces reach a maximum, which is equal to the loading force (F_{max}). The curve from (1) → (4) is called the approach curve (depicted red in **Figure 3-3b**. Upon retracting the cantilever repulsive forces decrease continuously (5→ 6). The maximum attractive force can be measured when the tip separates from the surface, where another mechanical instability is observed known as the so-called snap-off (8), which is visible immediately after the minimum of the curve (7). The maximum attractive force is a measure of the adhesive forces. The cantilever then returns to zero force (8→ 9). The curve from (5) → (9) is called the retraction curve (depicted in blue in **Figure 3-3b**.

The adhesion energies and interaction potentials between tip and sample usually can be quantified from an AFM measurement, if the exact tip geometry is known. However, the high sensitivity of a few piconewton provides the necessary resolution, to probe the response of individual molecules to external forces under ambient conditions. While imaging is often done in air for different reasons (e.g. easy sample preparation, faster image acquisition and lower noise at higher resonance frequencies), the force experiments are usually carried out in aqueous environment basically for two reasons: first, the capillary forces in air often exceed the forces to be investigated and secondly, often investigated biological molecules perform their functions in aqueous buffer. In principal, AFM measurements are also possible in other organic solvents as long as the experiment does not suffer from high solvent volatility.

3.4 Capillary Forces

In air, most samples have several nanometers of water adsorbed on the surface. This water layer forms a bridge between the tip and the substrate as shown in the **Figure 3-4 a**. Thus the capillary bridge is pulled when the tip is retracted causing large forces known as the capillary forces,[5] given by:

$$F = 4\pi R\gamma_L \cos\theta \qquad \text{equation (2)}$$

where R is the radius of the probe γ_L is the surface energy between the tip and the sample and θ is the angle related to the geometry of the tip-sample contact.

Thus the main source of adhesion in air is due to the capillary bridge formed between the tip and the sample, which leads to a hysteresis in the cantilever approach-retraction cycle as shown in the **Figure 3-4 b**. The figure shows the cantilever deflection Δz vs. the tip- sample distance z_P. At large distances there is no deflection and the plot is horizontal. As the cantilever is retracted away from the surface, the tip remains stuck to the sample: the capillary force holds it and the linear deflection-distance dependence extends below the horizontal axis until the capillary bridge is broken. At this position the mechanical instability (snap off) occurs and the tip goes back to its undeflected position. Thus one can observe a large hysteresis.

3-4 a)

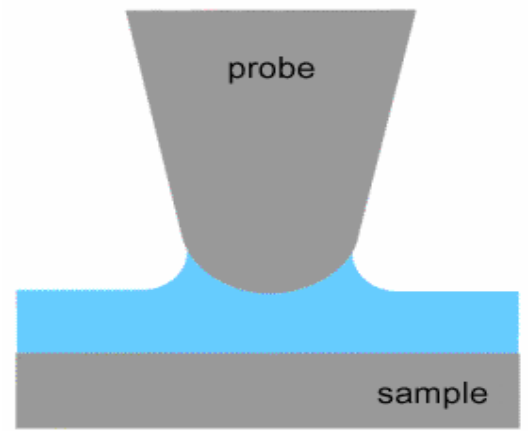

b)

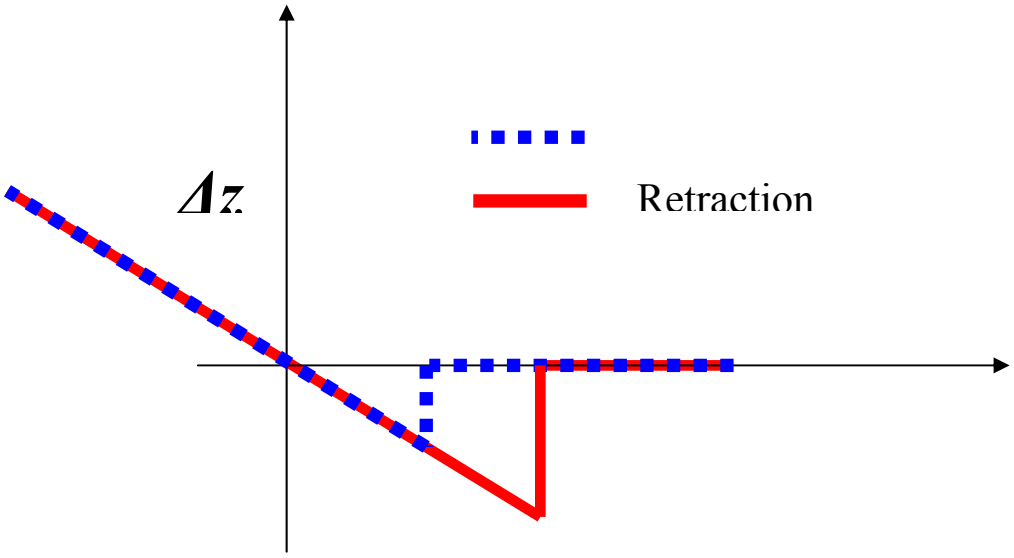

Figure 3-4 a) A capillary bridge formed between the tip and the sample. b) A typical deflection as a function of tip-sample separation showing hysteresis due to capillary forces.

3.5 Applications of SMFS

The first SMFS experiments by means of AFM were done on individual ligand receptor pairs: in these experiments a receptor-coated AFM tip was brought into contact with a sample surface coated with corresponding ligand and then pulled off. Statistical analysis of the recorded force-distance traces allowed the determination of the adhesion force.[6,7] While these first experiments were done with commercial instruments originally developed for image acquisition, custom-built instruments were soon optimized for SMFS. The force resolution of the best instruments is only limited by the thermal noise at room temperature and their spatial resolution along the z-axis is in the sub-nanometer range.[8] Another important development is the implementation of a single-molecule force clamp, which allows AFM measurement under conditions of constant force.[9] This new mode was recently used for studying the force dependence of the unfolding probability of protein modules.

3.5.1 Intra- and Intermolecular Forces

The intramolecular force measurements include the force-distance characteristics of single polymer chain. Typically, these underlying molecular processes follow equilibrium pathways under the conditions of the AFM experiment, which will be an important requirement for their potential use in the development of artificial switches and machines.

All unbinding and desorption processes in which the interaction is transmitted through the surrounding medium come under the class of intermolecular forces. This includes the rupture of covalent chemical bonds,[10] or the unbinding of all kinds of intermolecular aggregates based on non-covalent binding interactions such as ligand-receptor pairs or hydrogen bonded systems.[11]

To summarize, the underlying interaction forces can be classified into intramolecular and intermolecular forces as shown in the **Table 3-1**.[12]

Table 3-1

Intramolecular forces	Intermolecular force
entropic and enthalpic elasticity of single polymer chains	ligand-receptor pairs, DNA melting cell adhesion, protein unfolding
conformational transitions along polymer chains	covalent bond rupture, coordination complexes
	polymer desorption from solid substrates.

3.5.2 Stretching of Single Polymer Chains

Flexible polymers adopt a random coil conformation in solution and Brownian motion causes a permanent fluctuation of the molecule around a mean equilibrium conformation. Due to its large number of degrees of freedom, a single polymer chain made up of hundreds to thousands of monomers has to be treated by means of statistical physics.

Stretching a molecule causes two kinds of restoring forces viz. *entropic* and *enthalpic*. At small displacements, *entropic* forces dominate. Extending the molecule drastically reduces the number of conformations. This loss of conformational entropy is reflected in the so-called elastic entropy. Large displacements lead to a tension of the molecular backbone, in which bonds are stretched in the direction of the pulling force. This effect is called *enthalpic elasticity*.

The direct measurement of the intramolecular forces can be done using force spectroscopy on single molecules. The polymer is immobilized on the substrate and interacts with the tip specifically or nonspecifically (if the molecule is physisorbed to the tip). On retraction of the cantilever the molecules are stretched revealing important information about their conformation. The forces of interest are mostly weaker than those associated with bond rupture, thus a special treatment of the probe can be avoided.

Many single molecule experiments need to be performed and a large number of experimental data need to be obtained, then statistical results can be deduced. Fitting the

data with polymer models or by combining the data with computer simulations can help to determine microscopic parameters for example the mechanical quantities such as flexibility of the molecule[13,14] and the thermodynamic and kinetic parameters such as the energy barrier between the folded state and unfolded state of proteins.[15]

3.6 Molecule Specific Force Spectroscopy

As pointed out above, a large number of force profiles need to be recorded for the statistical analysis in order to study the local properties of the molecule. The interpretation of such data can however be complex. The tip randomly picks up the molecule and stretches it, thus it is unknown if the molecule is picked up at one of its end or closer to the center in which case we end up stretching a loop as shown in the **Figure 3-5**, which drastically affects the results.

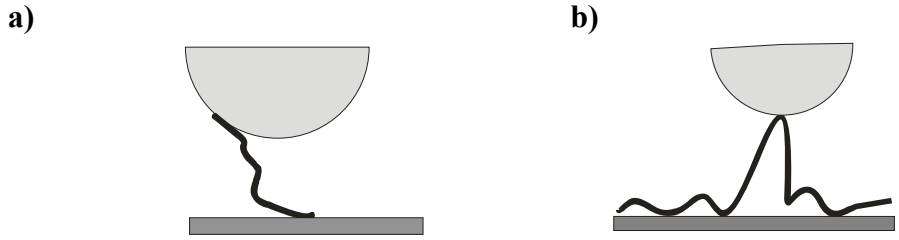

Figure 3-5 a) Tip picks up the molecule at one of its end. b) Tip picks up the molecule closer to its center, thereby stretching a loop.

Secondly, force induced conformational changes in individual molecules have been studied using single molecule force spectroscopy on a statistical basis. Only recently a new method was introduced wherein individual molecules were imaged and manipulated by combining AFM and SMFS techniques.[16] This technique i.e. “molecule specific force spectroscopy”, may help to resolve the complex force extension curves as well as help to monitor the force induced conformational changes *in-situ*.

3.7 Fly-fishing Mode

It is possible to manipulate a single molecule repeatedly before reaching its rupture limit by using the "fly fishing mode"[17] as shown in the schematics in **Figure 3-6**. In this mode the tip is allowed to approach and retract step by step without indenting deep into the sample film until a binding event was registered. This is done in order to minimize the number of multiple attachments, which typically occurs when the tip penetrates the polymer film. This mode is very effective in studying force induced conformational changes in individual molecules.

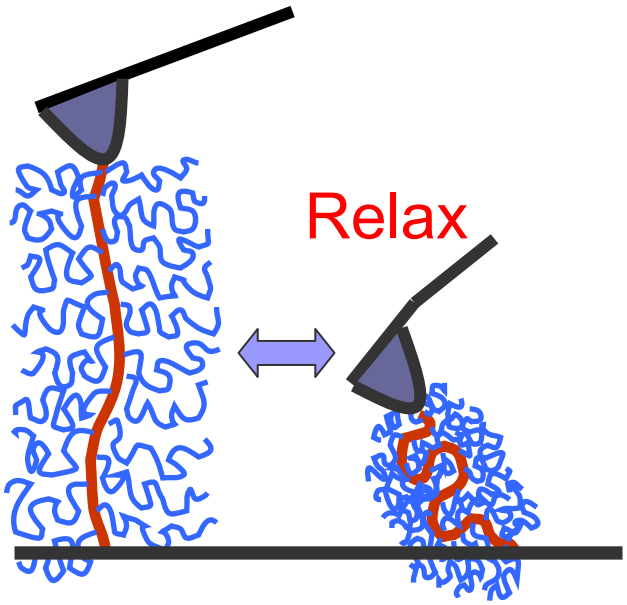

Figure 3-6 Schematics of repeatedly stretching the same cylindrical brush molecule in the "fly-fishing" mode.

3.8 Polymer Models from Statistical Mechanics

When a polymer chain is stretched a restoring force sets in which is strictly proportional to the relative extension of the chain, $F \propto x/L$ where x is the end-to-end distance of the polymer chain and L is the contour length of the polymer. Assuming a

Gaussian distribution for the random polymer chain, the force is a linear function of x for small extensions and the polymer behaves as an ideal spring. At higher forces i.e. approaching full extension of the polymer chain, the actual end-to-end distance cannot be larger than the contour length and the restoring force is a non-linear function of x/L. The two well-known theoretical models that satisfy this boundary condition are the freely jointed chain (FJC)[18] and the wormlike chain (WLC).[19,20]

Figure 3-7 shows the schematic representation of the two basic polymer models witht the FJC (left) describes a polymer of n rigid segments with a Kuhn length l_K that are attached with flexible joints.

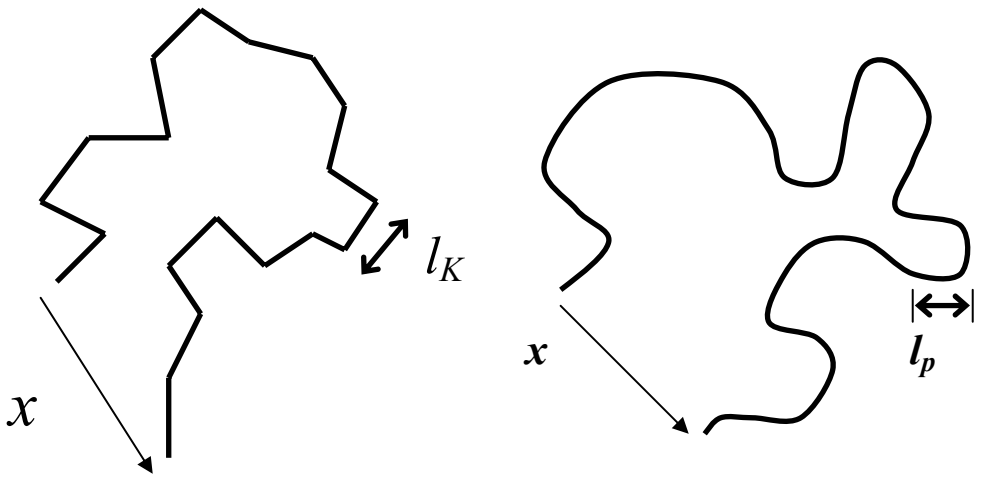

Figure 3-7 Schematics of the freely jointed chain (left) and the wormlike chain (right).

The schematics to the right shows the WLC that describes the polymer as an irregularly curved filament that is linear on the scale of the persistence length l_P. x is the end-to-end distance of the polymer chain. The force-extension behavior of individual polymer chains are well described by these two models.[1,12] The selection of elasticity models for the fitting of force-extension curves of single polymer chains in the entropic and enthalpic regime has discussed in detail by Janshoff et. al.[1]

3.9 Stiff chains

Stretching of stiff chains was first introduced by Odjik using a semiclassical model.[21] For a semiflexible chain there are three important length scales viz. (1) total length (L), (2) persistence length (l_p) and (3) deflection length (λ).

The flexibility of a polymer chain is given by the persistence length l_p which is the distance over which the two segments of the chain remain directionally correlated

$$l_p = \frac{A}{k_b T} \qquad \text{equation (2)}$$

where, A is the bending stiffness and $k_b T$ is the thermal energy.

A more relevant length scale for stiff polymer chains is the deflection length (λ), introduced by Odjik.[22]

$$\lambda = \sqrt{A/F} = \sqrt{k_b T l_p / F} \qquad \text{equation (3)}$$

For molecules larger than the deflection length $\lambda = \sqrt{k_b T l_p / F} \approx 2-6$ and forces larger than $F = k_b T / 4 l_p \approx 0.01$ pN:

$$F = \frac{k_b T}{4 l_p} \frac{1}{\left(1 - x/L\right)^2} \qquad \text{equation (4)}$$

where, x approaches L as $F^{-\frac{1}{2}}$.[23] Equation (4) applies up to moderate forces. This model describes the stretching of a semiflexible chain as an intermediate between a rigid rod and a flexible coil that accounts for the local stiffness.

In the high force regime i.e. 5-50 pN, chemical bonds are slightly modified by the strong stretching which leads to a small increase in the length of the molecule, however above 60 pN a drastic change in structure of the chain occurs leading to sudden changes in length. The failure of the inextensible model in the high force regime can be ascribed to a change from entropy dominated restoring forces to the elasticity-dominated regime. As a consequence a modified version, of the inextensible model, the so called extensible model was given by Odjik to account for the enthalpic contribution:

$$\frac{x}{L} = 1 - \frac{1}{2}\left(\frac{k_b T}{F l_p}\right)^{\frac{1}{2}} + \frac{F}{\Phi} \qquad \text{equation (5)}$$

where ϕ denotes the elastic stretch modulus. In the high force regime i.e. when the chain is stretched beyond its contour length the equation shows a more or less linear behavior effectively representing Hooke's law governed by bond angle deformation and bond stretching as shown in the **Figure 3-8 (**red continuous line**)** as compared to the model given by equation (4) (blue continuous line).

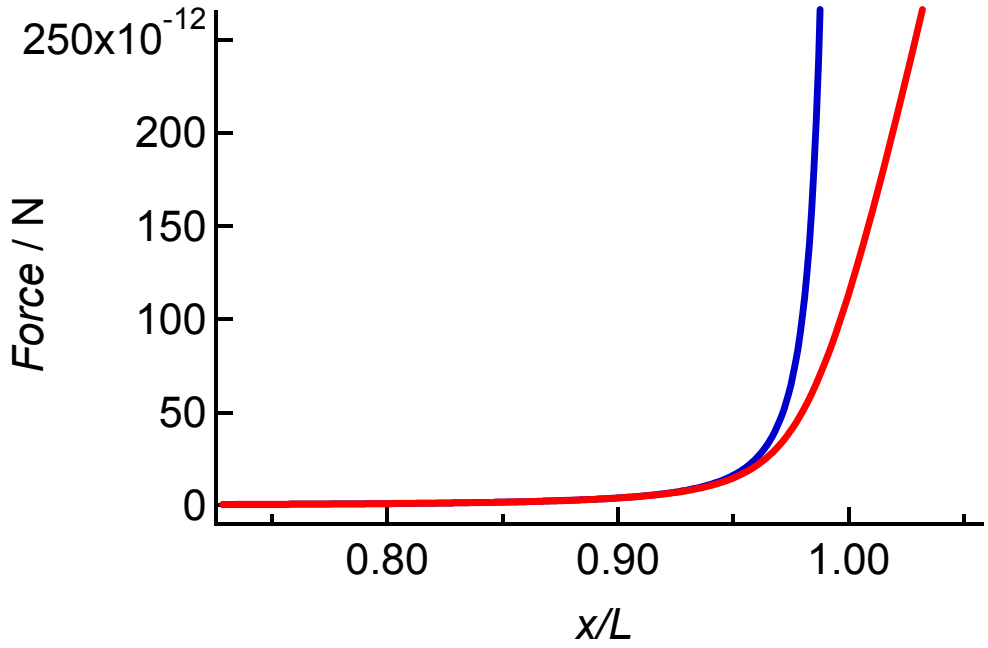

Figure 3-8 Comparison between the force laws given by equation (4) (blue continuous line) and equation (5) (red continuous line).

3.10 References

(1) Janshoff, A.; Neitzert, M.; Oberdörfer, Y.; Fuchs, H. *Angew. Chem. Int. Ed.* **2000**, *39*, 3212.

(2) Rief, M.; Gautel, M.; Oesterhelt, F.; Fernandez, J. M.; Gaub, H. E. *Science* **1997**, *276*, 1109.

(3) Hugel, T.; Holland, N. B.; Cattani, A.; Seitz, M.; Gaub, H. E. *Science* **2002**, *296*, 1103.

(4) Kellermayer, M. S. Z. *Physiol. Meas.* **2005**, *26*, R119.

(5) Weisenhorn, A. L.; Hansma, P. K.; Albrecht, T. R.; Quate, C. F. *Appl. Phys. Lett.* **1989**, *54*, 2651.

(6) Florin, E. L.; Moy, V. T.; Gaub, H. E. *Science* **1994**, *264*, 415.

(7) Lee, G. U.; Chris, L. A.; Colton, R. J. *Science* **1994**, *266*, 771.

(8) Sarid, D. *Scanning Force Microscopy*; Oxford University Press : Oxford U.K.: Oxford, 1991.

(9) Fernandez, J. M.; Hongbin, L. *Science* **2004**, *303*, 1674.

(10) Grandbois, M.; Beyer, M.; Rief, M.; Clausen-Schaumann, H.; Gaub, H. E. *Science* **1999**, *283*, 1727.

(11) Zou, S.; Schönherr, H.; Vancso, G. J. *Angew. Chem. Int. Ed.* **2005**, *44*, 956.

(12) Hugel, T.; Seitz, M. *Macromol. Rapid Commun.* **2001**, *22*, 989.

(13) Ortiz, C.; Hadziioannou, G. *Macromolecules* **1999**, *32*, 780.

(14) Bemis, J.; Akhremitchev, B. B.; Walker, G. C. *Langmuir* **1999**, *2799*.

(15) Rief, M.; Fernandez, J. M.; Gaub, H. E. *Phys. Rev. Lett.* **1998**, *81*, 4764.

(16) Oesterhelt, F.; Oesterhelt, D.; Pfeiffer, M.; Engel, A.; Gaub, H. E.; D.J., M. *Science* **2000**, *288*, 143.

(17) Rief, M.; Oesterhelt, F.; Heymann, B.; Gaub, H. E. *Science* **1997**, *275*, 1295.

(18) Flory, P. J. *"Statistical Mechanics of Chain Molecules"*: Hanser, München, 1988.

(19) Doi, M.; Edwards, S. F. *"The Theory of Polymer Dynamics"*; Oxford University Press: Oxford, 1998.

(20) Kratky, O.; Porod, G. **1949**, *68*, 1106.

(21) Odijk, T. *Macromolecules* **1995**, *28*, 7016.

(22) Odijk, T. *Macromolecules* **1983**, *16*, 1340.

(23) Marko, J. F.; Siggia, E. D. *Macromolecules* **1995**, *28*, 8759.

4 MATERIALS INSTRUMENTS AND PREPARATIONS

4.1 Instruments

In this thesis two instruments were used for the imaging and force spectroscopy experiments. Imaging in air was carried out by the AFM Multimode from digital instruments and the imaging in solution and force spectroscopy experiments were carried out using the Molecular Force Probe from Asylum research.

4.2 Substrates

Here, substrate denotes a solid base on which the molecules of interest are immobilized. The criteria for use of a particular substrate for AFM imaging are 1) It needs to be atomically flat, 2) should have a chemically well-defined surface and 3) should be easy to clean. All these results can be best fulfilled with layered materials since one can obtain a clean and atomically flat surface by just cleaving them prior to adsorption.

The choice of the substrate for AFM imaging depends on the experiment, since the interaction between the molecule and substrate determines adhesion and mobility of the adsorbate. For stable imaging it is necessary to have strong adsorption and low mobility.

In this thesis, mica substrate was used for all experiments. Mica is the most commonly used substrate for scanning force microscopy imaging, since it is easily cleavable and cheap. Due to its hydrophilic nature it allows molecule deposition from aqueous solutions, making it an ideal choice for investigations of biological macromolecules. Muscovite mica was obtained from PLANO (W. Plannet GmbH, Wetzlar, Germany).

4.3 Spin Caster

Homemade temperature controlled spin caster shown in **Figure 4-3** was used to spin cast the dilute polymer solutions onto the mica surface. Prior to spin casting the mica surface and polymer solution were kept in the spin caster box overnight to attain constant temperature.

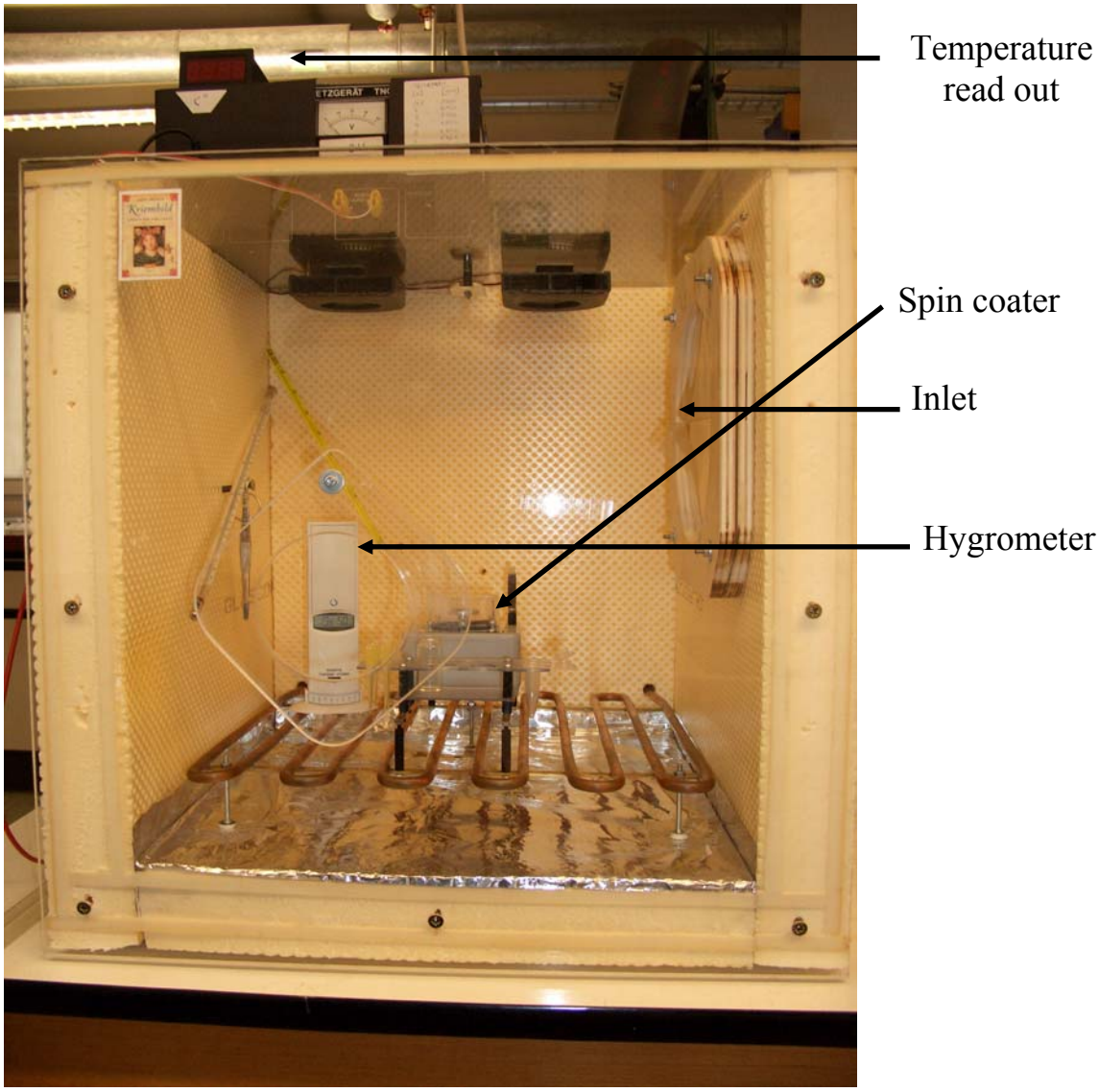

Figure 4-3 Picture temperature controlled spin caster.

4.4 AFM cantilevers and Spring Constant Measurement.

Silicon cantilevers purchased from Nanosensors, Nanoworld, Mikromasch were used for tapping mode AFM imaging. The cantilevers exhibited a nominal spring constant of ~ 40 N/m and a resonance frequency ranging from 250-300 kHz. **Figure 4-4** show scanning electron microscope images of a typical AFM tips attached to a microfabricated cantilevers.

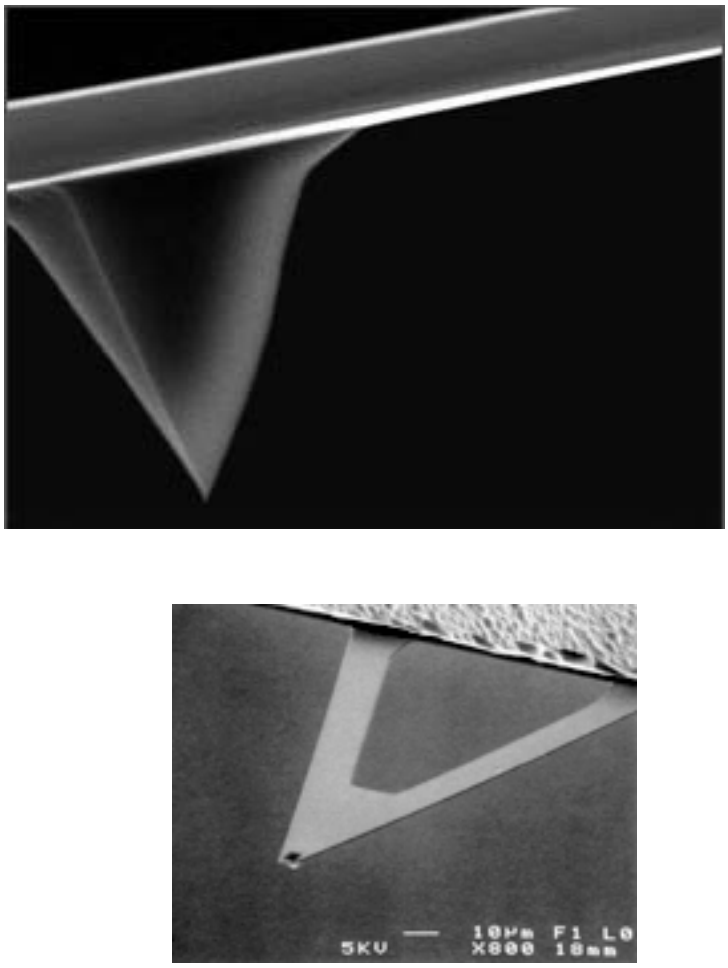

Figure 4.4 Scanning electron microscope image of a) silicon cantilever and tip and b) V-shaped silicon nitride cantilever.

Silicon Nitride cantilevers from Olympus and Veeco were used for tapping mode, contact mode AFM imaging and single molecule force spectroscopy in solution. There are several ways of determining the spring constant of a cantilever which include Added Mass method (Cleveland),[1] Sader method,[2] Hydrodynamic Drag method[3] and Thermal Noise method[4-6] Here the Thermal Noise Method was used to determine the spring constant of the cantilevers.

Thermal Noise Method

The thermal noise method is based on the *equipartition theorem*, which states that the thermal energy present in all terms in the Hamiltonian of a system that are quadratically dependent on a generalized coordinate is equal to $k_B T/2$, where k_B is Boltzmann's constant and T is the absolute temperature (in Kelvin). If one can treat the cantilever as an ideal spring of constant k, a measurement of the thermal noise $\langle x^2 \rangle$ in its position allows the spring constant to be determined as [4]

$$k = \frac{k_B T}{\langle x^2 \rangle} \qquad (1)$$

4.5 References

(1) Cleveland, J. P. et. al. *Rev. Sci. Instrum*. **1993**, 64, 1868.

(2) Sader, J. E., W. M. Chon, et al. *Rev. Sci. Instrum.* **1999**, 70, 3967

(3) Sader, J. E. *J.Appl. Phys.* **1998**, 84, 64.

(4) Hutter, J. L. and J. Bechhoefer *Rev. Sci. Instrum*. **1993**, 64, 1868.

(5) Butt, H. J. and M. Jaschke *Nanotechnology* **1995**, 6, 1

(6) Hutter, J. L. *Langmuir* **2005**, 21, 2630.

5 VISUALIZATION OF CYLINDRICAL POLYMER BRUSH MOLECULES

5.1 Introduction to Single Molecule AFM Imaging

The conformational characteristics of linear macromolecules constitute one of the most important physical aspects for the precise understanding of their properties. The possibility of visualizing individual macromolecules has been pursued since the appearance of scanning tunneling microscope[1] - the pioneering scanning probe microscopy technique. Numerous attempts to obtain images of DNA macromolecules on different substrates, which were undertaken with STM, had not been fully convincing until AFM[2] was introduced and successfully applied for this purpose. After that AFM studies of DNA,[3,4] proteins[5] and other molecular species of biological origin[6] became routine. Hashimoto et al first applied AFM for the visualization of single synthetic polymer molecules, i.e. polystyrene-block-poly (methyl methacrylate) diblock copolymers.[7] Since then AFM has been used extensively to study the conformations of single polymer macromolecules on surfaces as it can be used in virtually any environment.

5.2 Poly (2-vinylpyridine) Cylindrical Polymer Brushes

Cylindrical of poly-2-vinylpyridine (PVP) brush molecules were prepared by polymerization of the corresponding macromonomers as shown in **Scheme 5-1**, described elsewhere.[8] PVP can be converted to a polyelectrolyte by quarternization reaction. **Figure 5-1** shows an AFM topography image of a single PVP brush molecule along with the 3-dimensional image. The wormlike nature of the molecule is clearly visualized. The average height of these molecules was 2 ± 0.2 nm.

Previously *in-situ* adsorption of polyelectrolyte PVP brushes on mica surface before and after adding NaCl salt was observed by AFM imaging using the magnetic AC mode (MAC Mode^{TM}).[9] It was observed that the coverage of mica with the polyelectrolyte brushes increased by adding NaCl to the polyelctrolyte solution. This result is reconfirmed here by using intermittent contact mode AFM imaging. **Figure 5-2a**

shows an AFM topographic image of the quarternized PVP brushes without pre-adsorbing, i.e. the dilute polyelectrolyte solution (0.1 mg/ml) was injected into the fluid cell containing 200 µl Milli Q water and immediately imaged. The surface coverage was calculated by scanning probe image processor (SPIP) software to 29 %. **Figure 6-2b** shows the AFM topographic image after addition of 50 µl of 0.1M NaCl solution.

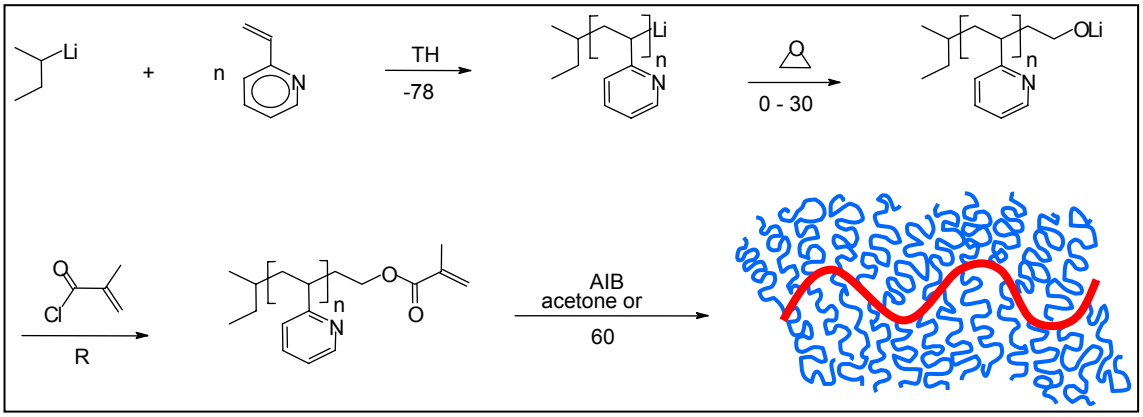

Scheme 5-1 Synthesis of poly-2-vinylpyridine (PVP) cylindrical brush molecules.

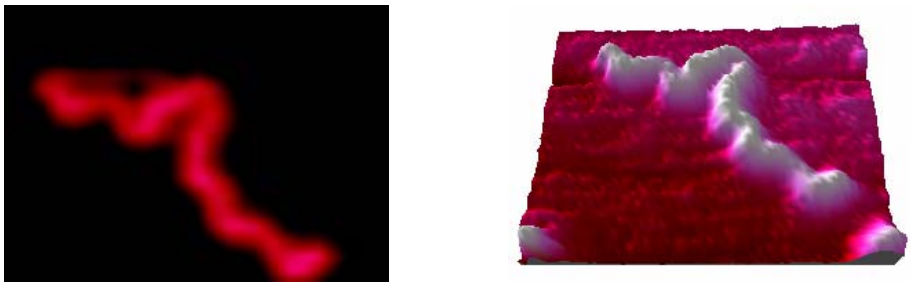

Figure 5-1 An AFM topography image of a single PVP brush molecule and its corresponding 3 dimensional image.

We can observe the sudden increase in coverage of the mica surface after 2 min of addition at exactly the same area of scan. An almost twofold increase of coverage can be observed and was calculated to 58 %. And after 30 min. we observe more or less complete film formation with a surface coverage of 69 % as shown in **Figure 5-2c**.

5-2 a)

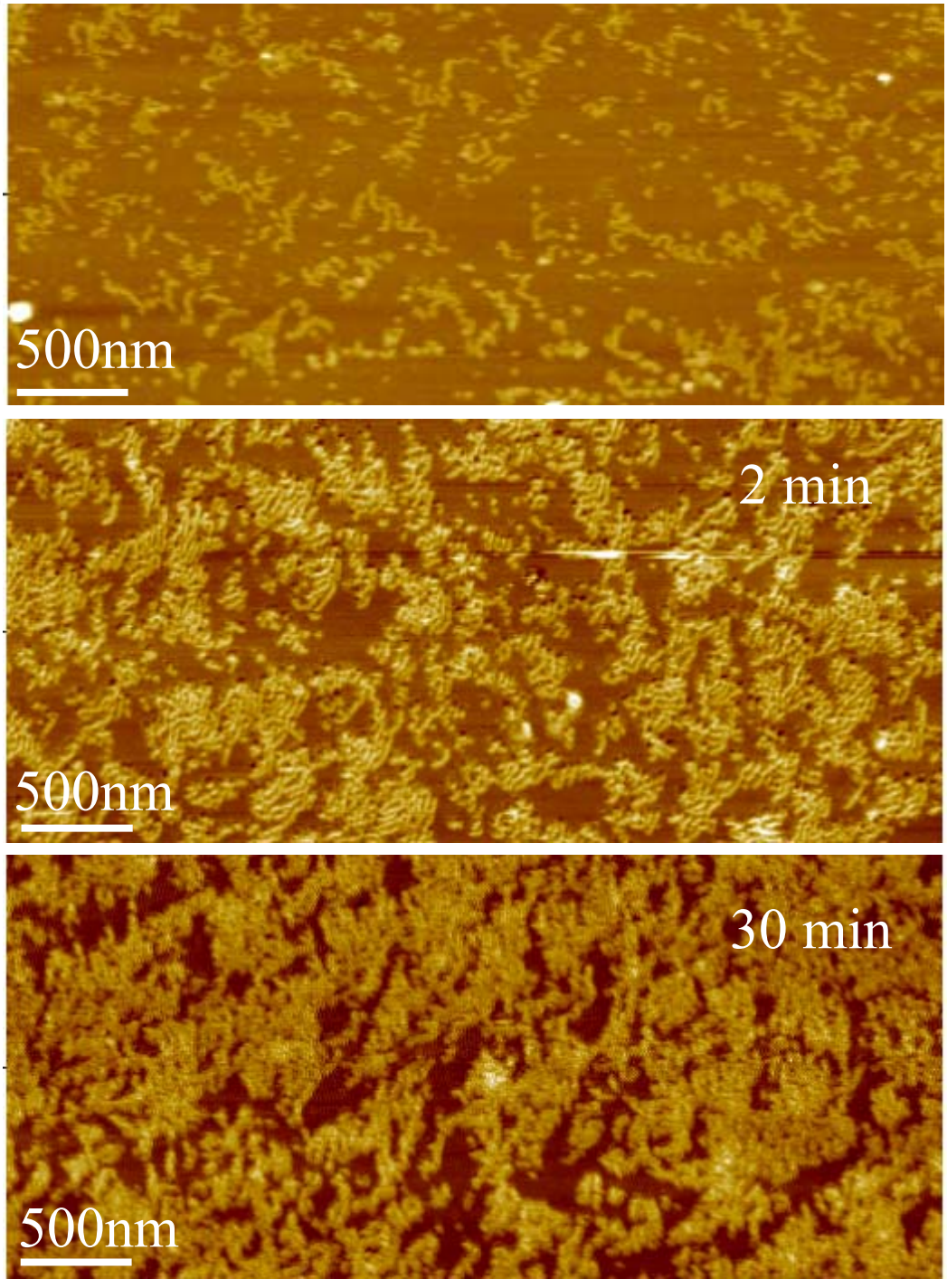

b)

c)

Figure 5-2 In-situ adsorption of cylindrical PVP brush molecules in presence of 0.1 M NaCl salt solution. a) no NaCl added. b) 2 min. after addition of NaCl. c) 30 min. after addition.

5.3 Micelles Formed by Cylindrical Brush-Coil Block Polymers

Recently amphiphilic cylindrical brush-coil block copolymers consisting of a polystyrene coil and a cylindrical brush block with poly (acrylic acid) side chains were synthesized using the "grafting from" technique as shown in **Scheme 5-2** by Khelfallah et. al.[10] Light scattering results in 10^{-3} M CsBr revealed an increase in molar mass and radius of gyration as compared to single blockcopolymer chains because of the expected formation of micellar aggregates. It was speculated that these polymers form micelles consisting of 4-5 block copolymers on average. To confirm the light scattering results AFM measurements were carried out in air and in aqueous solution.

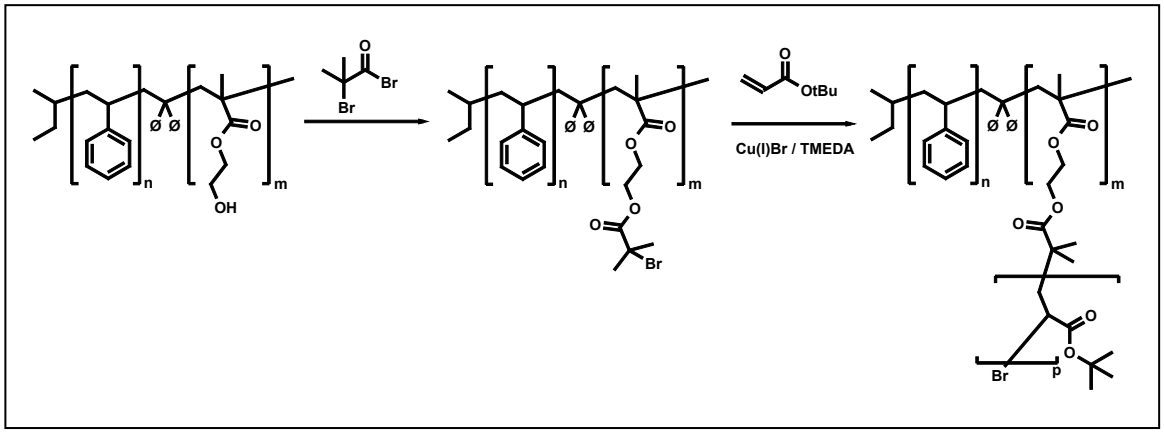

Scheme 5-2 Synthesis of the coil-cylindrical brush block copolymer.

The schematics of the cylindrical brush-coil copolymer, which forms micelles is shown in **Figure 5-3** along with the 3 dimensional AFM image depicting a single micelle consisting of 7 block copolymers. Polystyrene coil is shown in red and the negatively charged poly (acrylic acid) side chains are shown in blue.

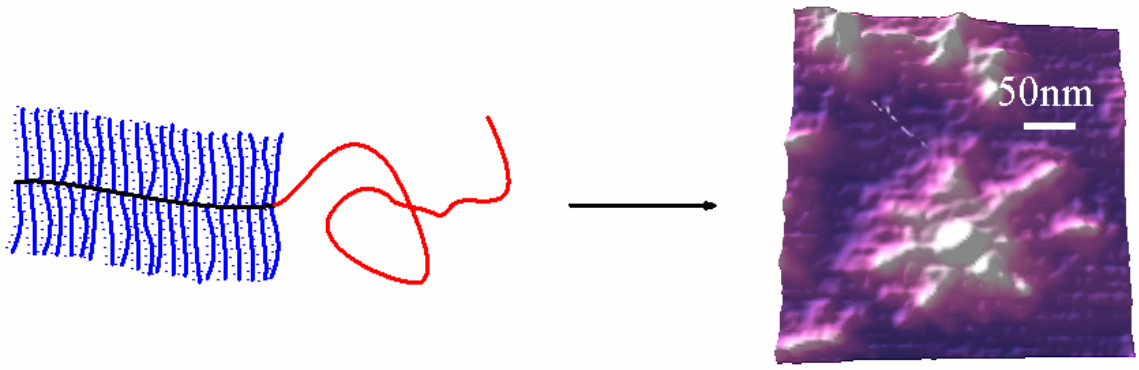

Figure 5-3 Schematics of the cylindrical brush-coil copolymer and the 3 dimensional image showing a single micelle consisting of 7 block copolymer chains.

The samples for imaging in air were prepared by spin casting a dilute aqueous solution on freshly cleaved mica surface or by the dip coating procedure. **Figure 5-4a** and **b** show the AFM topography and phase image of a spin-coated sample. It can be seen that the coverage of the mica is not homogeneous due to the spin-casting process. Interestingly single block copolymers coexist with micelles. The PS core in the micelles is clearly discernable in the 3 dimensional image above and in the AFM image below, whereas the PS block of the single block copolymers is not observed. We speculate that the PS blocks are "hidden" beneath the PAA-brush block. This very much explains the presence of the single block copolymer molecules well above the critical micellar concentration (CMC), because the PS block is not available for association and hence cannot induce micelle formation. The AFM phase image in **figure 5-4b** shows a strong phase contrast. The PAA side chain corona, the main chain and the PS block are clearly distinguished.

The PS-PAA brushes were also imaged under aqueous solution without pre-adsorbing the molecules. **Figure 5-5a** shows the AFM topography image in aqueous solution. Only globules could be visualized. The average height of the globules is 7 ± 2 nm. **Figure 5-5b** shows the height profile of an individual globule. However when the PS-PAA brush molecules were imaged in the presence of 1mM CsBr solution a similar AFM image was obtained as acquired in the dry state i.e. single block copolymer

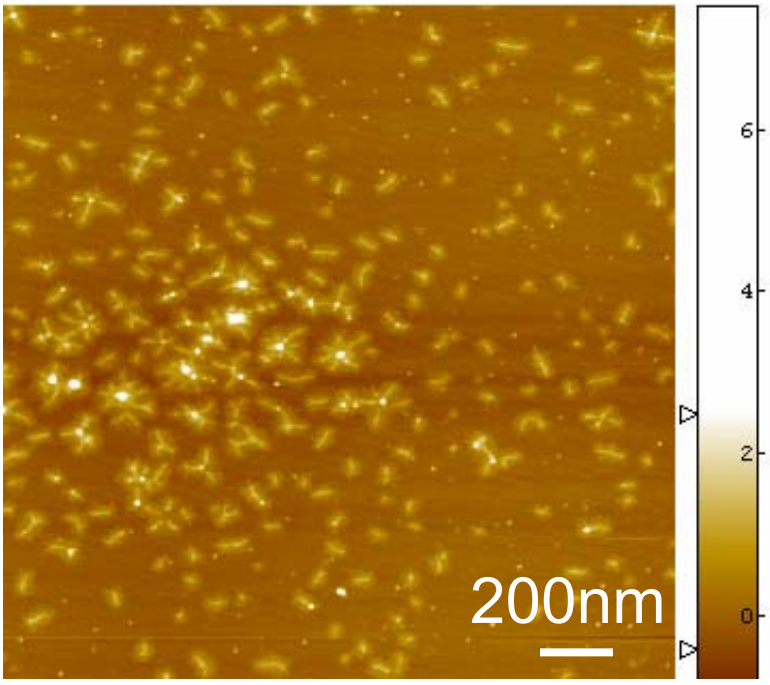

Figure 5-4a AFM topographic image of PS-PAA cylindrical brush-coil sample spin cast from an aqueous solution.

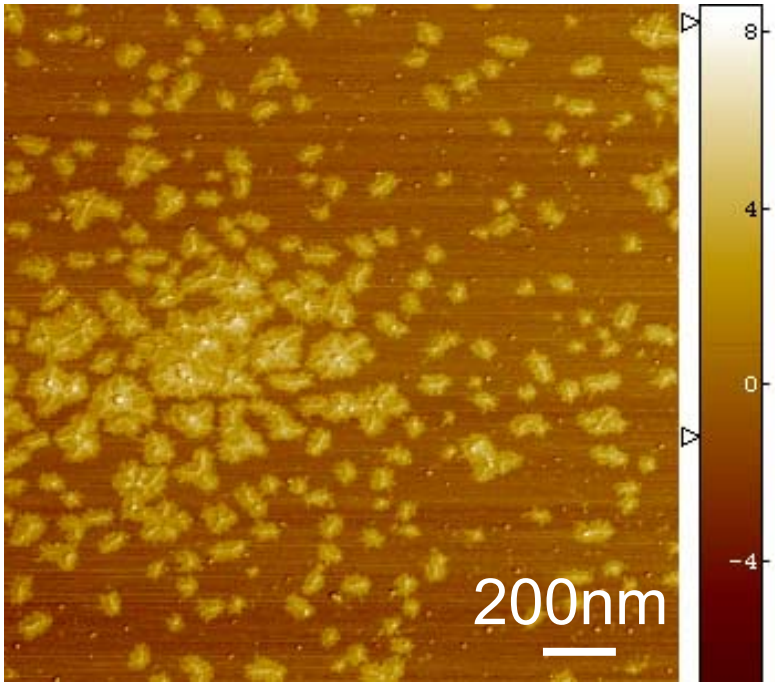

Figure 5-4b AFM phase image of PS-PAA cylindrical brush-coil sample spin cast from an aqueous solution.

a)

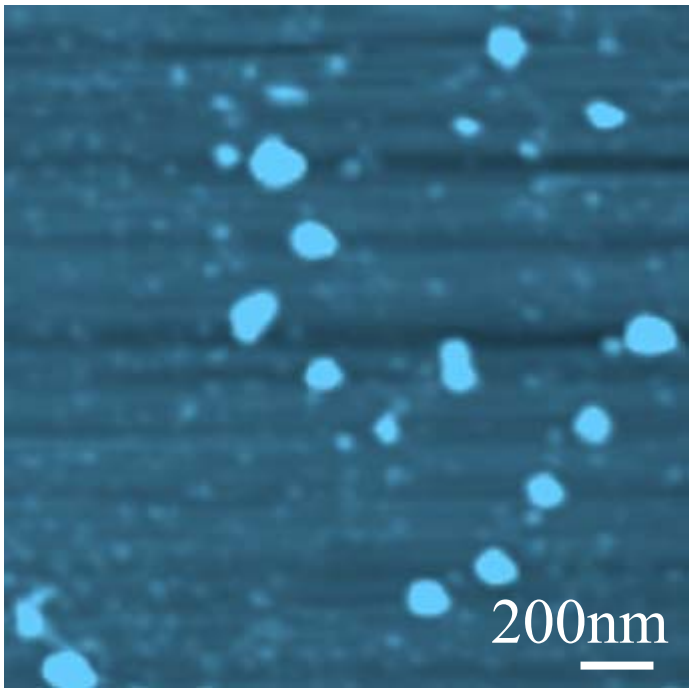

b)

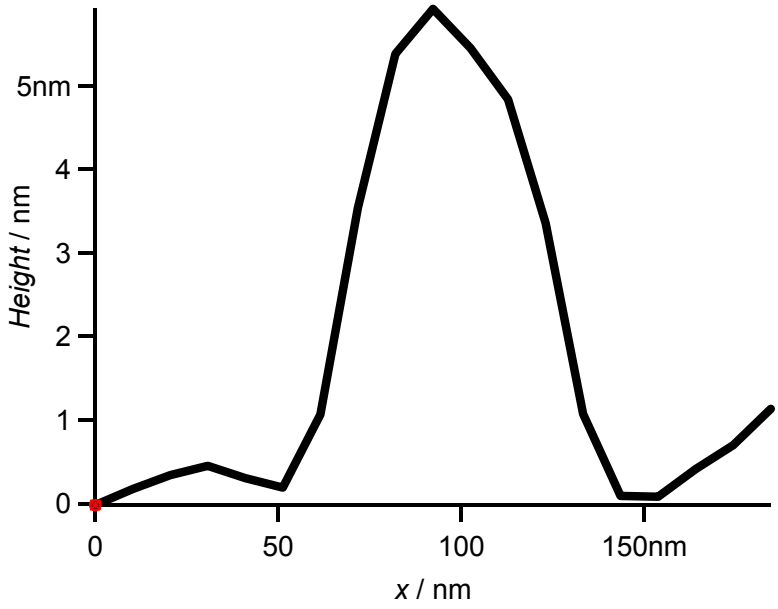

Figure 5-5 a) AFM topographic image of PS-PAA cylindrical brush-coil sample measured in aqueous solution b) Height profile.

molecules coexist with the micelles. **Figure 5-6** shows an AFM topography image in the presence of 1mM salt solution.

5-6)

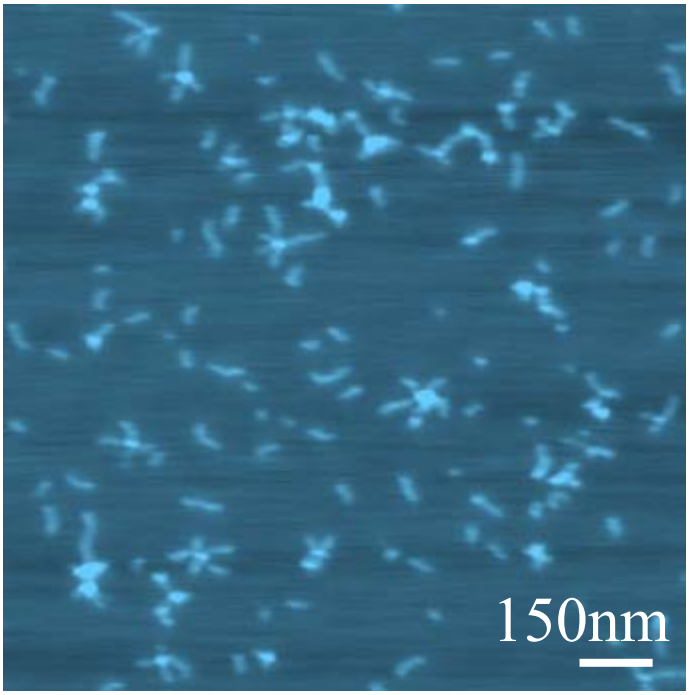

Figure 5-6 AFM topography image of PS-PAA cylindrical brush-coil sample measured in aqueous CsBr solution (1mM).

5.4 Thermally Responsive Cylindrical Brush Polymers.

Recently it has been shown that polymethacrylates with densely grafted poly-*N*-isopropylacrylamide (PNIPAM) side chains change their shape at the lower critical solution temperature (LCST) from cylindrical brushes to spherical structures. Synthesis of PNIPAM cylindrical brushes has been reported using atom transfer radical polymerization (ATRP) as shown in Scheme 5-3. PNIPAM is known to exhibit a LCST of around 33 ^{0}C. Above LCST water behaves as a poor solvent for PNIPAM[11] and the side chains collapse onto the main chain compelling the main chain to also collapse. The *in-situ* conformational transition from a cylinder to a sphere was observed by light

scattering experiments as reported by Li et. al.[12] A rough estimate of the molar mass of the side chains is M_w = 13 000 g /mol.

The motivation was to image the cylindrical brush molecules below and above the LCST and observe the conformational changes as a function of temperature and to carry out a detailed conformational analysis.

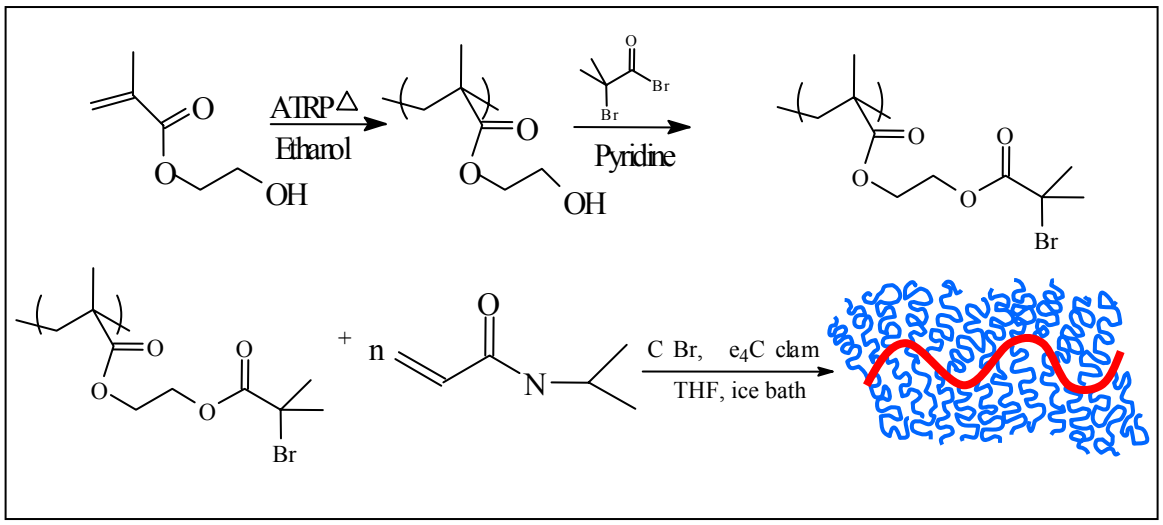

Scheme 5-3 Synthesis of poly-(N-isopropylacrylamide) cylindrical brush molecules.

5.4.1 AFM characterization of thermally responsive cylindrical brush molecules.

AFM imaging of the PNIPAM cylindrical brush polymers was carried out in air and under aqueous solution. **Figure 5-7a** shows the AFM topographic image of the PNIPAM cylindrical brushes in the dry state, obtained by spin casting a dilute aqueous solution (c = 0.1 g / l) on a freshly cleaved mica at 20 ^{0}C. The wormlike nature of the cylindrical brush molecules is clearly observed. The contour lengths of the brush molecules were determined by using a software to analyze the AFM images.[13] **Figure 5-7b** shows the histogram of the contour lengths yielding a weight average and number average contour lengths, L_w = 110 nm, L_n = 89.4 nm and a polydispersity, L_w/L_n = 1.23. The analysis was carried out for (n = 152) molecules.

AFM imaging was employed in aqueous solution to look into the conformation of the PNIPAM brush molecules without pre-adsorbing the molecules. **Figure 5-8a** shows the AFM topographic image of the PNIPAM cylindrical brushes in the solution at 20 ^{0}C. The brushes have an average height of 0.8 nm. A systematic contour length analysis was carried out in a similar way as for the molecules in the dry state. **Figure 5-8b** shows the histogram of the contour lengths yielding a weight average and number average contour lengths of L_w = 109 nm, L_n = 89.3 nm and a polydispersity, L_w/L_n = 1.22 (n = 152). This suggests that the conformation of the cylindrical brush polymer does not significantly change during the drying process. The cylinder length per monomer, *l*, is calculated to l = 0.25 L_w^{AFM} / L_w^{LS} = 0.14 nm. The small value of *l* suggests that the main chain could be locally coiled on the surface. It has generally been observed that the contour lengths obtained from AFM imaging are way less than that obtained from light scattering. One reason could be that when the molecule adsorbs onto the surface it might take up a conformation different from that in free solution with the backbone slightly locally coiled as depicted in the exaggerated scheme in **Figure 5-9**. These bends may not be observed by AFM imaging and might be the reason for the lower contour length values.

5-7 a)

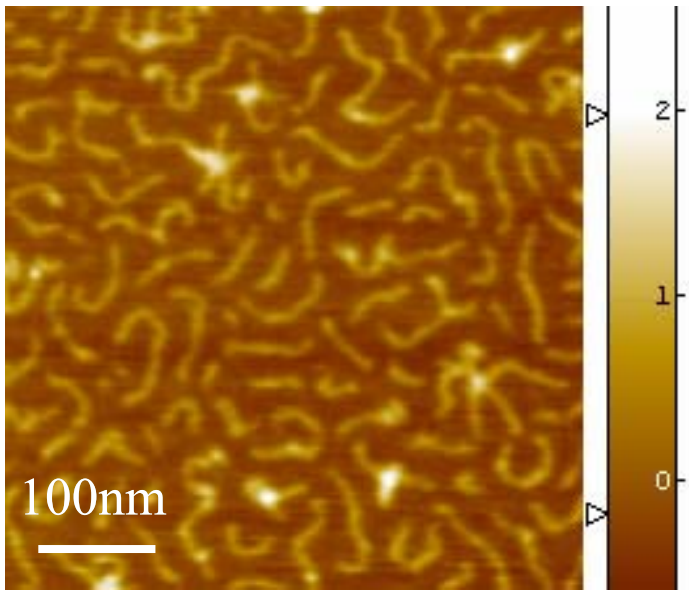

b)

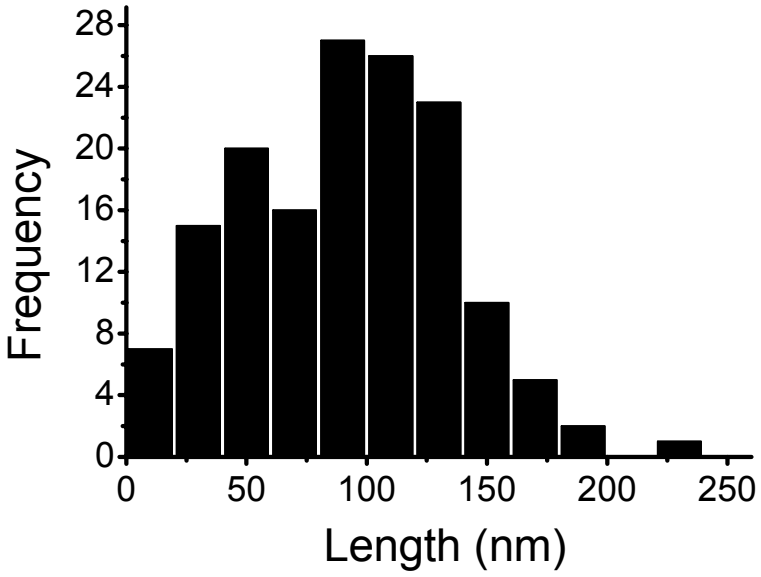

Figure 5-7 a) Topographic AFM image of the cylindrical PNIPAM brush molecules spin cast at 20 ^{0}C from aqueous solution. b) Histogram of the contour length yielding Lw = 110 nm, L_w/L_n = 1.23.

5-8 a)

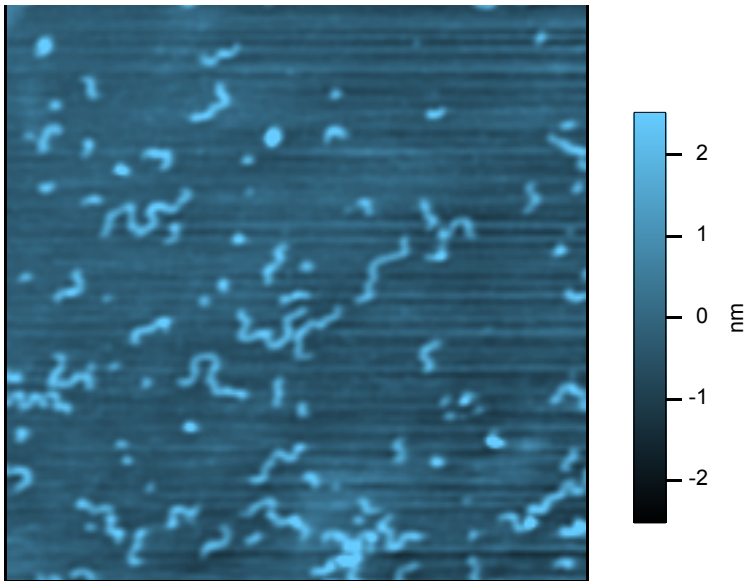

b)

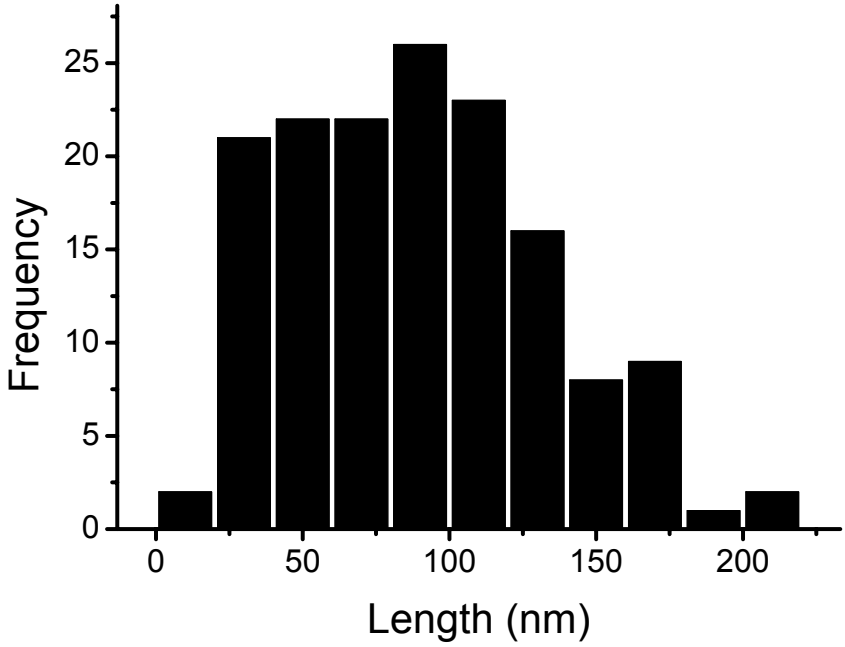

Figure 5-8 a) Topographic AFM image of the cylindrical PNIPAM brush molecules in aqueous solution at 20 ^{0}C without pre-adsorbing. b) Histogram of the contour length yielding L_w = 109 nm, L_w/L_n = 1.22.

5-9)

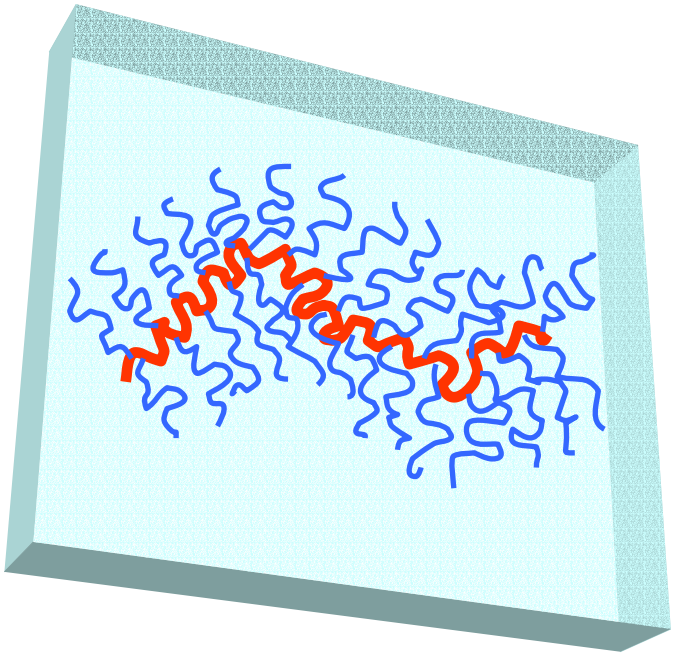

Figure 5-9 Schematics of a locally coiled backbone on the substrate.

Figure 5-10 shows the phase image of the PNIPAM cylindrical brush molecules spin cast from a dilute acetone solution (c = 0.1 g / l). The side chain corona is clearly resolved and we anticipate that this picture best resembles the situation of the swollen PNIPAM side chains in solution. The maximum extension of the side chains is estimated to be 20 nm from the image.

5-10)

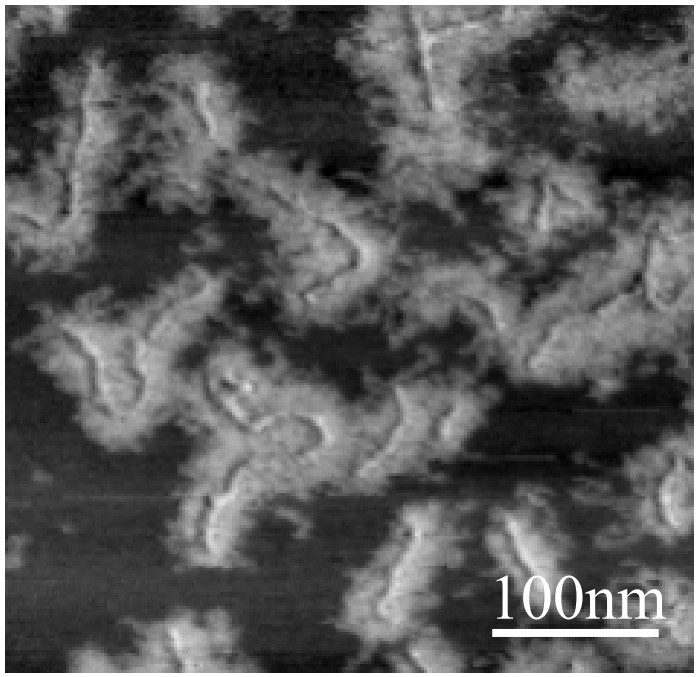

Figure 5-10 AFM phase image of the PNIPAM cylindrical brushes spin cast from a dilute acetone solution at 20 ^{0}C.

Since for the PNIPAM cylindrical brushes the solvent quality of water decreases with temperature the cylinder length was also investigated for samples spin cast from aqueous solution at 30 ^{0}C, carried out in a homemade temperature controlled spin caster. **Figure 5-11a** shows an AFM image of the cylindrical brush molecules at 30 ^{0}C. Interestingly, a significantly smaller contour length, L_w = 94 nm (Only individual molecules that could be distinguished were used for contour length analysis) was observed by performing a similar contour length analysis, which might be explained by the reduced repulsive forces between the side chains. This would suggest that the side chains should be partly collapsed which can be confirmed from the height analysis. The

brushes have an average height of 1.2 nm. **Figure 5-11b** shows the height profile of a single brush molecule.

When the known LCST of the PNIPAM side chains is reached, the transition from a cylindrical brush polymer to a collapsed structure takes place. **Figure 5-12** shows an AFM image of the cylindrical brush molecules at 33 ^{0}C. The collapsed main and side chains are clearly discernable in this picture, the white bright spot being that of the main chain which is compelled to be in a collapsed conformation, while the pale yellow corona is that of the collapsed side chains.

5-11 a)

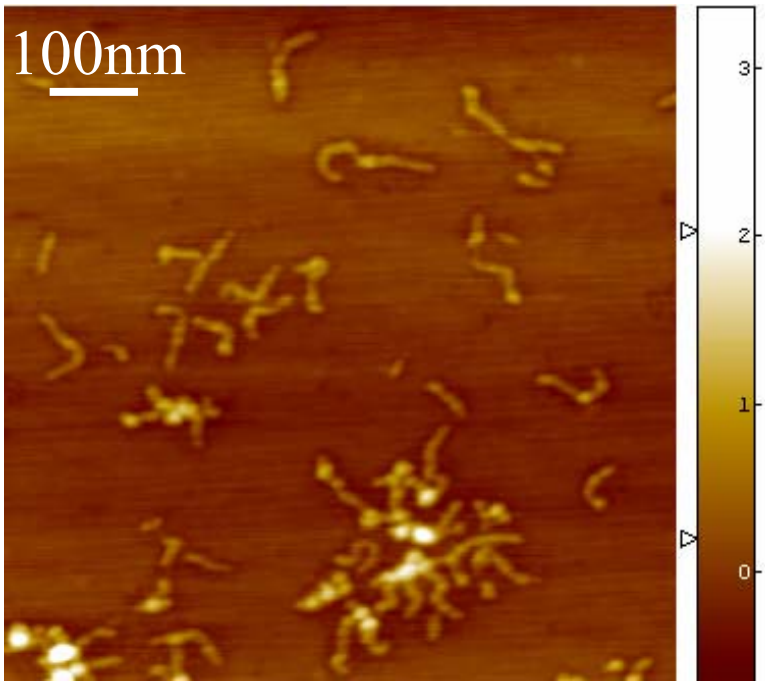

b)

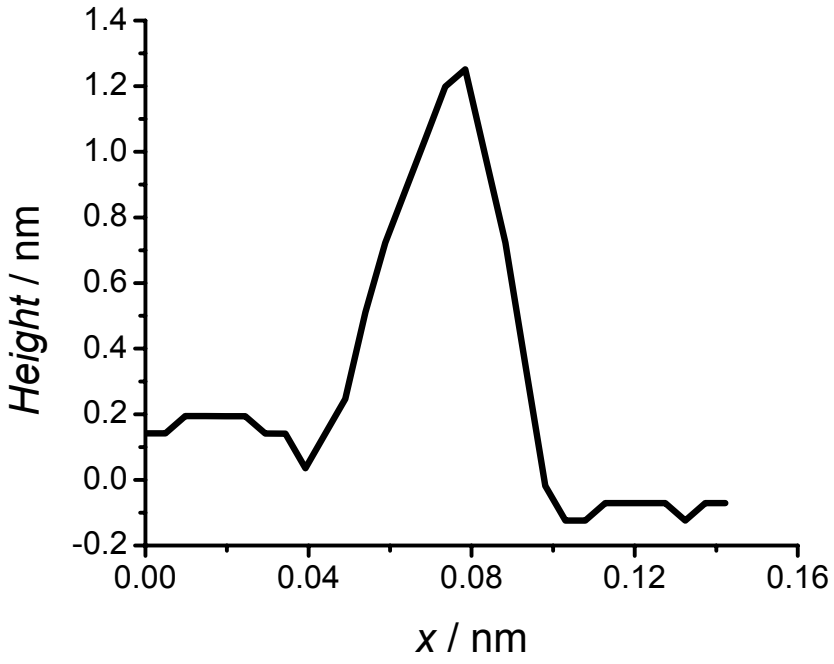

Figure 5-11 a) AFM topography image of PNIPAM cylindrical brush molecules spin cast from dilute aqueous solution at 30 ^{0}C. b) Height profile.

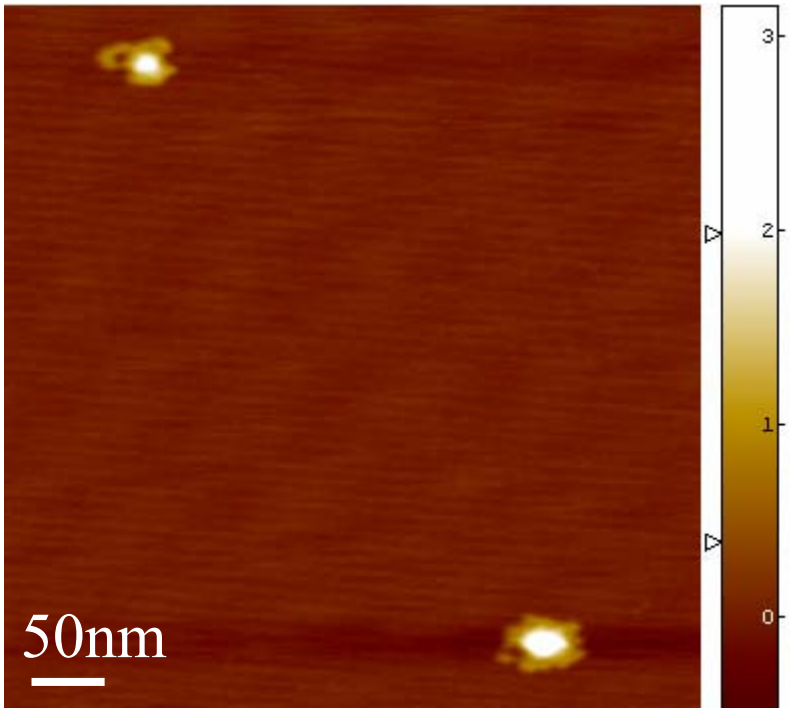

Figure 5-12 a) AFM topography image of PNIPAM cylindrical brush molecules spin cast from dilute aqueous solution at 33 ^{0}C.

The solution remains stable up to 38 ^{0}C above which aggregation and finally precipitation takes place. The PNIPAM brush molecules were imaged at 38 ^{0}C in air and under aqueous solution. **Figure 5-13 a** shows an AFM image in air, of the brush molecules spin cast at 38 ^{0}C and **Figure 5-13 b** shows the under water AFM image taken in a temperature controlled fluid cell. The average diameter and height of the molecules were determined from the images to be 50 ± 6 nm and 3 ± 0.5 nm respectively. **Figure 5-14** shows a height profile of a single collapsed globule under aqueous solution.

5-13 a)

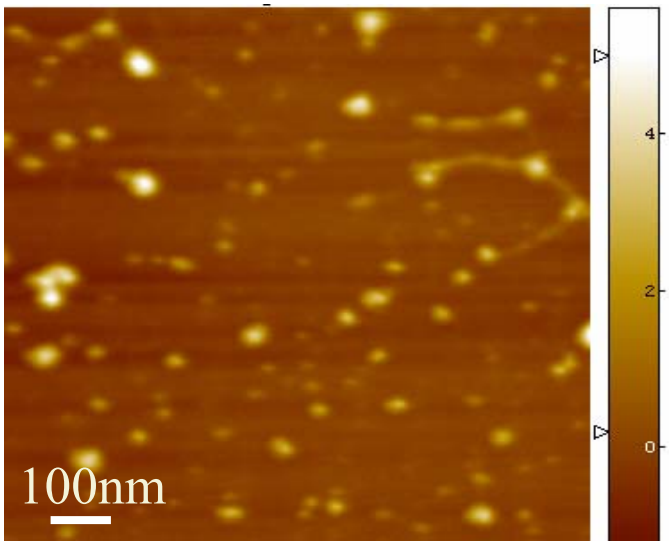

b)

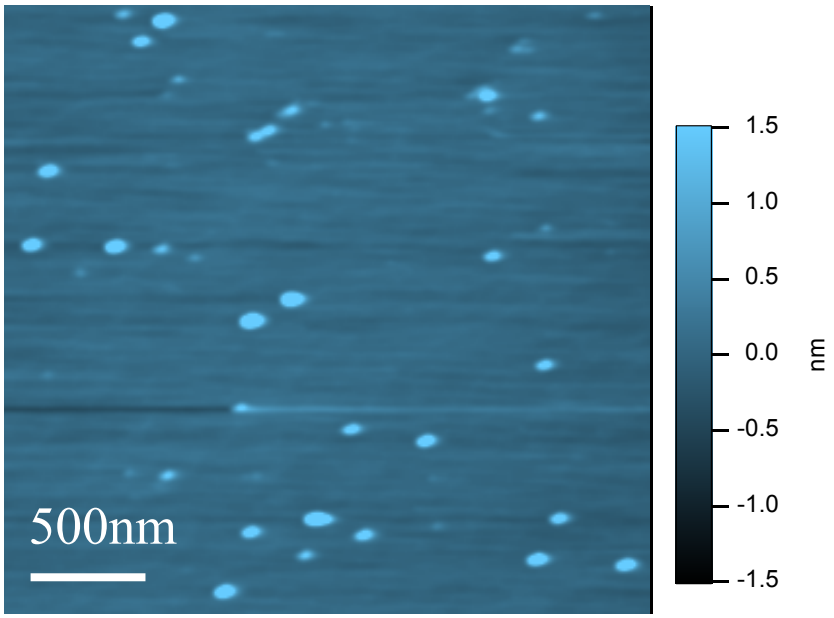

Figure 5-13 a) AFM topography image of PNIPAM cylindrical brush molecules spin cast from dilute aqueous solution at 38 ^{0}C. b) Topography AFM image of the brushes at 38 ^{0}C without pre-adsorbing.

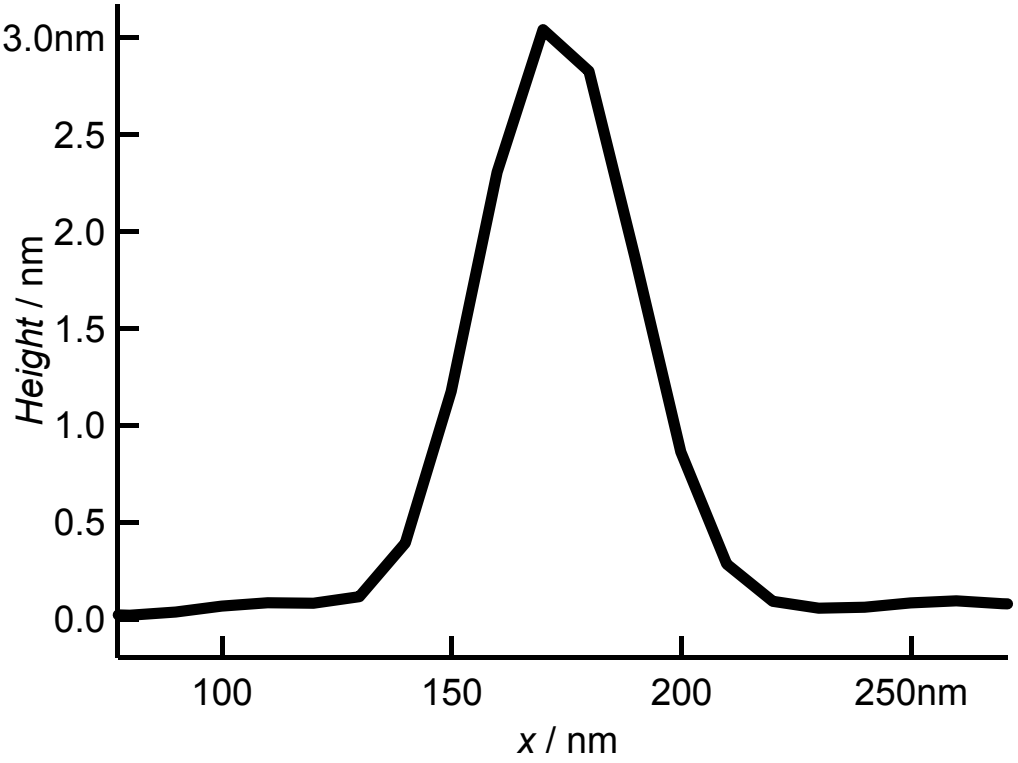

Figure 5-14 Height profile of a collapsed PNIPAM brush molecule under aqueous solution.

It was observed that when the PNIPAM brush molecules were adsorbed on the mica surface at 20 ^{0}C and the temperature was increased in order to observe *in-situ* conformational change from a cylinder to a sphere, no conformational change occurred. This can be attributed to the strong adsorption of the molecules on the mica surface. So in order to observe the conformational change on the surface, several surfaces were used like gold (111) surface, gypsum and graphite. But no conformational change was observed on either of the surfaces. The molecules either didn't adsorb at all, or once adsorbed, change in temperature did not cause a conformational change.

Evidently, surface modification is necessary to reduce the interaction energy between the brush molecules and the surface in order to allow for conformational switching on the surface. For this purpose the mica surface was modified with a mixture of silanes viz. aminopropyltriethoxy silane (APTES) and n-propyltriethoxy silane (n-PTES). A series of mixtures of APTES: n-PTES was prepared, with varying percentage of amino silane. The best results were obtained for 5% amino silane. Then the mixture of silane was vapor deposited onto the mica. In short, three 20 μl droplets of the mixture of silanes were placed on the inner side of a Petri dish. The freshly cleaved mica surface was placed in the Petri dish and then sealed. 18 hours of deposition time was allowed. Once the surface was modified the experiments were immediately carried out, as the modified surfaces were not stable over a long period of time.

Figure 5-15a shows the AFM topography image of the cylindrical PNIPAM brushes adsorbed on a silane-modified surface at 20 ^{0}C. Individual brush molecules are resolved. The height of the modified surface is ~ 0.3 nm. The temperature was increased to 38 ^{0}C and imaged at exactly the position. The whole experiment was performed in air under a humid environment. **Figure 5-15b** shows the AFM topographic at 38 ^{0}C. The white square indicates exactly the same position. After increase in temperature from 20 ^{0}C to 38 ^{0}C a thermal drift of ~ 200 nm was observed. The image clearly shows the conformational change from a cylinder to a globule. The aggregates formed are due to the mobility of the molecules on the surface. Unfortunately, the reverse transition, i.e. globule to cylinder on decrease in temperature below the LCST, was not observed. Hence the conditions have to be refined to realize the reversible transition on the surface. This project will be continued in the future.

5.4.2 Cylinder-globule-cylinder reentrant transition observed by AFM.

The phase behavior of PNIPAM in solutions composed of water and methanol has been studied extensively. It has been shown that, water and methanol, two good solvents for PNIPAM, at certain proportions of the mixture behave as a poor solvent. It was shown that as the volume percent of methanol in aqueous PNIPAM solution increases, the polymer chains collapse and with further increase of methanol content the chains were

swollen. This phenomenon is known as cononsolvency.[14-16] It was suggested that poor solvent condition occurs as a result of complexation of water and methanol.[17] Cononsolvency in linear PNIPAM chains have been observed in several organic solvent-water mixtures.[18]

Here the motivation was to observe the cononsolvency effect of PNIPAM side chains, using water and acetone as solvents, on the overall conformation of the cylindrical brush molecules.

As explained before, water and acetone are good solvents for the PNIPAM cylindrical brush molecules (**Figures 5-7a** and **5-10** show the AFM images spin cast from water and acetone respectively). A similar experiment was carried out using water-acetone mixtures. A dilute (c = 0.1 mg/ml) aqueous solution of PNIPAM cylindrical brush sample was prepared. Then acetone was added dropwise and AFM images were taken at regular intervals. We observed a similar reentrant behavior, i.e. at 0.2 volume % of acetone we observed that the cylindrical brush molecules were collapsed, so a cylinder to globule conformational change takes place. And as we increased the acetone content, at 0.3 volume % the cylindrical brush molecules reappear. Thus a reentrant cylinder-to-globule-to-cylinder transition takes place. **Figures 5-16 a-d** show the AFM topography images of the cylinder-to-globule-to-cylinder transition. We can observe in Figure 5-16 b, at 0.15 volume % of acetone there is a coexistence of extended cylindrical brush molecules and collapsed brush molecules. **Figure 5-16 c** shows the AFM image of single collapsed globules having an average diameter and height of 50 nm and 3 nm, respectively similar to the collapsed globules above the LCST. **Figure 5-16 d** shows the globule to cylinder transition. The cylinder conformation is preserved with further acetone content. But the *in-situ* conformational transition could not be observed due to strong adsorption of the molecules as discussed before.

5-15 a)

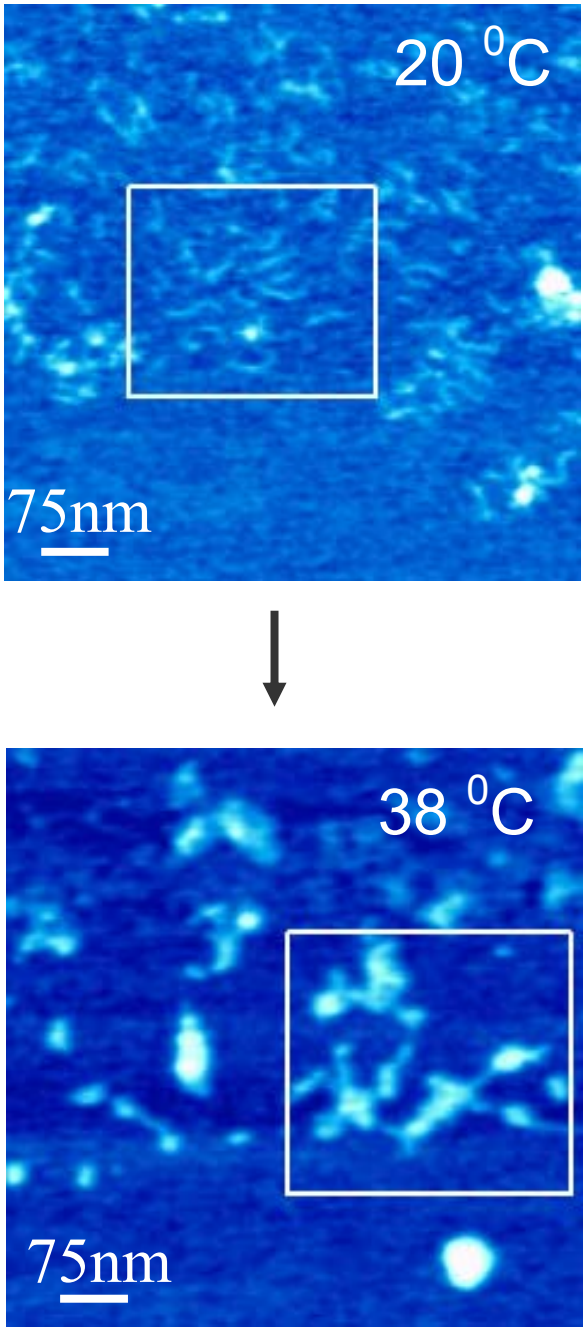

b)

Figure 5-15 a) AFM topography image of PNIPAM cylindrical brush molecules deposited on the modified mica surface at 20 ^{0}C. b) Topography AFM image of the brushes at 38 ^{0}C, at exactly the same area of scan.

a)

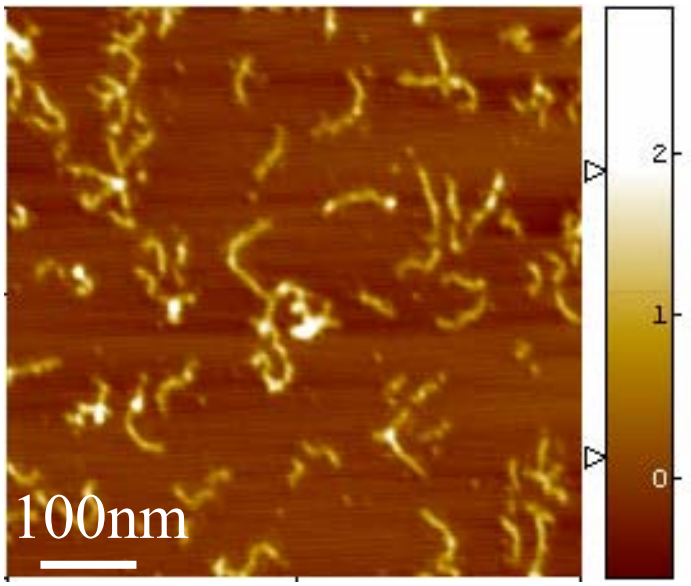

b)

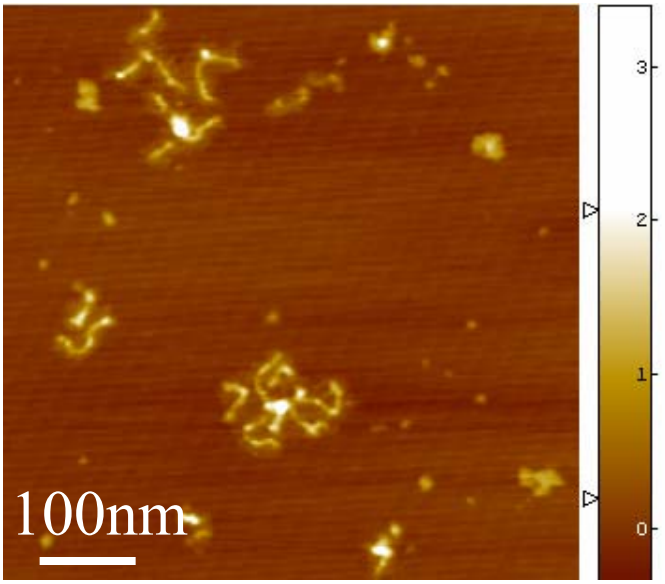

Figure 5-16 a) AFM topography image of PNIPAM cylindrical brush molecules spin cast from a dilute solution with acetone vol % = 0.1 b) AFM topography image of PNIPAM cylindrical brush molecules spin cast from a dilute solution with acetone vol % = 0.15

a)

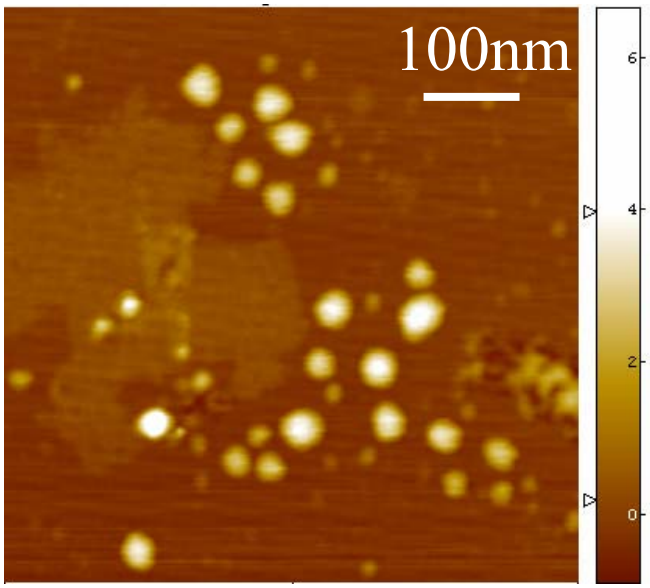

b)

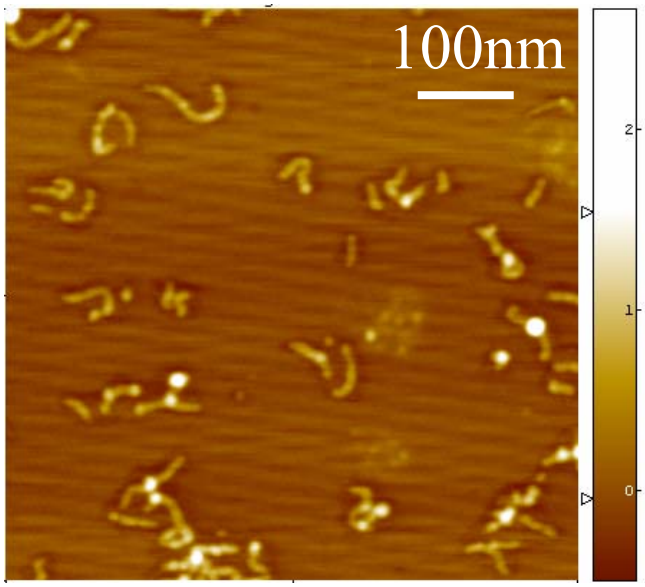

Figure 5-16 c) AFM topography image of PNIPAM cylindrical brush molecules spin cast from a dilute solution with acetone vol % = 0.2 d) AFM topography image of PNIPAM cylindrical brush molecules spin cast from a dilute solution with acetone vol % = 0.3

5.5 Conclusions

We have shown that AFM imaging is a powerful tool to characterize the molecular conformations of cylindrical brush molecules in various environmental conditions. Micelle formation of cylindrical brush-coil (PS-PAA) molecules was observed in air and under solution. Also, thermally responsive PNIPAM cylindrical brush molecules were characterized by AFM as a function of temperature. Finally reentrant cylinder-globul-cylinder conformational transitions due to cononsolvency effect of PNIPAM side chains were studied using AFM imaging.

5.6 References

(1) Binnig, G.; Rohrer, H.; Gerber, C.; Weibel, E. *Phys. Rev. Lett.* 1982, *49*, 57.

(2) Binnig, G.; Quate, C. F.; Gerber, C. *Phys. Rev. Lett.* 1986, *56*, 930.

(3) Hansma, P. K.; al., e. *Appl. Phys. Lett.* 1994, *71*, 2394.

(4) Rippe, K.; Mucke, N.; Langhton, C. A. *Nucleic Acids Res.* 1997, *25*, 1736.

(5) Arakawa, H.; Umemura, K.; Ikai, A. *Nature* 1992, *358*, 171.

(6) Marti, O.; Elings, V.; Huaugan, M.; Bracker, C. E.; Schneir, J.; Drake, B.; Gould, S. A.; Gurley, J.; Hellemans, L.; Shaw, K. *J. Microsc.* 1988, *1521*, 803.

(7) Kumaki, J.; Nishhikawa, Y.; Hashimoto, T. *J. Am. Chem. Soc.* 1996, *118*, 3321.

(8) Dziezok, P.; Sheiko, S. S.; Fischer, K.; Schmidt, M.; Möller, M. *Angew. Chem. Int. Ed.* 1997, *36*, 2812.

(9) Schmidt, U.; Prokhorova, S.; Sheiko, S. S.; Möller, M.; Dziezok, P.; Schmidt, M. *Molecular Imaging (Application Notes)*.

(10) Khelfallah, N.; Gunari, N.; Fischer, K.; Gkogkas, G.; Hadjichristidis, N.; Schmidt, M. *Macromol. Rapid Commun.* 2005, *26*, 1693.

(11) Schild, H. G. *Prog. Polym. Sci.* 1992, *17*, 163 and references therein.

(12) Li, C.; Gunari, N.; Fischer, K.; Janshoff, A.; Schmidt, M. *Angew. Chem. Int. Ed.* 2004, *43*, 1101.

(13) provided by Sheiko S. S. Univ. of North Carolina, U.

(14) Winnik, F. M.; Ringsdorf, H.; Venzmer, J. *Macromolecules* 1990, *23*, 2415.

(15) Winnik, F. M.; Ottaviani, M. F.; Bossmann, S. H.; Garcia-Garibay, M.; Turro, N. J. *Macromolecules* 1992, *25*, 6007.

(16) Schild, H. G.; Muthukumar, M.; Tirrell, D. *Macromolecules* 1991, *24*, 948.

(17) Zhang, G.; Wu, C. *Phys. Rev. Lett.* 2001, *86*, 822.

(18) Shimizu, S.; Seyama, T.; Sekine, R.; Kurita, K. *J. Appl. Cryst.* 2003, *36*, 694.

6 PERSISTENCE LENGTH OF CYLINDRICAL BRUSH MOLECULES MEASURED BY ATOMIC FORCE MICROSCOPY

6.1 Introduction

Manipulation of single molecules by optical tweezers and atomic force microscopy has provided invaluable insight into the elasticity of various macromolecules ranging from nucleic acids,[1,2] polysaccharides,[3] proteins[4,5] and synthetic polymers[6] to end grafted polymers.[7] Extension of single macromolecules attached to an AFM tip allows forces to be measured from 10 pN up to several tens of nanonewtons, sufficient to break covalent bonds,[8] while optical tweezers cover the lower force range from 100 fN to 10 pN rendering both techniques complementary.

Among the different molecules of interest, semiflexible chains are of pivotal importance due to their prevalence in nature. The mechanical properties of molecules such as actin, DNA, and microtubules have attracted extraordinary attention by both experimentalists and theorists strongly based on their function in a living cell associated with mechanical demands.[9,10]

The mechanical behavior of individual semiflexible chains, which are characterized by a persistence length of the same order of magnitude as the contour length, is captured by the wormlike chain (WLC) model.[11,12] The WLC model describes the statistical mechanics of linearly elastic rods, in which the bending energy is quadratic in curvature and where the elastic energy is microscopically a combination of energetic and entropic contributions.

The relevant physical parameter of the WLC model is the persistence length l_p giving an estimate of the length scale over which the tangent vectors along the contour of the chain backbone correlate. Double stranded DNA, for instance, exhibits a persistence length of approximately 50 nm.[13] While excluded volume effects can safely be ignored if molecules under tension are considered,[14] it is, however, necessary to account for

enthalpic stretching in the high force regime as first suggested by Odijk[15] assuming a cylindrical rod of homogeneous elasticity.

Linear flexible chains with densely grafted linear or dendritically branched side chains exhibit the shape of cylindrical brushes provided that the main chain is much longer than the side chain.[16-21] The properties of the side chains e.g. chemical structure, dimensions, stiffness, and mutual interaction are proven to be determining factors for the conformational behavior of the molecule.[16] This opens an opportunity to control the properties of the molecule of interest by synthesizing cylindrical brushes with predefined side chain characteristics, i.e. to adjust these characteristics by external stimuli, such as the solvent quality, pH, or temperature, and responsive materials may be synthesized, accordingly.[17]

The interest in cylindrical brushes is due to conformational effects caused by competition of the entropic restoring force of the extended backbone and the repulsive, steric interaction forces between the side chains. So far, much theoretical attention has been focused on the study of cylindrical brushes in solution, particularly on the conformational properties in terms of main and side chain bond angle correlation functions and on the formation of liquid crystalline phases characterized by l_k/d the ratio of the Kuhn length ($l_k = 2l_p$) to the cross-sectional dimension d of the cylindrical brush polymers. Many experimental studies on various cylindrical brush polymers in solution exist with partly contradictory results concerning the cylinder length per main chain monomer, l, the Kuhn length l_k and the cross-sectional dimension d.[22-25]

It is therefore of interest to improve the understanding of the mechanical properties of cylindrical brush molecules as a function of side chain structure and length as well as solvent quality on a single molecule level. Here we present for the first time force extension experiments using PNIPAM bottle brush molecules investigating the entropic and enthalpic restoring forces.

6.2 Experimental

Synthesis of cylindrical poly-N-isopropylacrylamide brushes by atom transfer radical polymerization using poly-2-bromo-isobutyryl-oxyethyl-methacrylate is described

elsewhere.[17] The characterization data relevant for the macro initiator and the polymer brushes as well as a scheme illustrating the synthesis of the brush are compiled in the supporting information. For AFM imaging of the PNIPAM brush molecules in air a dilute aqueous solution was spin cast on freshly cleaved mica (c = 0.1mg/mL). The molecular architecture of the adsorbed polymer was studied under ambient conditions (air) with a Multimode AFM (Nanoscope IIIa controller, Veeco, Santa Barbara, CA, USA) operating with amplitude feedback in the intermittent contact mode. Silicon tips from Nanosensors™ (Neuchatel, Switzerland) with a mean radius of ~ 5 nm, an average spring constant of 42 N/m and a resonance frequency of 250-300 kHz were used.

For measurements in solution, a droplet of 50µl MilliQ water was placed on a freshly cleaved mica surface and mounted in a homemade AFM PTFE fluid cell. The polymer was dissolved in MilliQ water and then injected into the fluid cell to roughly achieve the same concentration as the spin casting solution used for in air measurements. Intermittent contact mode AFM images were obtained in water employing a MFP 3D microscope from Asylum Research, Santa Barbara, CA, USA. V-shaped silicon nitride cantilevers purchased from Olympus (PSA 400) with spring constants in the range of ~ 0.5 N/m were used for the measurement.

Force spectroscopy measurements were carried out by placing a droplet of 50 µl of the polymer solution (c = 0.1 mg/mL) on freshly cleaved mica and incubated for 1h. Subsequently the surface was rinsed with water to remove excess of unbound polymer molecules. Force distance curves were recorded at 20 ^{0}C using the MFP 3D microscope. V-shaped silicon nitride cantilevers purchased from Olympus (PSA 400) exhibiting a nominal spring constant of ~ 0.01 N/m were used for the pulling experiments. The exact spring constants were determined by thermal noise analysis prior to each experiment.[26]

6.3 Results and discussion

Figure 6-1a shows an AFM phase image of cylindrical PNIPAM brush molecules adsorbed on mica using intermittent contact mode in air. The molecules were spin cast at 20 °C from a dilute aqueous solution on a freshly cleaved mica surface. Both the backbone and the tightly adsorbed side chains can be distinguished. The weight average

contour length determined by AFM was calculated to L_w = 110 nm.[17] **Figure 6-1b** shows a height image of the cylindrical PNIPAM brushes deposited by adsorption from solution imaged in aqueous solution also using intermittent contact mode exhibiting an average height of 3 nm. **Figure 6-1c** displays a typical surface coverage, which has been used using for the pulling experiments. A relatively high coverage was chosen in order to increase the probability of observing stretching events.

6-1 a)

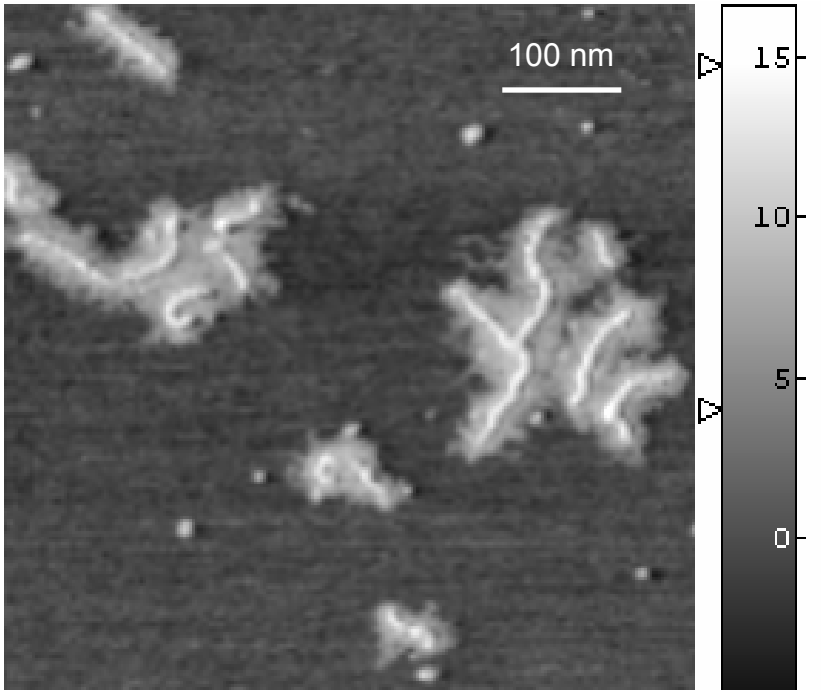

b)

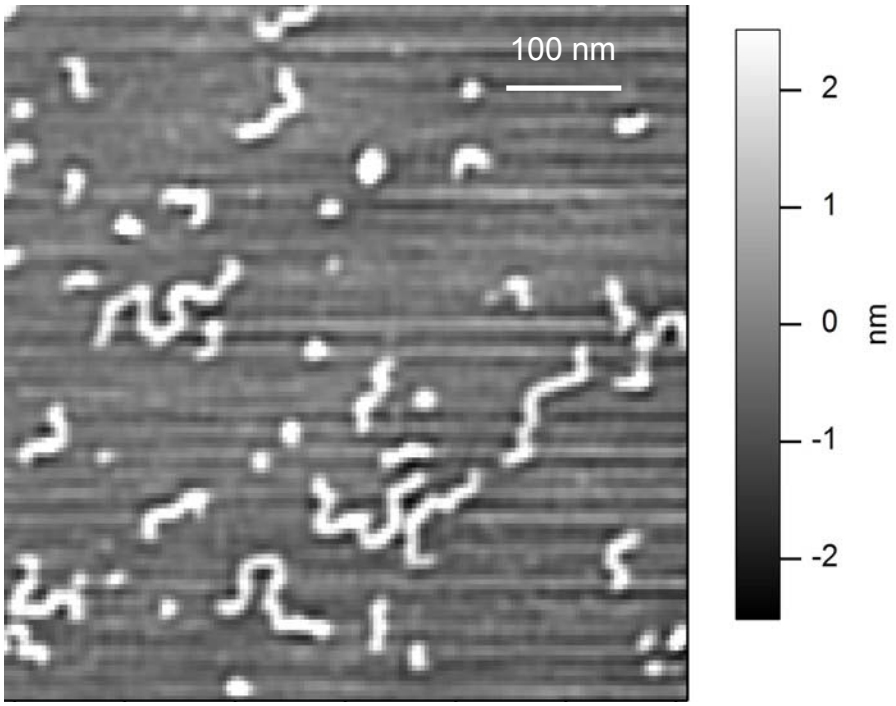

c)

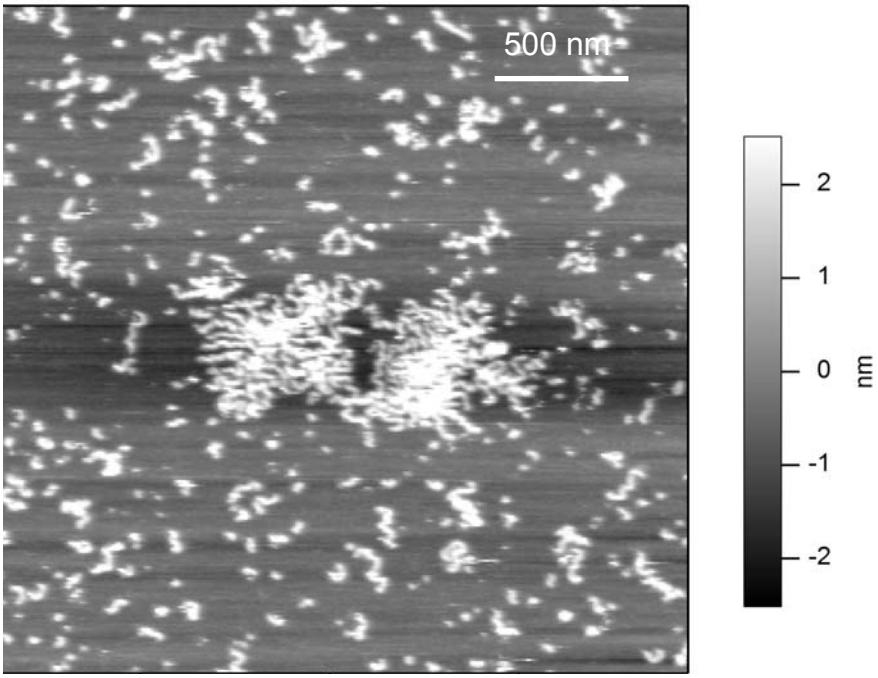

Figure 6-1: a) AFM phase image of the cylindrical PNIPAM brushes spin cast on mica at 20 °C from aqueous solution. b) Cylindrical PNIPAM brushes imaged by AFM in water also at 20 °C. c) AFM image of polymer brushes in water showing the typical surface coverage as used for the pulling experiments.

Experimentally, there are two complementary ways to evaluate the persistence length l_p of the molecules from the AFM images in the framework of the WLC model. One method makes use of the local curvature employing the fact that the bond correlation function gives the average cosine angle Θ between the tangents along the brush molecule separated by distance s:

$$\langle \cos(\Theta) \rangle = e^{-\frac{s}{l_p}} \qquad (1)$$

Equation (1) shows that the persistence length l_p is essentially the decay length through which the memory of the initial orientation of the molecule persists.[27]

The second method relies on the equation of Kratky-Porod, which relates the mean square end-to-end distance $\langle R^2 \rangle$, the contour length L and the persistence length l_p in two dimensions (equation (2)):[27]

$$\left\langle R^2 \right\rangle_{2D} = 4 l_p L \left(1 - \frac{2 l_p}{L} \left(1 - e^{-\frac{L}{2 l_p}} \right) \right) \tag{2}$$

A different formula results if the molecule on the surface is a projection from 3-D space onto the x-y plane:

$$\left\langle R^2 \right\rangle_{3D\text{-proj}} = \frac{4}{3} l_p L \left(1 - \frac{l_p}{L} \left(1 - e^{-\frac{L}{l_p}} \right) \right) \tag{3}$$

The wormlike nature of the polymer is clearly visible in the AFM images and the persistence length has been analyzed by means of equations (2) and (3). **Figure 6-2** shows a graph of end-to-end distance $\left\langle R^2 \right\rangle$ as a function of contour length as well as the corresponding fit of equation (2). The image size used for the analysis was $1 \times 1\ \mu m^2$ with 512×512 pixels. Bends in the range below 2 nm can thus not be resolved. The persistence length obtained from the fit was $l_p = (29 \pm 3)$ nm for equation (2) and $l_p = (100 \pm 7)$ nm for equation (3). A projection of the molecules from 3D to 2D might, however, be inadequate so close to the rod limit. In summary, determination of the persistence length using AFM images has a serious drawback related to the interaction of the molecules with the substrate. Bustamante and coworkers recently demonstrated that virtually any conformation of DNA on mica from outstretched to coiled can be obtained by changing the buffer conditions and thus modifying the interaction potential of the surface with the molecule.[28] Molecules might be kinetically trapped or in their equilibrium state. As a consequence, it is appropriate if not necessary to measure force extension curves of the molecule by employing single molecule force spectroscopy (SMFS) enabling one not only to determine the persistence of the molecule in a more direct manner but also to explore the mechanical properties of the cylindrical PNIPAM brushes in a force regime beyond the purely entropic restoring forces.

Figures 6-3a-d show the different classes of events typically observed in stretching adsorbed cylindrical PNIPAM brushes in aqueous solution. A total of n = 690 force curves are considered and only retraction curves are shown in the following graphs.

6-2)

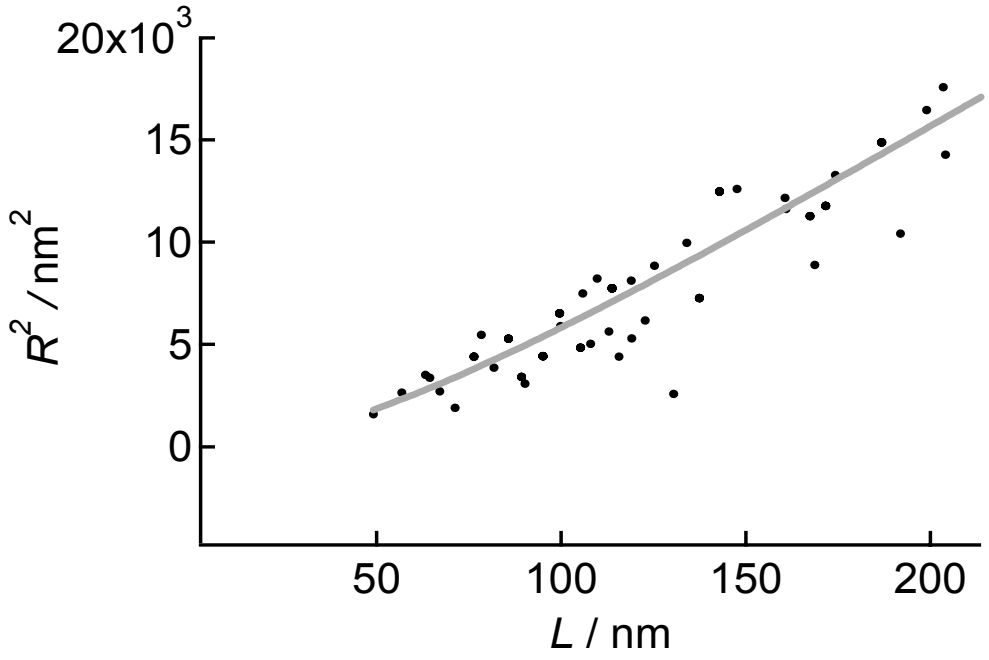

Figure 6-2: Mean-square end-to-end distance $\langle R^2 \rangle$ as a function of brush contour length *L*. The continuous grey line is the corresponding fit of equation (2) yielding a persistence length of l_p = (29 ± 3) nm.

Figure 6-3a shows a force extension curve in which no polymer bridge is formed between the tip and the substrate. The absence of stretching events is found in only 15% of all curves. Force-extension curves as displayed in **Figure 6-3b** were observed in 38% of the force spectroscopy experiments. The force curve is attributed to the stretching of an individual cylindrical PNIPAM brush molecule displaying a nonlinear extension with force. It is, however, also conceivable that the molecule is picked up in a way that two

strands of the same molecule are stretched simultaneously resulting in an increased persistence length (inset). At high enough extensions, the elastic restoring force of the chain exceeds the physisorption force tethering the molecule either to the tip or to the substrate and the molecule detaches. As shown in **Figure 6-3c**, a large number, as high as 30 %, of all force extension curves exhibits desorption events indicative either of the stretching and the subsequent detachment of two physisorbed molecules or might be interpreted as desorption of the molecule from two sites consecutively as illustrated in the inset. 14% of the force curves display multiple detachment events in which more than one or two molecules are involved (**Figure 6-3d**). Since the sample is polydisperse and we cannot control the point at which the polymer brush is picked up by the tip, the apparent contour length of the polymer, which is defined as the contour length L_{app} between tip and substrate, varies. The desorption force also varies due to its non-specific nature and can be as high as 600 pN.

Stiff chains under tension revealing weak undulations are best described by a semiclassical model first introduced by Odijk.[15] Kulic et al. recently presented a different approach employing an analogy with instantons in quantum mechanical tunneling problems to arrive at the same result.[29] For molecules longer than the deflection length $\lambda = \sqrt{k_b T l_p / F} \approx 2-6$ and forces larger than $F = k_b T / 4 l_p \approx 0.01\text{pN}$, the following equation holds up to moderate forces:

$$F = \frac{k_b T}{4 l_p} \frac{1}{\left(1 - x/L\right)^2} \tag{4}$$

This model describes semiflexible chains under tension as an intermediate between a rigid rod and a flexible coil accounting for both local stiffness and long-range flexibility. The flexibility of the chain is parameterized by the persistence length l_p, the distance over which the two segments of the chain remain directionally correlated. The persistence length represents the flexibility of the molecule being directly proportional to the bending modulus of the molecule. In other words, molecules with a low persistence length have a tendency to form coils.

6-3 a)

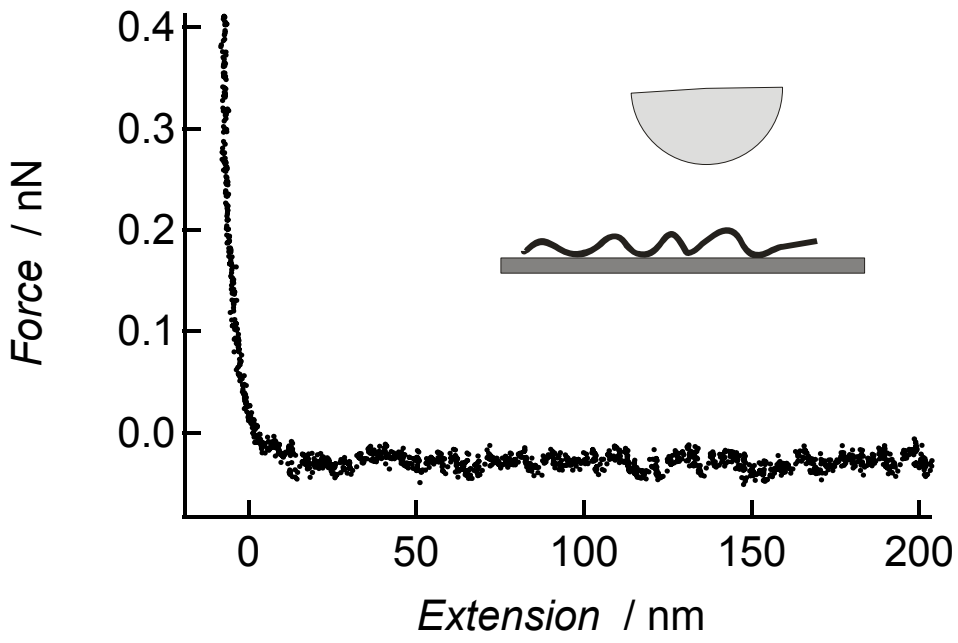
0.4
0.3
0.2
0.1
0.0
Force / nN
0
50
100
150
200
Extension / nm

b)

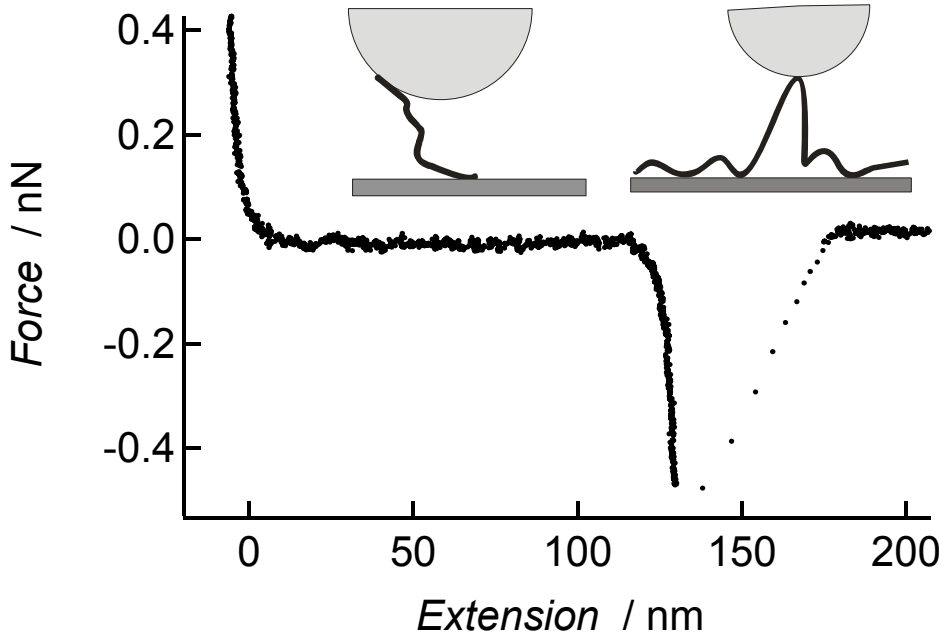
0.4
0.2
0.0
-0.2
-0.4
Force / nN
0
50
100
150
200
Extension / nm

c)

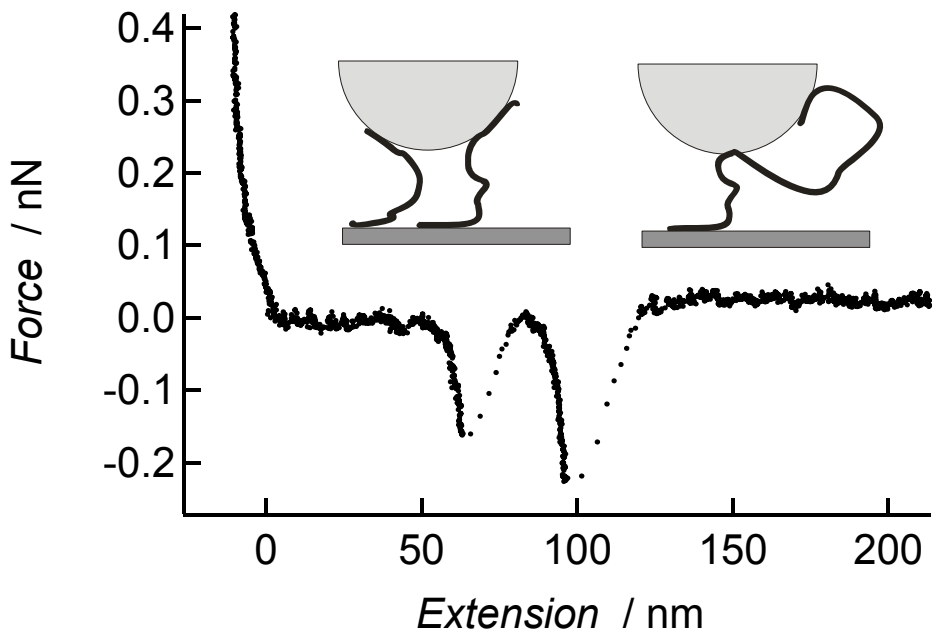

d)

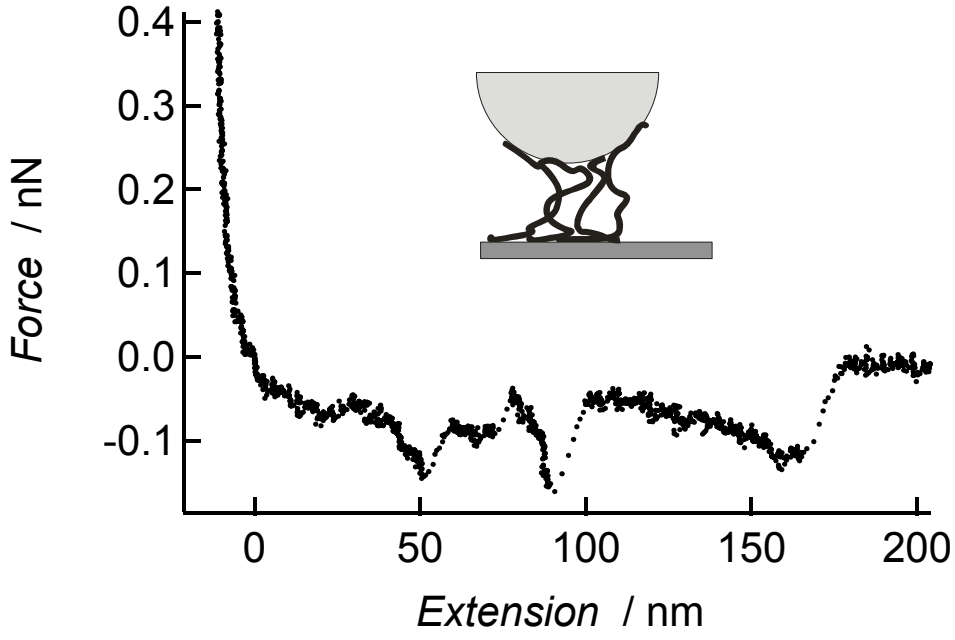

Figure 6-3: a) Force extension curve representing 15 % of all curves (*n* = 690) showing no stretching event. b) Force extension curve showing a single stretching

event attributed to extension of an individual cylindrical PNIPAM brush molecule (38 % of the force spectroscopy experiments). c) Retraction curve exhibiting desorption events indicative of either stretching and detachment of two physisorbed molecules or desorption of the molecule from two sites (30 % of all force curves). d) 14 % of all force curves display multiple detachment events in which two or more molecules are involved as shown in the inset.

The failure of the inextensible model in the high force regime can be attributed to a change from the entropy dominated restoring forces to the elasticity dominated regime as the level of stress on the molecule is increased. This infers extension of the molecule beyond its equilibrium contour length. As a consequence we utilize a modified version of equation (4), the so called extensible model to fit the persistence length to the data:[15]

$$\frac{x}{L} = 1 - \frac{1}{2}\left(\frac{k_b T}{F l_p}\right)^{\frac{1}{2}} + \frac{F}{\Phi} \tag{5}$$

Φ denotes the elastic stretch modulus. According to equation (4) x approaches L as $F^{-\frac{1}{2}}$. In this regime the brush molecules can also be enthalpically stretched beyond the contour length L as apparent from equation (5). At $x \geq L$ in the high force regime equation (5) shows approximately linear behavior effectively representing Hooke's law governed by bond angle deformation and bond stretching. In general, there need not be a simple relationship between the stretch modulus and the persistence length. Supposing that the molecule behaves like a cylindrical rod one might use linear elasticity theory to find $\Phi = 16 k_B T l_p d^{-2}$ leaving Φ in the range of nanonewtons for polymer brushes.[15] Recently, enthalpic stretching of covalent bonds has been quantified as a mixture of bond extension and bending of the bond angles using density functional theory and *ab initio* approaches. Netz found a stretch modulus of 28 nN for a C-C bond in the *trans* conformation.[30] **Figure 6-4a** shows a nonlinear curve fit employing the extensible Odijk model (equation (5)) providing a persistence length of (23 ± 4) nm and a segment elasticity of (6.5 ± 0.4) nN. The extensible model (equation (5)) corresponds well to the experimental data in particular in the high force regime emphasizing that the elasticity of the cylindrical

PNIPAM brushes at low forces is dominated by entropic contributions, while in the high force regime the elasticity is governed by enthalpic stretching and deforming of bonds. Fortunately, *self-avoiding* of the chains does not play a role in our case since $L < 3l_p$ and already at small extensions self-avoidance would be suppressed by reduction in brush concentration.

It is instructive to perform continuous stretching experiments with a single chain to prove reproducibility and to gauge the impact of substrate polymer interaction as displayed in **Figure 6-4b**. Here, the bottle brush molecule has been gathered by the tip extended with a threshold force just below the detachment forces and then relaxed without touching the surface. The stretching of the suspended molecule is carried out in repeated cycles. We found highly reproducible force distance curves, i.e. all relaxation and extension curves lie on top of each other, and thus we conclude that interference of the force extension curve arises from adhesion of the molecule is highly improbable.

6-4 a)

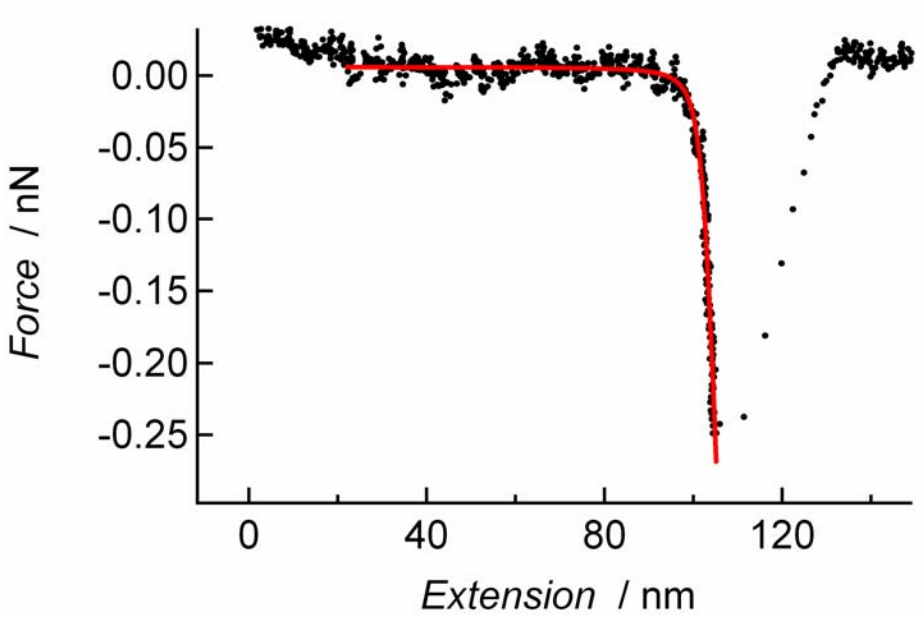

b)

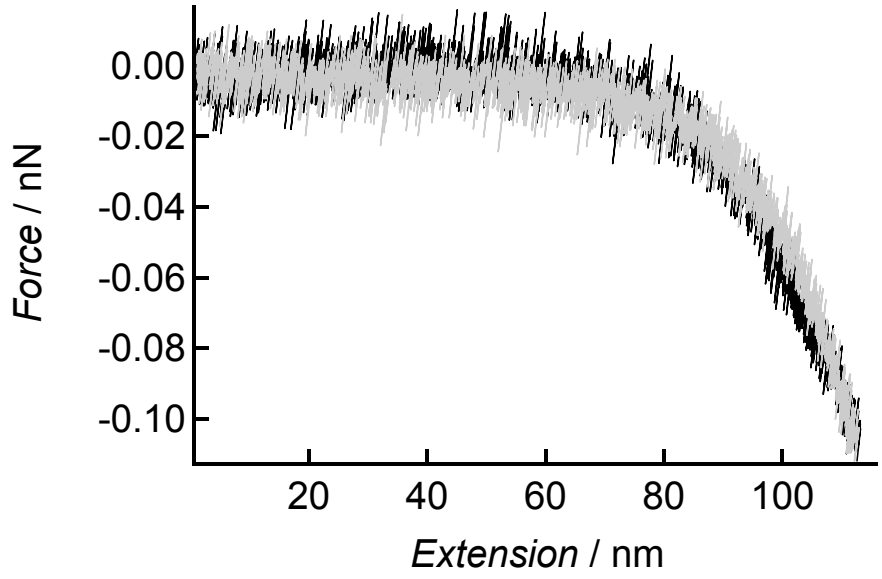

Figure 6-4: a) Measured force extension curve of a cylindrical PNIPAM brush molecule and the corresponding nonlinear curve fit employing the extensible Odijk-model (equation 5) providing a persistence length of (23 ± 4) nm and a segment elasticity of (6.5 ± 0.4) nN. b) Stretching of a single polymer brush without detachment of the molecule. Both relaxation (grey) and extension (black) exhibit the same elasticity, which suggests that adhesion to the surface does not play a dominant role in the force extension curves.

Figure 6-5 shows two histograms of the apparent persistence length l_p^{app} and the apparent contour length L_{app} obtained from employing the extensible WLC model to fit a large number (n = 77) of force-extension curves resulting in an average persistence length of (43 ± 2.4) nm and an average contour length of (80 ± 2.5) nm assuming normal distribution. The elastic stretch modulus Φ ranges between 2-11 nN in satisfying accordance with theoretical models and previous studies.[15,30] The histogram displayed in **Figure 6-5** exhibits a rather broad distribution of apparent persistence lengths l_p^{app}, which might be attributed to two inherent problems associated with pulling at individual brush

molecules. Firstly, it is conceivable that side and main chain are extended simultaneously and secondly the attachment of the chain to the tip and surface might reduce the apparent persistence length as first reasoned by Kulic et al.[29]

Stretching of the brush molecule might occur by anchoring of one or more side chains to the tip. As a consequence main and side chains are extended simultaneously as depicted in **Figure 6-6a** showing different possible scenarios. The restoring force experienced by the cantilever is thus a mixed contribution from stretching the side and main chain, which can be envisioned as two nonlinear springs in series.

6-5 a)

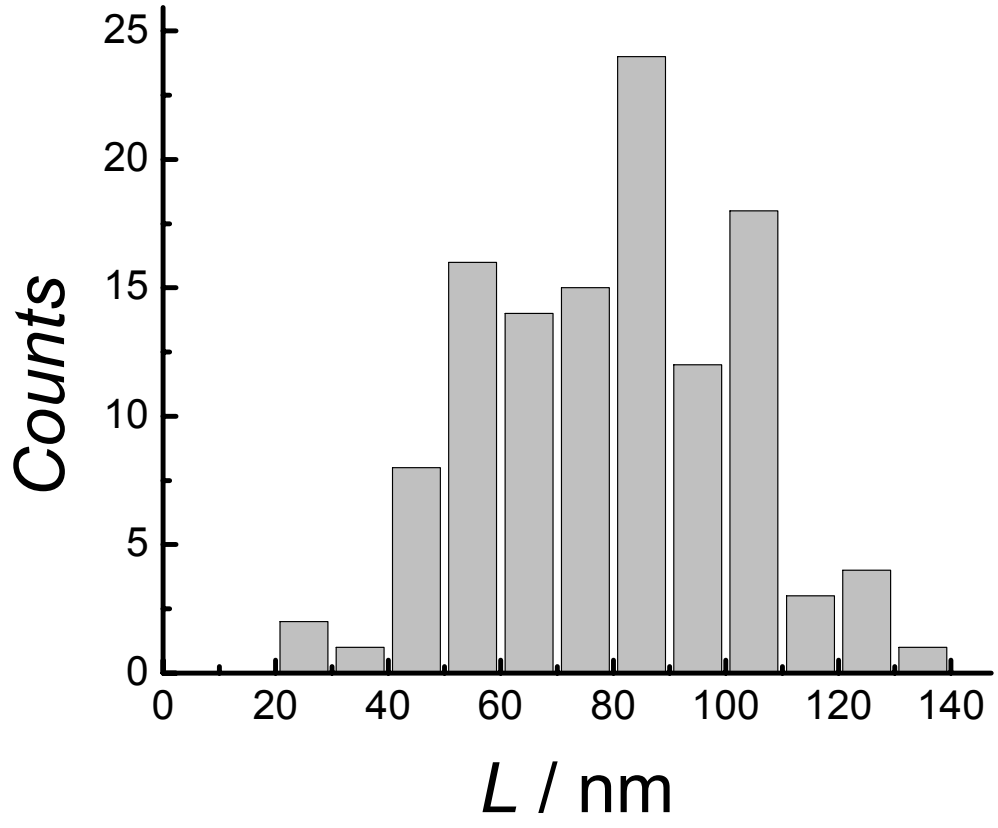

b)

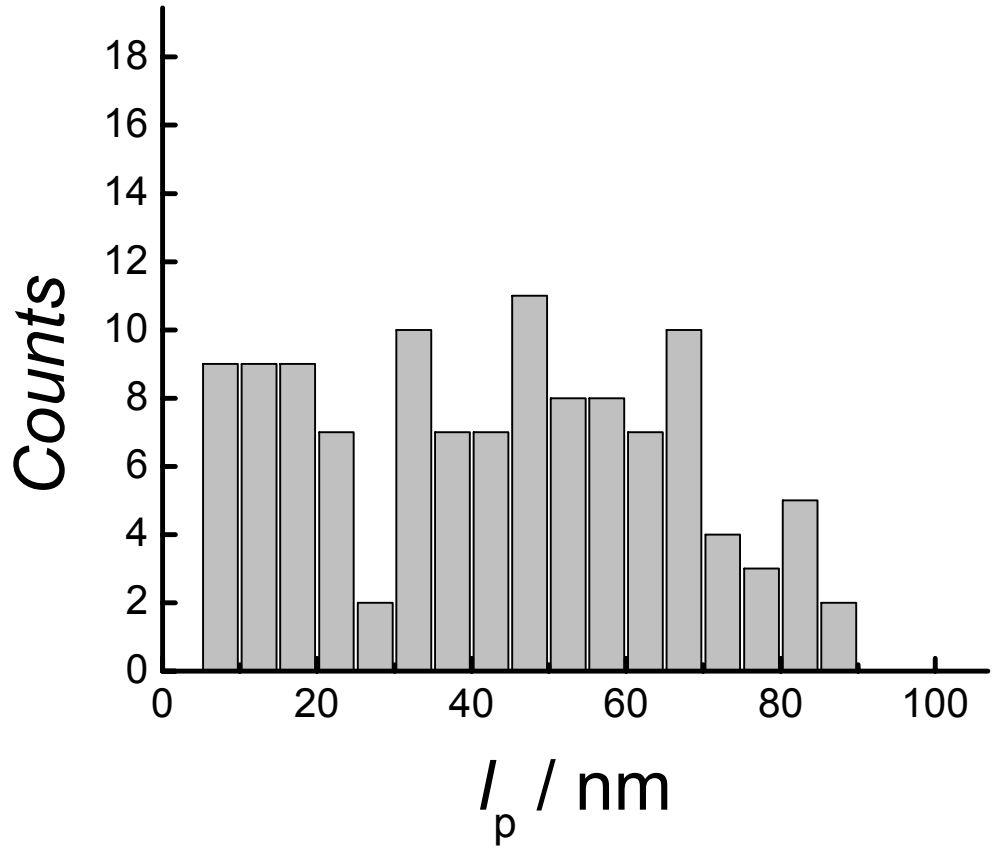

Figure 6-5: a) Histogram of extension lengths *L* with an average apparent contour length of (79 ± 23) nm and b) histogram of measured persistence lengths exhibiting a mean value of l_p = (43 ± 22) nm.

Hence, the apparent persistence length observed in our experiments might be lowered substantially as compared to those molecules in which merely the main chain is extended by the AFM tip. The decrease of the apparent persistence length is a function of the individual main and side chain contour length that is suspended between tip and substrate. The situation gets even more intricate if several side chains are pulled simultaneously each with a different apparent length, which increases the apparent persistence length due to reducing the force exerted on each side chain.

6-6 a)

i) **ii)** **iii)**

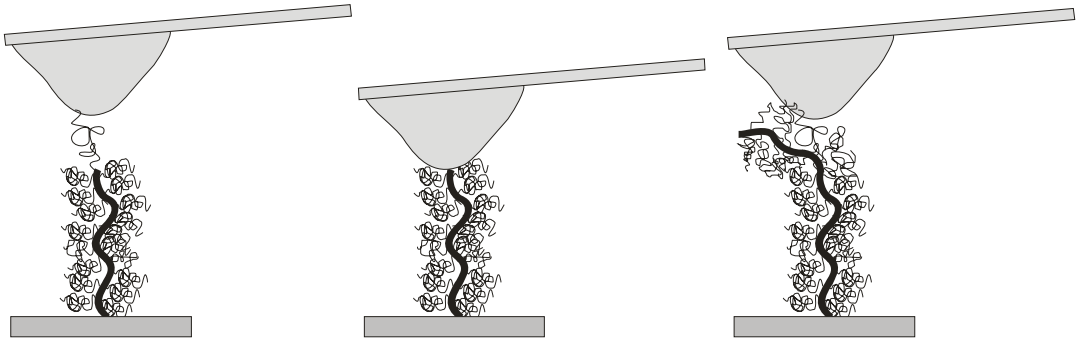

b)

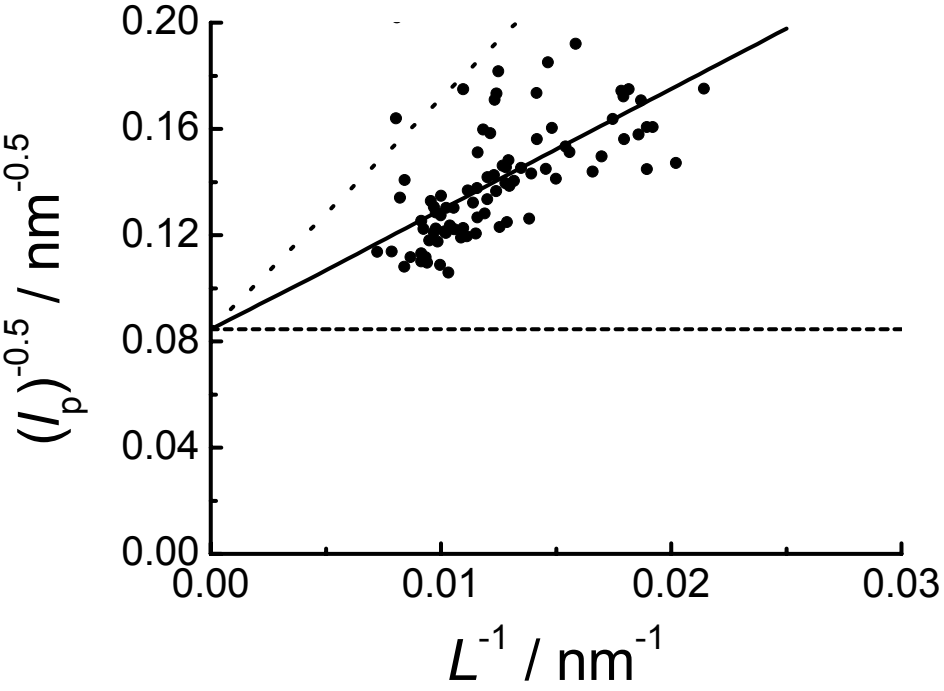

Figure 6-6: a) Illustration of different conceivable scenarios when stretching a polymer brush. i) One side chain is attached to the tip. ii) Only the main chain is extended between tip and sample. iii) Several side chains are anchored simultaneously to the tip.
b) Extrapolation of the "true" persistence length as a function of inverse apparent contour length to infinite contour length employing equation (8). Robust linear fitting (——) yields a "true" persistence length of 140 nm assuming a side chain length of 7 nm and a persistence length l_{p2} of 2 nm. Line (---) models a brush pulled only at the main chain and (···) denotes pulling at a side chain exhibiting a length between tip and sample attachment site of 14 nm instead of 7 nm.

Stretching of a brush molecule at a single side chain (persistence length: l_{p2}; contour length: L_2) *and* the main chain (persistence length: l_{p1}; contour length: L_1) simultaneously, can be described by adding the extension of two nonlinear chains since both chains experience the same force and thus the overall extension reads:

$$x = x_1 + x_2 = L_1 + L_2 - \frac{L_1}{2}\left(\frac{k_b T}{F l_{p1}}\right)^{\frac{1}{2}} - \frac{L_2}{2}\left(\frac{k_b T}{F l_{p2}}\right)^{\frac{1}{2}} + \frac{F\left(L_1 + L_2\right)}{\Phi}, \tag{6}$$

which can be readily cast in an equation for a single chain with an apparent persistence length l_p^{app} and an overall contour length $L_{app} = L_1 + L_2$:

$$\frac{x}{L_{app}} = 1 - \frac{1}{2}\left(\frac{k_b T}{F l_p^{app}}\right)^{\frac{1}{2}} + \frac{F}{\Phi}. \tag{7}$$

The apparent persistence length l_p^{app} as a function of contour length L can be linearized to:

$$\frac{1}{\sqrt{l_p^{app}}} = \frac{1}{\sqrt{l_{p1}}} + \left(\frac{1}{\sqrt{l_{p1}}} - \frac{1}{\sqrt{l_{p2}}}\right) L_2 L_{app}^{-1}. \tag{8}$$

Hence, a plot of $\left(l_p^{app}\right)^{-\frac{1}{2}}$ as a function of L_{app}^{-1} provides a means to determine the "true" persistence length of the main chain from a linear fit and the corresponding *y*-intercept ($\lim_{L\to\infty}\left(l_p^{app}\right)^{-\frac{1}{2}} = \left(l_{p1}\right)^{-\frac{1}{2}}$).

Figure 6-6b shows a graph displaying the experimentally determined persistence length from fitting equation (6) to each individual force extension curve as a function of the apparent contour length. Fitting of equation (8) to the data (solid line) gives a "true" persistence length of 140 nm at an average side chain persistence length of 2 nm and a mean side chain length of 7 nm. The dashed line denotes solely the pulling of a main chain (l_{p1} = 140 nm), while the dotted line displays the situation for a longer side chain (l_{p2} = 2 nm, L_2 = 14 nm) maintaining the parameters for the main chain.

It might also be conceivable that several side chains are extended simultaneously, which diminishes the impact of the side chain elasticity on the apparent persistence length. Notably, the persistence length of the side chains attached to the tip scales with $nl_p^{\text{side chain}}$, with n the number of side chain with equal length. As mentioned above (figure 3b (inset)), it might also be possible that the persistence length is larger due to loop formation while picking up the molecule close to the center and thus extending two chains in parallel.

Secondly, the measured apparent persistence length is also influenced by structural parameters as already pointed out by Marko and Siggia[14] as well as recently shown by Kulic et al.[29] who found that l_p^{app} decreases according to $l_p^{\text{app}} = l_p \cos(\tau) \Big/ \left(1 + c l_p / L\right)^2$ in which c denotes a structural parameter representing intrinsic bending, loop formation or the geometry of attachment of the chain to either the substrate or the tip. $\cos(\tau)$ accounts for the direction of force not being collinear with the attachment point of the molecule. As a consequence deviations from the true persistence length decrease with increasing contour length for all contributions. However, side chains attached to the tip might reduce the impact of attachment geometry on the measured persistence length rendering this problem of minor importance in our special case.

A "true" persistence length of 140 nm seems to be rather high as compared to 29 nm obtained from image analysis assuming molecules in equilibrium on the surface. It is much more likely that the molecules are kinetically trapped on the surface suggesting a higher persistence length in three dimensions. In fact, we could not induce a collapse of the PNIPAM brush by increasing the temperature to exert poor solvent conditions due to

the strong adhesion of the molecule. Hence, the low persistence length of merely 29 nm might be due to kinetic effects due to polymer substrate interactions.

However, a persistence length of 140 nm is higher than expected from common knowledge on cylindrical brushes with different side chain length and with chemically different side chains. Typically, the stiffness of wormlike chains is investigated by static light scattering according to the Benoit-Doty formula, which describes the radius of gyration as function of the contour length L and of the persistence length l_p. However, for cylindrical brush polymers the contour length is not a priori known because the cylinder length per main chain repeat unit might be smaller than l = 0.25 nm which is usually adopted for repeat units and because of the contribution of the flexible side chain corona to both ends of the cylindrical brush. Recently combined light and neutron scattering investigations have shown that the cylinder length per repeat unit of the main chain is in fact l = 0.25 nm in free solution in contrast to the much smaller values typically observed by AFM for cylindrical brushes at surfaces.[31] The contribution of the side chain corona to both ends of cylindrical brushes may be estimated from the formula for the radius of gyration of coil-rod-coil structures derived by Huber.[32] Reevaluation of the LS-results given in ref. 17 according to the procedure mentioned above and described in some detail elsewhere, yields l_p = 60 nm which is about a factor of 2 smaller than that obtained by force spectroscopy.[33] Although this discrepancy appears large at a first glance, it should be noted that for wormlike chains close to the rod limit (i. e. $L/l_p \approx$ 1-3) small variations in R_g produce extremely large changes in l_p. For the present data, the change in l_p from 140 nm to 60 nm produces a variation in R_g by 17 %, only. Although for the SLS-data given in ref. 17 this deviation is certainly larger than the experimental error for R_g of about ± 5 %, a similar sensitivity of the fitted persistence length could be expected for the force distance curve analysis, as well. However, the primary source of uncertainty could originate from the extrapolation procedure shown in Fig. 6b. Clearly, much more reliable results could be expected from the investigation of much longer cylindrical brush polymer which, however, are presently not available with PNIPAM side chains.

A possible explanation for the high extrapolated value of the persistence length might be that the tip occasionally pulls two parts of one chain simultaneously as illustrated in the inset of figure 3b (right scheme) leading to an inseparable increase in

persistence length of the bottle brush molecule. It remains to be elucidated why the two approaches provide so substantially different values for the persistence length. In summary, the broad distribution of measured persistence lengths can be attributed to the chain attachment to tip and substrate and the influence of the side chain elasticity. Both effects are particularly important if the stretched contour length of the molecules is short.

6.4 Conclusions

We have directly measured the force versus separation profiles of individual cylindrical PNIPAM brushes as they are extended between an AFM tip and the substrate. The nonlinear force extension curves are best described by the extensible Odijk-model accounting for the deformation of bond angles as well as stretching of the bonds.

From imaging of bottle brush molecules on mica we inferred an average persistence length of 29 nm assuming that the molecules are in their equilibrium state on the surface. Stretching experiments, however, suggest a considerably higher persistence length biased by the contour length, which has been attributed to the influence of side chain elasticity. In fact, the measured persistence lengths are shifted systematically to lower values due to side chains attached to the tip. In conclusion, persistence lengths inferred from AFM imaging of adsorbed brush molecules are systematically smaller than those from stretching experiments, which might be attributed to the substrate interactions of the brush molecules.

6.5 References

(1) Bustamante, C.; Marko, J. F.; Siggia, E. D.; Smith, S. B. *Science* **1994**, *265*, 1599-1600.

(2) Rief, M.; Gautel, M.; Schemmel, A.; Gaub, H. E. *Biophys. J.* **1998**, *75*, 3008-3014.

(3) Rief, M.; Oesterhelt, F.; Heymann, B.; Gaub, H. E. *Science* **1997**, *275*, 1295-1297.

(4) Rief, M.; Gautel, M.; Oesterhelt, F.; Fernandez, J. M.; Gaub, H. E. *Science* **1997**, *276*, 1109-1112.

(5) Oesterhelt, F.; Oesterhelt, D.; Pfeiffer, M.; Engel, A.; Gaub, H. E.; D.J., M. *Science* **2000**, *288*, 143-146.

(6) Ortiz, C.; Hadziioannou, G. *Macromolecules* **1999**, *32*, 780-787.

(7) Zhang, D.; Ortiz, C. *Macromolecules* **2005**, *38*, 2535-2539.

(8) Grandbois, M.; Beyer, M.; Rief, M.; Clausen-Schaumann, H.; Gaub, H. E. *Science* **1999**, *283*, 1727-1730.

(9) Boal, D. *Mechanics of the cell*, 1 ed.; Cambridge University Press: Cambridge, 2002.

(10) Liu, X.; Pollack, G. H. *Biophys. J.* **2002**, *83*, 2705-2715.

(11) Kratky, O.; Porod, G. **1949**, *68*, 1106-1122.

(12) Kovac, J.; Crabb, C. C. *Macromolecules* **1982**, *15*, 537-541.

(13) Bustamante, C.; Smith, S. B.; Liphardt, J.; Smith, D. *Curr. Opi. Struct. Biol.* **2000**, *10*, 279-285.

(14) Marko, J. F.; Siggia, E. D. *Macromolecules* **1995**, *28*, 8759-8770.

(15) Odijk, T. *Macromolecules* **1995**, *28*, 7016-7018.

(16) Sheiko, S. S.; Möller, M. *Chem. Rev.* **2001**, *101*, 4099-4123.

(17) Li, C.; Gunari, N.; Fischer, K.; Janshoff, A.; Schmidt, M. *Angew. Chem. Int. Ed.* **2004**, *43*, 1101-1104.

(18) Gerle, M.; Schmidt, M.; Fischer, K.; Roos, S.; Müller, A. H. E.; Sheiko, S. S.; Prokhorova, S.; Möller, M. *Macromolecules* **1999**, *32*, 2629-2637.

(19) Sheiko, S. S.; Gerle, M.; Fischer, K.; Schmidt, M.; Möller, M. *Langmuir* **1997**, *13*, 5368-5372.

(20) Zhang, A.; Shu, L.; Bo, Z.; Schlüter, A. D. *Macromol. Chem. Phys.* **2003**, *204*, 328-339.

(21) Schlüter, A. D.; Rabe, J. P. *Angew. Chem. Int. Ed.* **2000**, *39*, 864-883.

(22) Wintermantel, M.; Gerle, M.; Fischer, K.; Schmidt, M.; Wataoka, I.; Urakawa, H.; Kajiwara, K.; Tsukahara, Y. *Macromolecules* **1996**, *29*, 978-983.

(23) Fischer, K.; Schmidt, M. *Macromol. Rapid Commun.* **2001**, *22*, 787-791.

(24) Terao, K.; Nakamura, Y.; Norisuye, T. *Macromolecules* **1999**, *32*, 711-716.

(25) Terao, K.; Hokajo, T.; Nakamura, Y.; Norisuye, T. *Macromolecules* **1999**, *32*, 3690-3694.

(26) Hutter, J. L.; Bechhoefer, J. *Rev. Sci. Instrum.* **1993**, *64*, 1868-1873.

(27) Rivetti, C.; Walker, C.; Bustamante, C. *J. Mol. Biol.* **1998**, *280*, 41-59.

(28) Rivetti, C.; Guthold, M.; Bustamante, C. *J. Mol. Biol.* **1996**, *264*, 919-932.

(29) Kulic, I. M.; Mohrbach, H.; Lobaskin, V.; Thaokar, R.; Schiessel, H. *Phys. Rev. E* **2005**, *72*, 0419051-0419055.

(30) Netz, R. R. *Macromolecules* **2001**, *34*, 7522-7529.

(31) Ratgeber, S.; Pakula, T.; Wilk, A.; Matyaszewski, K.; Beers, K. L. *J. Chem. Phys.* **2005**, *122*, 124904-124917.

(32) Huber, K. *Macromolecules* **1989**, *22*, 2750-2755.

(33) Zhang, B.; Gröhn, F.; Fischer, K.; S., P. J.; Schmidt, M. *in preparation* **2005**.

7 STRETCHING CYLINDRICAL BRUSHES UNDER POOR SOLVENT CONDITIONS BY ATOMIC FORCE MICROSCOPE

7.1 Introduction

Cylindrical polymer brushes or sometimes called bottle brushes, are long chain molecules consisting of a flexible backbone densely grafted with relatively long side chains provided that the main chain is much longer than the side chain. In the presence of excluded volume interactions, the densely grafted side chains try to avoid strong overlapping, which induces an extremely high chain stiffness of the backbone as explained in chapter 6.

Homopolymer cylindrical brushes, which spread on the air water interface, were found to adopt a spherical shape upon lateral compression of the monolayer.[1] Statistical copolymacromonomer chains were observed to exhibit a conformational transition from wormlike chain to regularly curved structures, such as horseshoe or meander-like shapes, when the side chains were made incompatible by chemical transformations.[2] More recently cylindrical polymer brushes with temperature responsive side chains, poly-isopropylacrylamide (PNIPAM) were synthesized which exhibited a cylinder to globule transition at the lower critical solution temperature (LCST) of PNIPAM.[3]

The force-extension behavior of single chains[4,5] has paralleled the study of the collapsed state of polymers in poor solvent.[6] The mechanical response has been studied for individual globules under extension and various compression regimes.[7]

More recently, experimental observations of DNA stretching in a poor solvent[8] and an improved theoretical understanding of semiflexible polymers in poor solvents[9] have lead to theories of globules with a well-defined internal structure.[10]

Atomic force microscopy (AFM)[11] and single molecule force spectroscopy (SMFS)[5,12] are well known techniques, which have provided invaluable insight into the structure and elasticity of macromolecules. Force induced unfolding of proteins,[13] heparin[14] and mechanical induced overstretching of DNA[15] have become prominent milestones in force spectroscopy of single molecules.

Recently a technique, which involves the combining of the two methods i.e. AFM and SMFS was used for the controlled manipulation of individual bacteriorhodopsins leading to a deeper insight into membrane proteins.[16] In this chapter the force extension behavior of PNIPAM bottle brush molecules which are adsorbed to a surface is investigated in poor solvent conditions. Further inherently combined AFM imaging and SMFS techniques are presented, which may serve as a kind of "molecule specific force spectroscopy". It is used to mechanically manipulate selected single molecules and map the effect of unfolding events after manipulation i.e. to observe force induced conformational transitions. The goal here was to overcome the kinetic barrier by lifting the polymer from the surface allowing the molecule to adopt the equilibrium conformation at the respective temperature.

7.2 Experimental

Synthesis of cylindrical poly-N-isopropylacrylamide brushes by atom transfer radical polymerization using poly-2-bromo-isobutyryl-oxyethyl-methacrylate was performed as described elsewhere.[3] Force spectroscopy experiments were carried out by placing a 50µl droplet of dilute aqueous PNIPAM solution (c = 0.1 g/L) on a freshly cleaved mica surface, subsequently mounted in a homemade AFM PTFE fluid cell and incubated for 1 h. The surface was then rinsed with MilliQ water to remove unadsorbed molecules. V-shaped silicon nitride cantilevers purchased from Veeco (thermomicroscopes) exhibiting a nominal spring constant of and 0.015 Nm^{-1} were used for the experiments. Prior to use the spring constant was determined by thermal noise method.[17]

Under water AFM imaging was carried out in contact mode. Briefly, a 50µl droplet of MilliQ water was placed on a freshly cleaved mica surface and then mounted in a homemade AFM PTFE fluid cell. The polymer was dissolved in MilliQ water and then injected into the fluid cell to roughly achieve a concentration of ~ 0.1 g/l. V-shaped silicon nitride cantilevers purchased from Veeco (thermomicroscopes) exhibiting a nominal spring constant of and 0.01 Nm^{-1} were used for the experiments.

SMFS and molecule specific force spectroscopy experiments were carried out using a MFP 3D microscope from Asylum Research, Santa Barbara, USA.

7.3 Results and discussion

7.3.1 Qualitative Analysis of stretching of individual collapsed cylindrical brushes

Figures 7-1a-f show the different classes of events typically observed in stretching experiments of the cylindrical PNIPAM brushes in aqueous solution. A total of n = 740 force curves are considered and only retraction curves are shown in the following graphs.

Figure 7-1a shows a typical large nonspecific adhesion which can exist between 0-60 nm extension lengths with adhesion force magnitudes up to 1.2 nN, typical for hydrophobic surfaces. 15 % of the curves show such a behavior. **Figure 7-1b** shows a force extension curve exhibiting multiple force plateaus of constant force with increasing extension. The multiple plateaus shown in **Figure 1b** could be due to stretching of multiple molecules or of a single collapsed globule, which however is not clear. Such kinds of events have been predicted previously and observed experimentally for synthetic polymers in poor solvents, which were interpreted in two ways. Firstly the findings can be interpreted in terms of a *Raleigh instability* which describes a first order transition into a "ball-string" configuration where the applied force draws out one monomer at a time into a thin filament from a collapsed, surface bound globule due to high polymer-solvent interfacial energy.[6] The second involves the assumption that the polymer chain is adsorbed on the surface in a series of loops and at slow enough extension rates the monomers have enough time to detach and reform several times so that the force is redistributed over all the monomers in the chain. In our case, if we consider that the multiple plateau events originate from a single collapsed globule then the events can be interpreted as one out of the two energy changes upon extension (i) the annihilation of attractive polymer-surface interactions as the side chains of the polymer brush are ripped off the surface;

7-1 a)

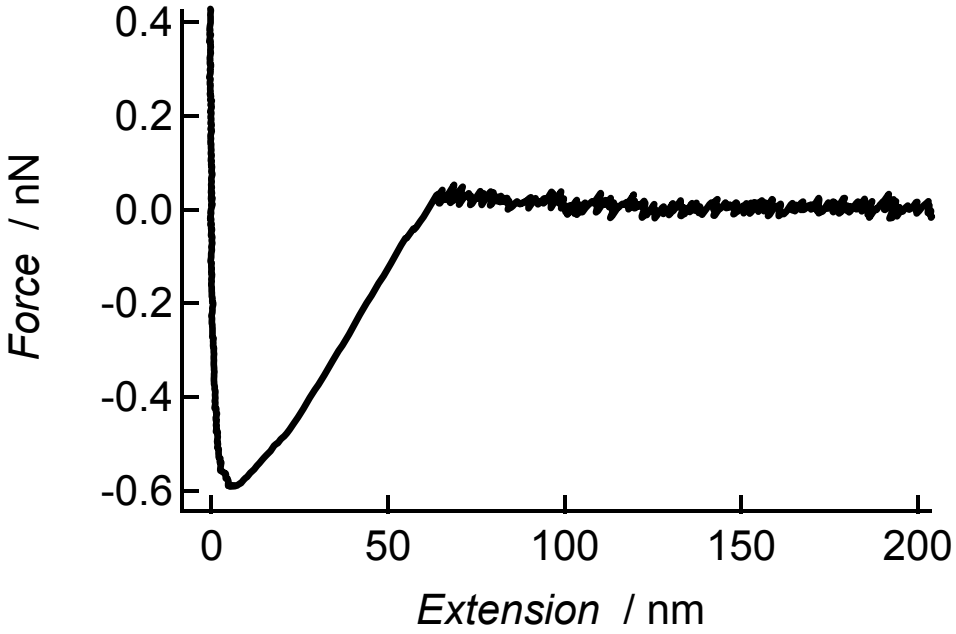
0.4
0.2
0.0
-0.2
-0.4
-0.6
Force / nN
0
50
100
150
200
Extension / nm

b)

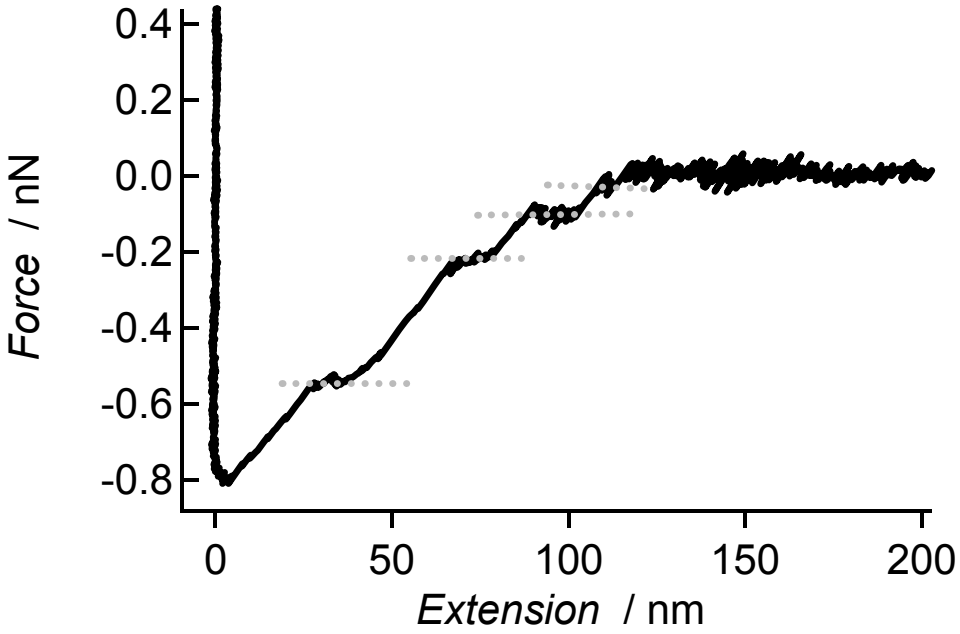
0.4
0.2
0.0
-0.2
-0.4
-0.6
-0.8
Force / nN
0
50
100
150
200
Extension / nm

c)

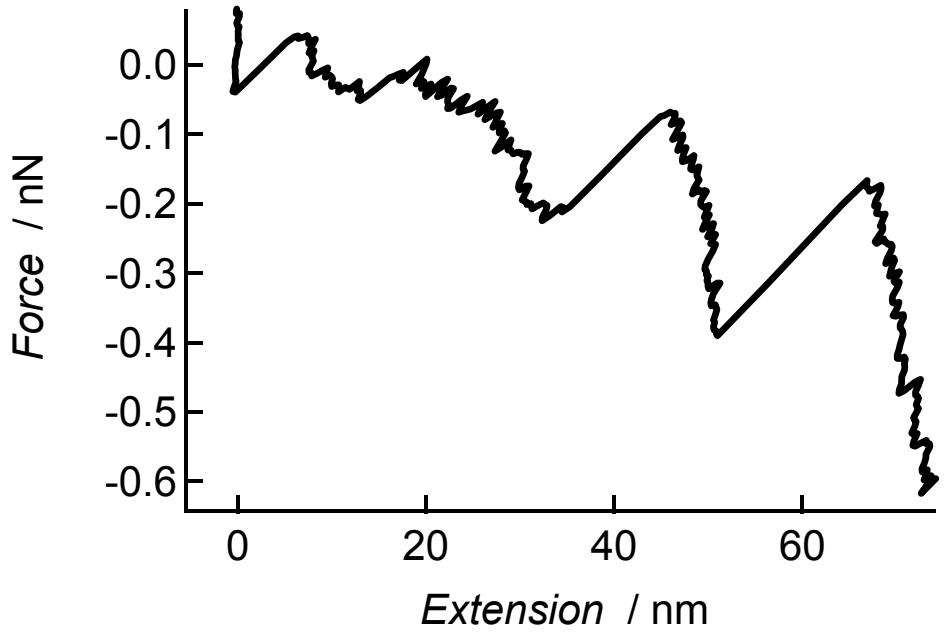
0.0
-0.1
-0.2
-0.3
-0.4
-0.5
-0.6
Force / nN
0
20
40
60
Extension / nm

d)

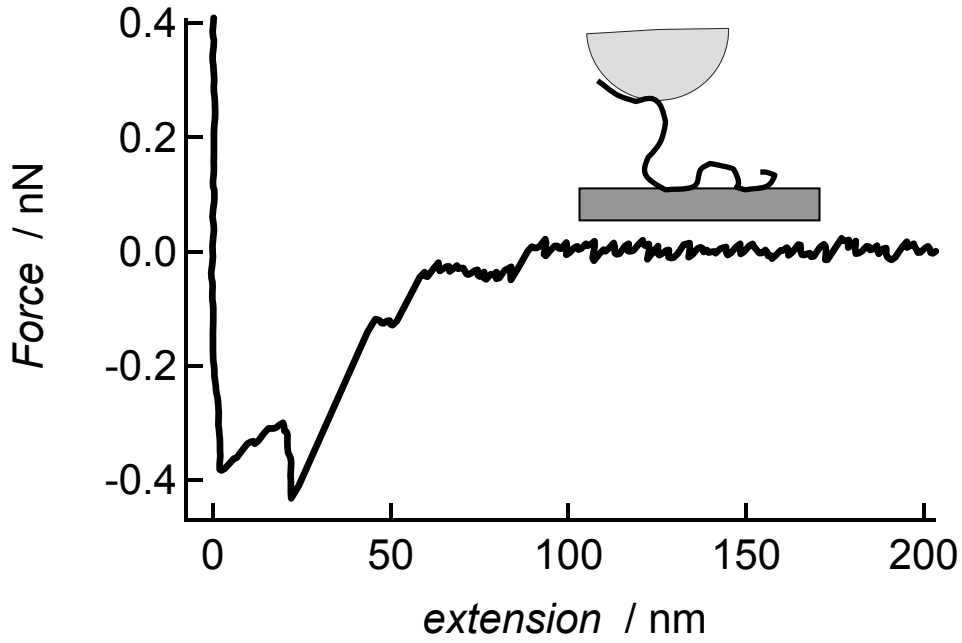
0.4
0.2
0.0
-0.2
-0.4
Force / nN
0
50
100
150
200
extension / nm

e)

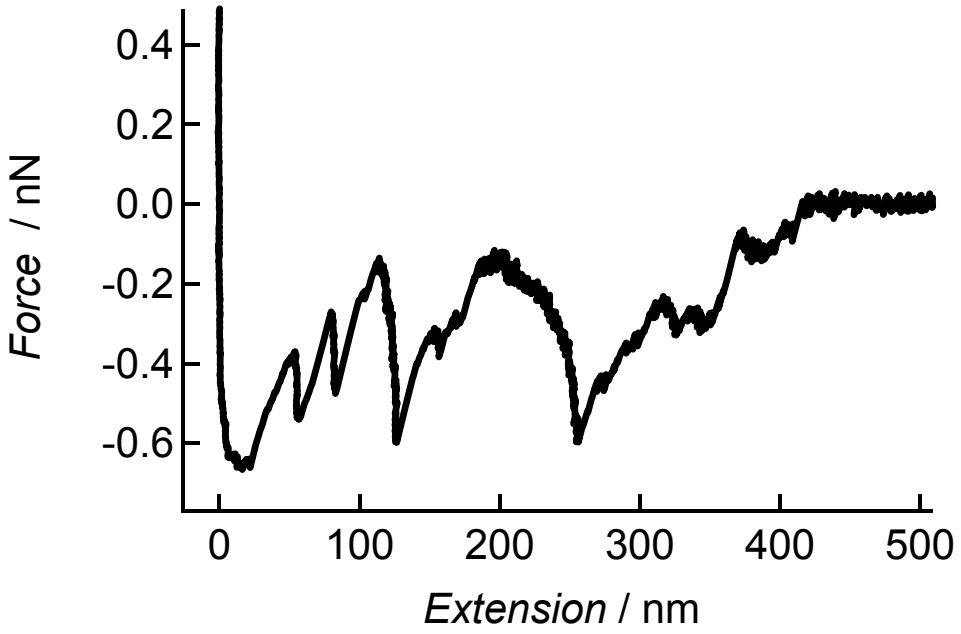
0.4
0.2
0.0
-0.2
-0.4
-0.6
Force / nN
0
100
200
300
400
500
Extension / nm

f)

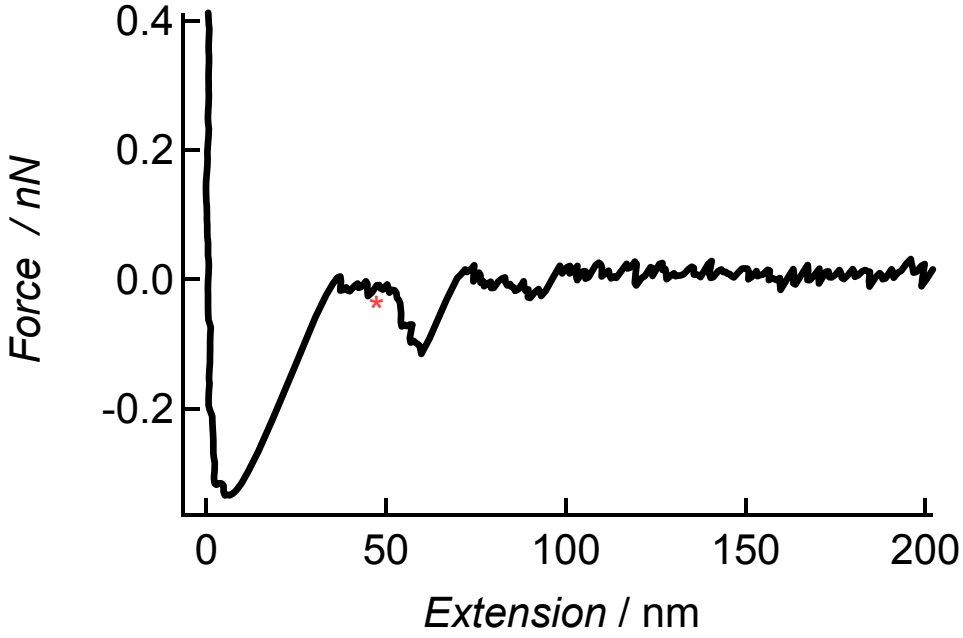
0.4
0.2
0.0
-0.2
Force / nN
0
50
100
150
200
Extension / nm

Figure 7-1a) No polymer bridge formed between the tip and the substrate 15 % of all curves (n = 740). b) Force-extension curve showing multiple plateau events (10 % of all curves). c) Force-extension curves showing multiple stretch events (45 % of force spectroscopy experiments). d) Complex force curves showing a stretch event followed by two plateaus (25 % of all curves). e) Stretching of a bunch of globules showing multiple stretch events (5 % of all force curves). f) Stretch event preceded by a plateau, shown by a red star (10 % of force curves showing saw tooth profile).

(ii) The creation of unfavorable polymer-solvent contacts, characterized by the interfacial tension, as the collapsed brush molecule is stretched out against the collapse forces. It is difficult to distinguish between the two energies in the force plateau. But it is indeed clear, in the case of PNIPAM brush molecules, that these plateau events are observed only in poor solvent conditions. However it should be noted that only 10 % of all the force extension curves show such a kind of behavior. **Figure 7-1c** shows a saw-tooth profile similar to those observed in the unfolding process of modular proteins.[13] The marked discontinuous changes in the force, indicates a polymer bridge between the tip and the sample. This bridge stretches out to a distance of 80 nm, which may correspond to the stretched out brush molecule. A large number, as high as 45 %, of all force extension curves exhibit saw-tooth profiles indicative of the stretching of the collapsed globule. Saw-tooth profiles could be due to the increase in number of surface contacts in poor solvent conditions. However it is uncertain if the stretch events are from single globules or multiple molecules.

Figure 7-1d shows a rather complex force extension curves exhibiting initially a stretch event followed by two plateau events, which might suggest the desorption of loops formed by the brush molecule on the surfaces as illustrated in the inset followed by desorption from the tip. 25 % of all force extension curves exhibited such a behavior. Finally we cannot avoid the stretching of two or more globules as we can observe in **Figure 7-1e** where we see the saw-tooth profile. Only 5 % of the all the force curves displayed such behavior. There was another interesting class of stretch events, which exhibited a saw tooth profile with a plateau preceding one of the stretch events. The plateau shown in **Figure 7-1f** with a star occurred at forces between 50-100 pN. 10 % of

the saw tooth profiles exhibited such a plateau. The plateau could be indicative of a conformational transition, but is not clear due to the complex stretch events. In order to resolve this detailed experiments in the "fly-fishing" mode were carried out which will be discussed in chapter 8.

7.3.2 Quantitative Analysis of stretching of individual collapsed cylindrical brushes

A total of n = 77 curves which displayed a saw-tooth profile (**Figure 7-1c**) were analyzed for the maximum extension length. **Figure 7-2a** shows the histogram of the apparent contour length of the polymer brushes spanned between tip and sample showing stretch events L_{app} = (86.2 ± 26) nm assuming a normal distribution. A similar analysis was carried out for the plateau events (**Figure 7-1b**), which gave a mean value of the apparent contour length of L^{*}_{app} = (83.2 ± 35) nm for a data set of n = 38. The histogram is shown in **Figure 7-2b**. The broad distribution of the apparent contour lengths could be due to the polydispersity of the polymer and due to the unknown nature of tip-sample interaction.

Furthermore the flexibility of the chain is parameterized by the persistence length l_p .The experimental curves were fit using an extended WLC model described by Odjik[18] which includes linear elastic contributions arising from the stretching of bond angles and covalent bonds:

$$\frac{x}{L} = 1 - \frac{1}{2}\left(\frac{k_b T}{F l_p}\right)^{\frac{1}{2}} + \frac{F}{\Phi} \qquad \text{equation (1)}$$

where Φ denotes the elastic stretch modulus. The last stretch event of the saw tooth profile was fit with the Odjik model. **Figure 7-3** shows a nonlinear curve fit (continuous blue line) employing the Odjik model (equation (1)) providing a persistence length of (0.31 ± 0.004 nm) and a segment elasticity of (1.2 ± 0.3) nN. The values obtained for the persistence length are physically impossible. One possible reason that could hamper the value obtained could be that the baseline (red continuous line, manually drawn) used for the fitting procedure could not be located precisely as can be observed in the Figure7-3.

Secondly most of the stretch events are too complex to be fitted as can be observed in **Figre7-1 c**.

7-2 a)

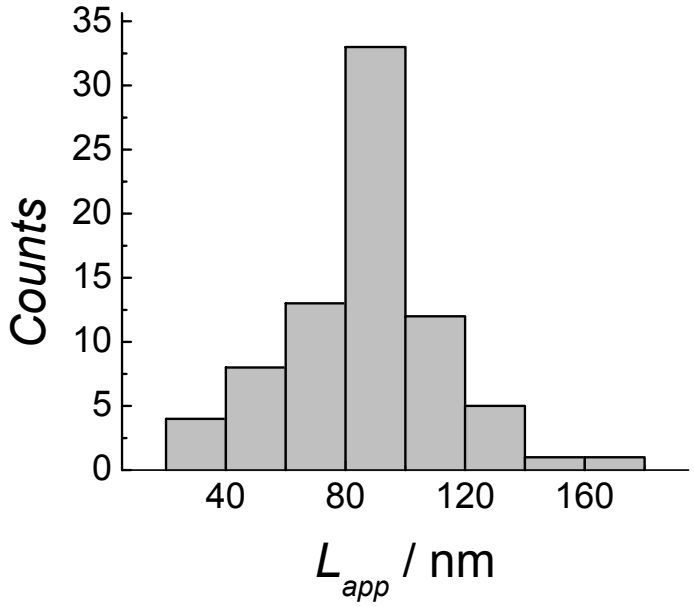

b)

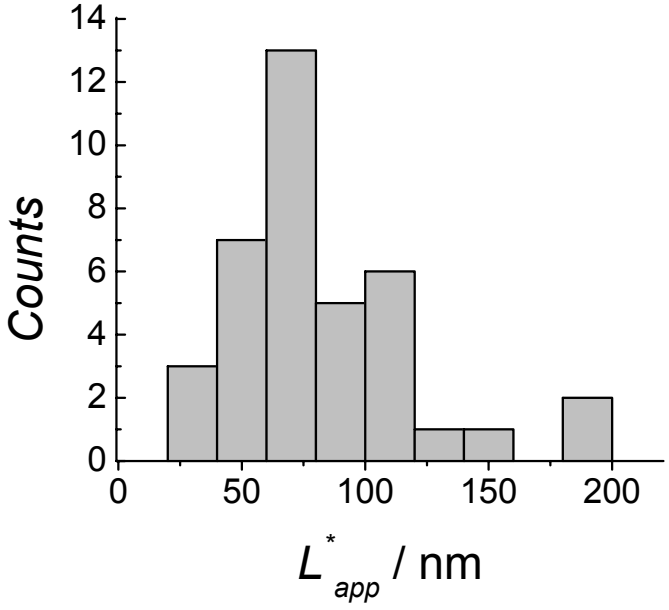

Figure 7-2 a) Histogram of extension lengths L_{app} with an average apparent contour length of (86.2 ± 26) nm b) Histogram of desorption lengths L_{app} with an average apparent contour length of (83.2 ± 35) nm

7.4 Molecule Specific Force Spectroscopy

In order to study the unwinding of the single PNIPAM globules in detail, molecule specific force spectroscopy, which combines AFM imaging and SMFS, was used to image and to selectively manipulate a single globule. For this experiment we immobilize the PNIPAM brush molecules at 38 ^{0}C (above the LCST) on a preheated freshly cleaved mica surface. After rinsing the mica surface with ultrapure water, the collapsed globules were imaged at 38 ^{0}C.

Figure 7-4a shows a contact mode AFM height image of a single collapsed globule. The deflection image shown in the inset depicts the contour of the collapsed molecule. After imaging, the AFM stylus was positioned over the collapsed globule and pressed onto the globule with a force of ≈ 1nN for about 1s. It was then retracted. The arrow indicates the point at which the molecule was stretched. **Figure 7-4b** shows the force-extension behavior of the collapsed PNIPAM globule. In this particular case we observe a strong nonspecific adhesion force was observed between 0-40 nm extension length with adhesion force magnitudes up to ≈ 0.7 nN, which nearly mask the initial stretch events. Subsequently a long plateau event at ≈ 220 pN follows until finally the stretched molecules desorbs from the tip at 225 nm. Such controlled stretching events have about 28 % occurrence while the rest 72 % experimental curves showed no stretch or plateau events suggesting no interaction of the tip with the collapsed globule.

Switching back to the image mode the same molecules were imaged in contact mode after manipulation. **Figure 7-4c** shows the contact mode AFM height image of the collapsed globule after mechanical manipulation. A conformational change is detected on the surface after the stretch event. This is clearly distinguished in the deflection image shown in the inset. The molecule is not stretched out on the surface even after manipulation because the temperature remained above the LCST of PNIPAM. Hence a collapsed structure would be expected even after manipulation, since this is the stable

conformation. As described above the conformation of these molecules do not change on reducing the temperature on the surface, because the adsorption force seems to be much higher than the driving force required for the conformational change on the surface.

7-3)

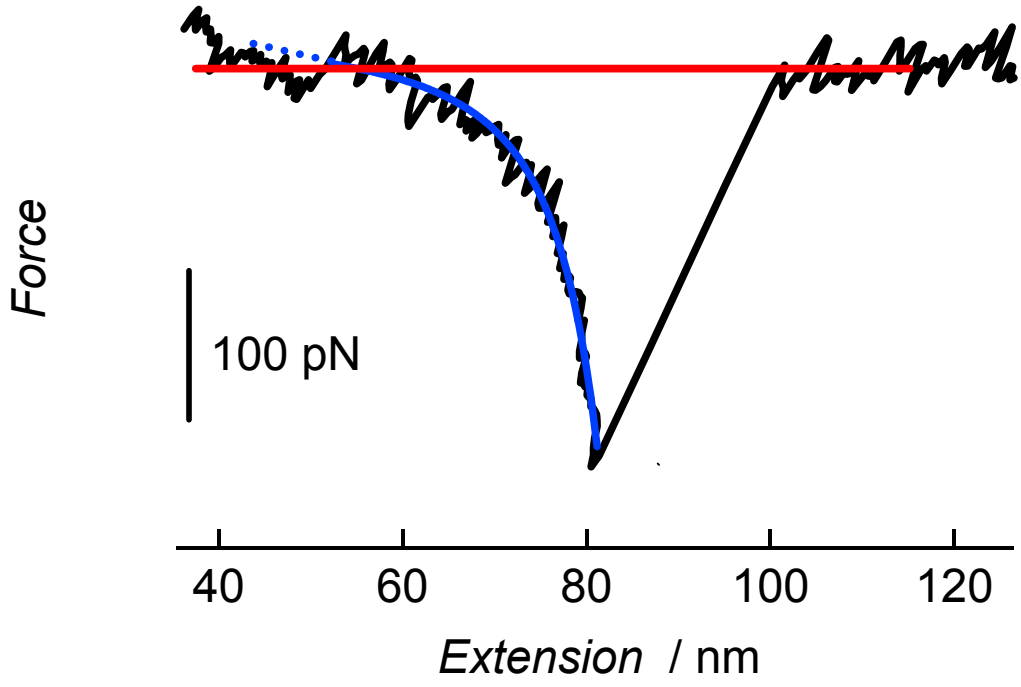

Figure 7-3 Measured force extension curve of a cylindrical PNIPAM brush molecule above LCST and the corresponding nonlinear curve fit (blue solid line) employing the extensible Odijk-model (equation 1) providing a persistence length of (0.31 ± 0.004) nm and a segment elasticity of (1.2 ± 0.3) nN. The red line is a manually drawn to show the uncertainty in locating the correct baseline for the fitting procedure.

Hence, a controlled mechanical manipulation of the collapsed brushes was performed by initially adsorbing the PNIPAM brush molecules on a preheated, freshly cleaved mica surface at 38 ^{0}C and then performing the combined AFM imaging and SMFS

spectroscopy experiment at 20 ^{0}C. **Figure 7-5a** shows a contact mode AFM deflection image of the collapsed globules. The images are similar to the globular structures as observed above LCST. The controlled manipulation of individual collapsed globules was carried out as described above. **Figure 7-5b** shows the force-extension behavior of the single collapsed PNIPAM globule (for the molecule marked 2). In this particular case a typical a saw-tooth profile is measured, which is similar to those found for the unfolding of modular proteins. As the PNIPAM globule is a disordered globule (not ordered like proteins) the unwinding saw-tooth profile also does not display a regular pattern.

After obtaining the force extension profile the PNIPAM brush molecules were visualized in the imaging mode as shown in **Figure 7-5c**. Only those molecules are marked which were mechanically manipulated except number (1) which is used as reference molecule. In case of molecule (2) a complete conformational transition from a globule to a fully extended cylinder is observed. This suggests that after the stretching events the molecule desorbs from the tip and not from the surface. As the experiment was carried out at 20 ^{0}C, the molecule once stretched completely prefers to remain in the stable cylindrical conformation. The molecule marked (3) in **Figure 7-5a** is stretched out and eventually completely desorbed from the mica surface since it is missing in the image after manipulation as shown in F**igure 7-5c.** Another example of the force induced conformational change is shown in **Figure 7-6 a-c.** An AFM deflection image of a single collapsed PNIPAM brush globule is shown in **Figure 7-6a** wherein the side chain corona and the collapsed backbone can be faintly visualized. The arrow indicates the point at which the molecule was stretched. **Figure 7-6 b** shows the force-extension behavior of the collapsed PNIPAM globule. In this particular case multiple stretch events occur. **Figure 7-6c** shows the AFM deflection image of the same molecule after manipulation, and exhibit an extended backbone. Interestingly only single plateau events are observed in "molecule specific force spectroscopy" experiments, i.e. multiple plateau events were absent. Thus it is concluded that single plateau events at an average force of (150 ± 30) pN are due to the desorption of the molecule as it is peeled off from the surface. Thus the multiple plateau events observed in the SMFS experiments can be interpreted as desorption of multiple molecules attached to the tip. As a consequence "molecule specific

force spectroscopy" helps to explain the statistical discrepancies, which are usually found in SMFS experiments.

7-4 a)

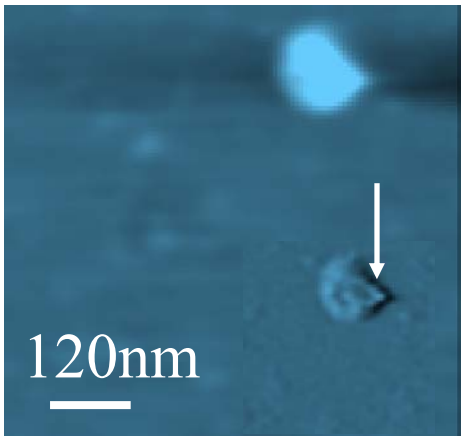

b)

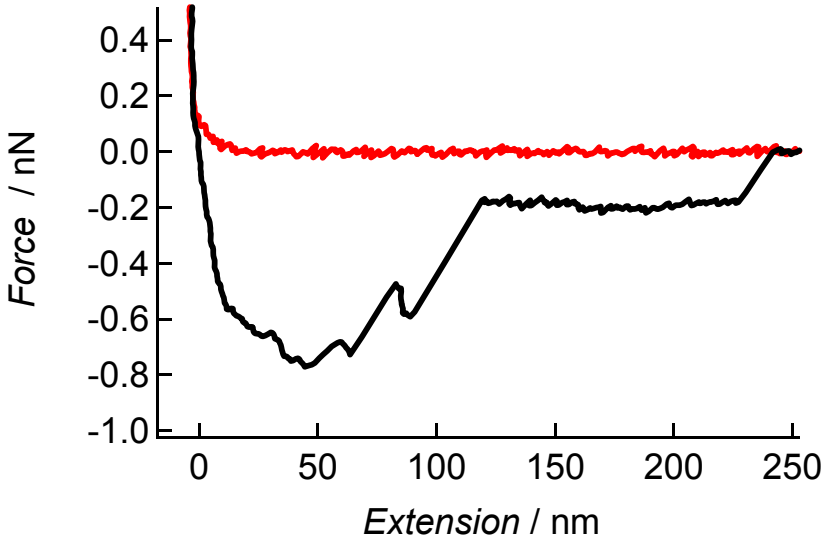

c)

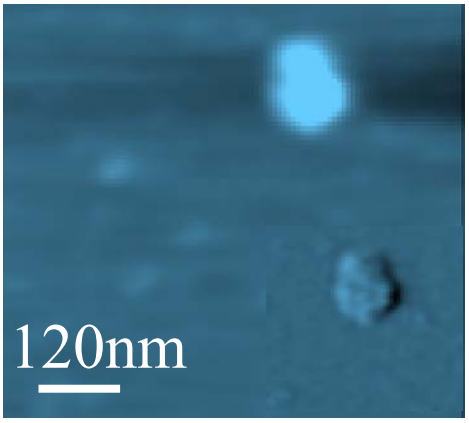

Figure 7-4 a-c) Molecule specific force spectroscopy of single collapsed PNIPAM brush molecule at 38 ^{0}C(detailed description given in text).

7-5 a)

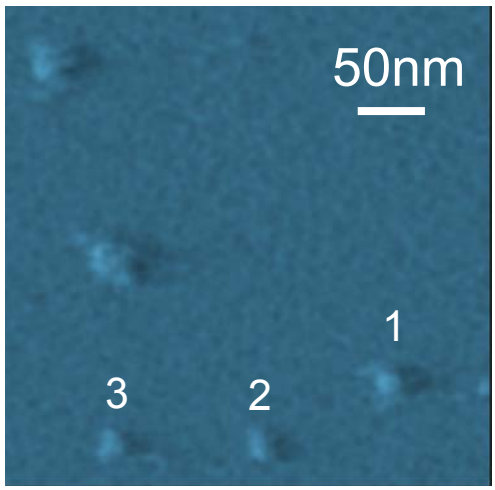

b)

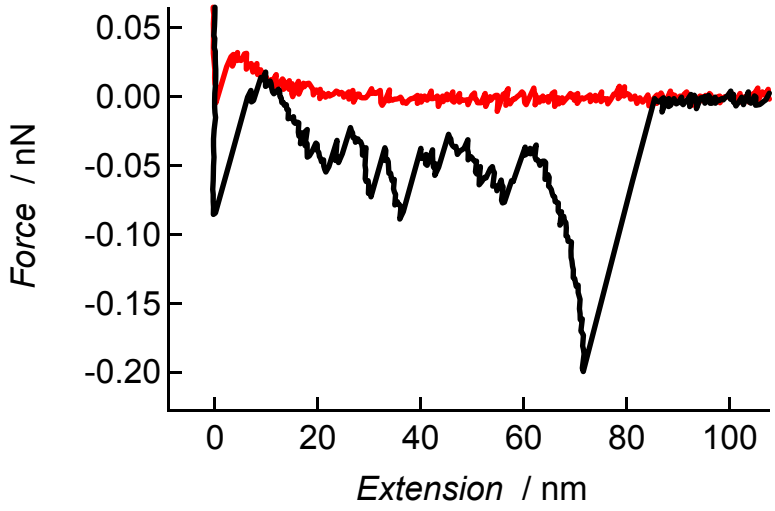

c)

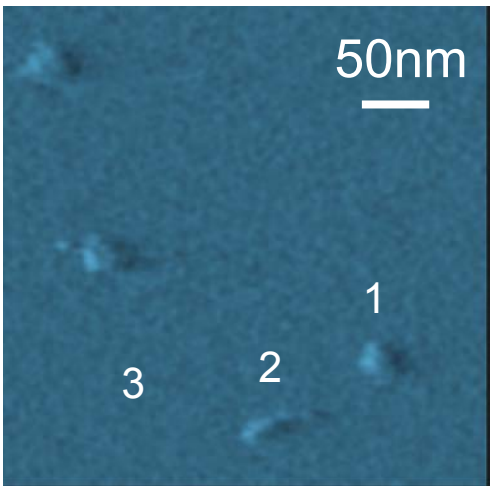

Figure 7-5 a-c) Molecule specific force spectroscopy of single collapsed PNIPAM brush molecule at 20 ^{0}C (detailed description given in text).

7-6 a)

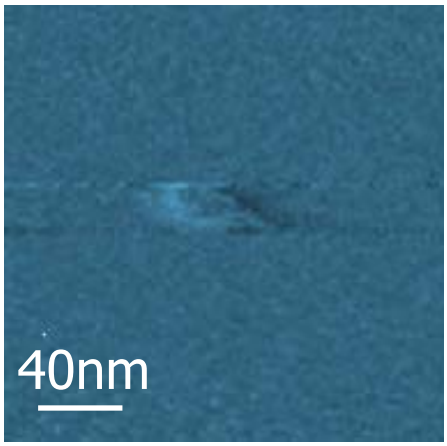

b)

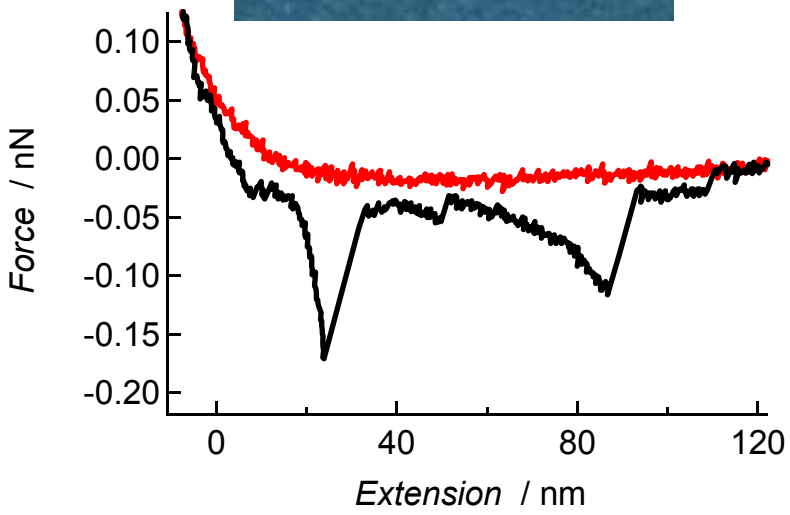

c)

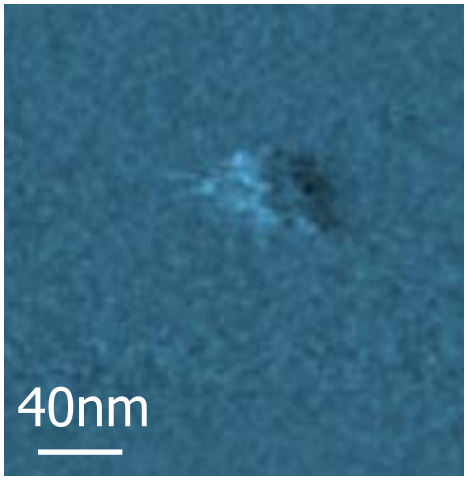

Figure 7-6 a-c) Molecule specific force spectroscopy of single collapsed PNIPAM brush molecule at 20 ^{0}C(detailed description given in text).

It should be possible to assign the stretch/plateau events to the conformation of the molecule by imaging before and after manipulation.

The force induced globule-to-cylinder conformational changes in PNIPAM brush molecules shown in **Figure 7-5 and 7-6** reveal that the pulling forces exerted by the AFM tip stretches out the brush molecule so that the PNIPAM side chains come into contact with the aqueous solution which is at 20 ^{0}C i.e. good solvent conditions for PNIPAM. Accordingly the brush molecule remains in the extended conformation after readsorption onto the surface.

7.5 Conclusions

We have directly measured the force versus separation profiles of individual cylindrical PNIPAM brushes in poor solvent conditions as they are extended between an AFM tip and the substrate. The force-extension behavior of the PNIPAM brushes is qualitatively different in poor solvent conditions from those in good solvents. Force induced globule-to-cylinder conformational changes were observed using the "molecule specific force spectroscopy".

7.6 References

(1) Sheiko, S. S.; Moeller, M. *Chem. Rev.* **2001**, *101*, 4099.

(2) Stephan, T.; Muth, S.; Schmidt, M. *Macromolecules* **2002**, *35*, 9857.

(3) Li, C.; Gunari, N.; Fischer, K.; Janshoff, A.; Schmidt, M. *Angew. Chem. Int. Ed.* **2004**, *43*, 1101.

(4) Rief, M.; Oesterhelt, F.; Heymann, B.; Gaub, H. E. *Science* **1997**, *275*, 1295.

(5) Hugel, T.; Seitz, M. *Macromol. Rapid Commun.* **2001**, *22*, 989.

(6) Haupt, B. J.; Senden, T. J.; Sevick, E. M. *Langmuir* **2002**, *18*, 2174.

(7) Halperin, A.; Zhulina, E. B. *Macromolecules* **1991**, *24*, 5393.

(8) Baumann, C. G.; Bloomfield, V. A.; Smith, S. B.; Bustamante, C.; Wang, M. D.; Block, S. M. *Biophys. J.* **2000**, *78*, 1965.

(9) Pereira, G. G.; Williams, D. R. M. *Biophys. J.* **2001**, *80*, 161.

(10) Craig, A.; Terentjev, E. M. *J. Chem. Phys.* **2005**, *122*, 194901.

(11) Binnig, G.; Quate, C. F.; Gerber, C. *Phys. Rev. Lett.* **1986**, *56*, 930.

(12) Janshoff, A.; Neitzert, M.; Oberdörfer, Y.; Fuchs, H. *Angew. Chem. Int. Ed.* **2000**, *39*, 3212.

(13) Rief, M.; Gautel, M.; Oesterhelt, F.; Fernandez, J. M.; Gaub, H. E. *Science* **1997**, *276*, 1109.

(14) Marszalek, P. E.; Oberdörfer, A. F.; Hongbin, L.; Fernandez, J. M. *Biophys. J.* **2003**, *85*, 2696.

(15) Smith, S. B.; Cui, Y.; Bustamante, C. *Science* **1996**, *271*, 759.

(16) Oesterhelt, F.; Oesterhelt, D.; Pfeiffer, M.; Engel, A.; Gaub, H. E.; D.J., M. *Science* **2000**, *288*, 143.

(17) Hutter, J. L.; Bechhoefer, J. *Rev. Sci. Instrum.* **1993**, *64*, 1868.

(18) Odijk, T. *Macromolecules* **1995**, *28*, 7016.

8 GLOBULE-CYLINDER TRANSITION OBSERVED BY FORCE SPECTROSCOPY

8.1 Introduction

With the advent of experimental techniques employing optical tweezers,[1] atomic force microscope,[2] and micropipipets,[3] able to probe the mechanical response of individual polymers to imposed tension, a systematic study of the complicated, three dimensional structure of interesting polymers is possible. Such experiments give detailed mechanical information on the global statistical conformation of flexible macromolecules as well as direct measurement of their important structural length scales.[4,5] It has also been possible to elucidate the mechanism of some force-driven phase transitions occurring at the single molecule level, the unfolding of the giant titin protein,[6] the stretching of collapsed DNA molecules,[7] and the force induced conformational transitions in Heparin, just to name a few.[8]

Cylindrical brushes consist of a highly stretched main chain the extension of which is caused by steric overcrowding of densely grafted side chains.[9-12] If we assume that such a tightly adsorbed polymer with two chemically different side chains whose mutual interaction parameters can be switched from attractive to repulsive by an external field, such a molecule can undergo a stimulated transition from an extended to a curled conformation. Recently, the synthesis of a polymeric system based on cylindrical polymer brushes with poly-N-isopropylacrylamide (PNIPAM) side chains was reported to exhibit a rod-globule transition upon external stimuli like temperature.[13]

The stretching of chains, which are collapsed in a poor solvent, was first studied theoretically by Halperin and Zhulina, who employed scaling theory arguing that at weak extensions the globule deforms into an ellipsoid and then into a cylinder as shown in the **Figure 8-1.**[14] The interplay of conformational entropy and surface energy gives rise to the three deformation regimes as shown in **Figure 8-1.** The weak deformation of the globule to an ellipsoid is associated with a linear restoring force (region I). For intermediate deformations f is weakly dependent on L and the polymer undergoes a sharp

transition into a "ball-string" conformation. This regime (II) is associated with a conformational transition involving the coexistence of the globule and a stretched string of so called Pincus blobs of size ξ_c. The plateau force is given by $f = kT/\xi_c$, neglecting finite size corrections. Finally for strong stretching the $f \sim L$ behavior of a Gaussian chain is recovered (region III).

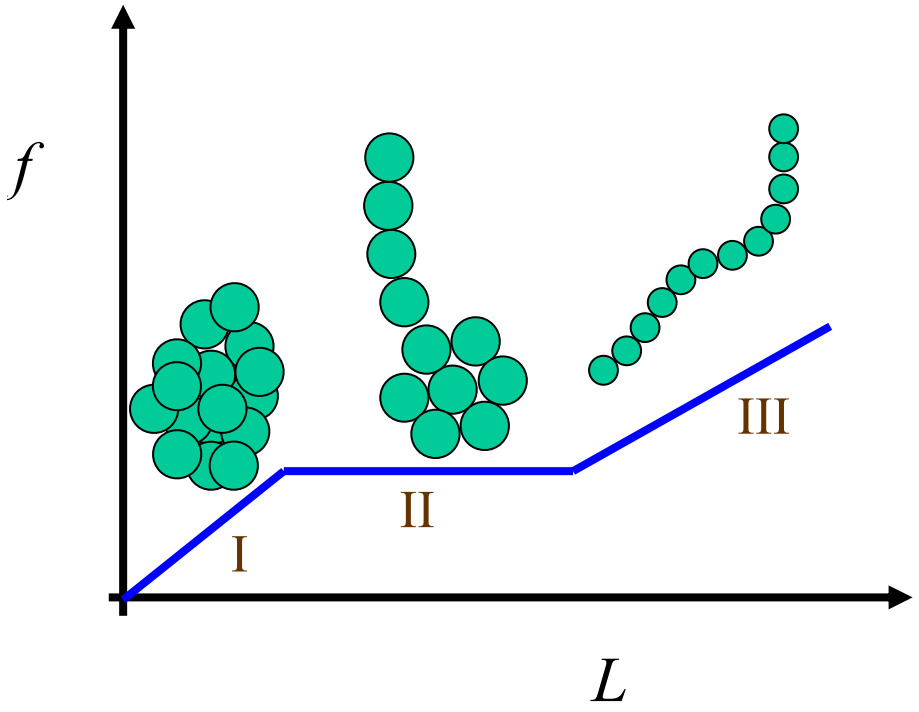

Figure 8-1 *f-L* (force-extension) diagram for the stretching of an isolated collapsed coil ignoring finite size effects. The sketches show the conformations corresponding to the various regimes. The plateau depicting a "ball-string" conformation.

AFM experiments on single globules have focused on protein unfolding,[6] polymer adsorption in poor solvent[15] or mechanical properties of α helices.[16] More recently, Craig et. al. theoretically studied the force extension behavior of polymers collapsed in poor solvent and distinguish between stretching of ordered and disordered globules.[17] They have also modified their theory to include the effects of semiflexibility where stiff

molecules, such as DNA adopt a toroidal conformation in poor solvents. They argue that the stretching of the toroids is similar to those of the globules with some modification in the surface-energy term.

However the experimental confirmation of the plateau forces on stretching individual collapsed globules, predicted initially by Halperin et.al. is missing. Here we describe the mechanical unfolding-folding behavior of single collapsed PNIPAM brush molecules by force spectroscopy using the "fly-fishing" technique. A force plateau ranging from 50-80 pN was observed in the force-extension curves. We also propose a new model for the stretching of the single collapsed brush molecules.

8.2 Experimental

Force Spectroscopy experiments were carried out by dissolving the polymer sample in MilliQ water to a final concentration of ~ 0.1 mg/mL. 50 μL of the aqueous solution were placed on freshly cleaved mica surface, subsequently mounted in a homemade AFM PTFE fluid cell and incubated for 1 h above the lower solution critical temperature (LCST) at 37°C. Prior to incubation the polymer solution, mica surface and fluid cell were placed in the oven at 37 °C overnight. Subsequently, the surface was rinsed with water to remove excess of unbound polymer molecules. Force distance curves were recorded at 38 °C, employing an MFP 3D microscope from Asylum Research, Santa Barbara, USA. Silicon nitride BioLever cantilevers (BL-R150VB-C1), purchased from Olympus, exhibiting a nominal spring constant of ~ 0.02 Nm^{-1} were used. Prior to use the spring constant was determined by thermal noise method[18] as described in chapter 4. All experiments were conducted at 100 nm/s pulling speed, unless mentioned.

8.3 Results and Discussion

Figure 8-2 shows a schematic representation of a cylindrical polymer brush under good solvent and the collapsed conformation under poor solvent conditions. These conformations have been visualized by AFM and the images of a single cylindrical PNIPAM brush molecule and the globular conformation above the LCST are shown

below in **Figure 8-2**. The compactness of the globule is maintained primarily by the hydrophobic effect.

For the characterization of the elastic properties of the collapsed PNIPAM globule, the AFM tip was brought into contact with the sample on the mica surface then kept in contact for 2 s to allow for polymer attachment. Subsequently, the cantilever was retracted. As discussed in chapter 7 the force-extension profile after tip-substrate interaction are somewhat complex (**Figure 7-1c**), consisting of contributions from stretching multiple molecules, adhesion and desorption of the molecule from the substrate. Therefore the elastic properties of the collapsed cylindrical brushes were studied using the "fly-fishing" mode.[19] In this mode the tip was allowed to approach and retract step by step without indenting deep into the sample film until a binding event was registered. If the molecule does not desorb from the tip or the substrate it is possible to repeatedly stretch and relax a single molecule before reaching its rupture limit.

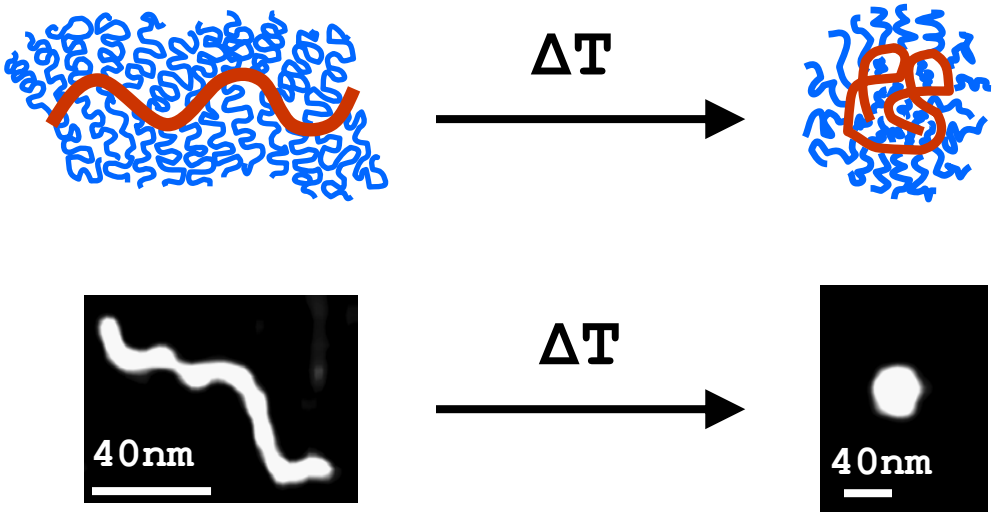

Figure 8-2 Schematic representation of a cylindrical polymer brush in a good solvent (left) and the collapsed conformation in poor solvent (right). Below are the AFM topography images of a single PNIPAM brush

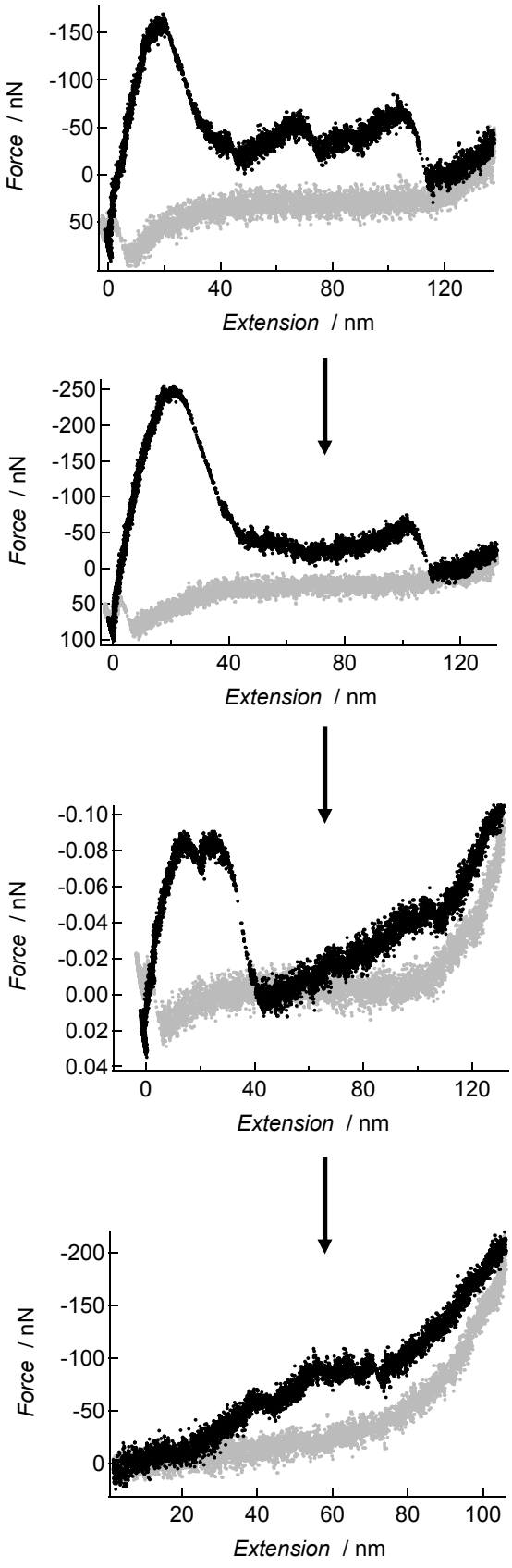
Force / nN
-150
-100
-50
0
50
0
40
80
120
Extension / nm
Force / nN
-250
-200
-150
-100
-50
0
50
100
0
40
80
120
Extension / nm
Force / nN
-0.10
-0.08
-0.06
-0.04
-0.02
0.00
0.02
0.04
0
40
80
120
Extension / nm
Force / nN
-200
-150
-100
-50
0
20
40
60
80
100
Extension / nm

Figure 8-3 A typical sequence of stretch-release cycles in the "fly-fishing" mode for a single collapsed PNIPAM brush molecule.

The "fly-fishing" mode was used in order to minimize multiple attachments to the tip. The typical sequence of stretch-relax cycles involved in the "fly-fishing" mode are shown in **Figure 8-3** wherein a single globule is stretched and subsequently retracted stepwise in order to reduce the adhesive force (to avoid indenting into the sample).

Figure 8-4 shows a typical stretch-release cycle of a single globular PNIPAM brush molecule. At low forces up to 50 pN the stretch curve shows a kind of linear behavior as depicted in the figure from B→C. Unlike the case of good solvent conditions where the stretching behavior at lower forces is dominated by entropy, in the poor solvent case the deformation behavior is dominated by the surface energy. The origin of the linear restoring force is due to stretching of the collapsed brush molecule, resulting in a deformation essentially creating an excess area that leads to an excess surface energy $F \propto \gamma h^2$, where γ is the surface tension and h is the maximal deviation from the flat surface i.e. extension. It should be noted that, $F \cong A\gamma$, where A is the area and $A \approx h^2$. Thus in this part of the curve the collapsed globule is deformed into an ellipsoid.

Subsequently, with further extension (40–70 nm) a plateau force of ≈ 50 pN was observed as shown in the **Figure 8-4** (C→D). At 40 nm extension length, one of the ends of the molecule is pulled out of the globule and stretched segment-by-segment. Thus there is a weak dependence of F on h. This could be the reason why a plateau force is observed on stretching the molecule (i.e. from extension length 40-70nm) and my display the coexistence of the densely collapsed brush and stretched segments. With further extension, the tip is able to provide the necessary energy to the molecule to overcome the energy barrier and the brush with collapsed side chains is stretched further giving rise to a linear increase in force, from (D→E). Subsequently, the molecule is relaxed and the curve follows the path (E→F). Clearly, a hysteresis is observed with no force plateau during the relaxation path.

The Halperin model cannot be applied because the collapsed polymer brushes because it is not likely to form a unique blob size for the side chains and the main chain simultaneously. Thus a new approach is used:

8-4)

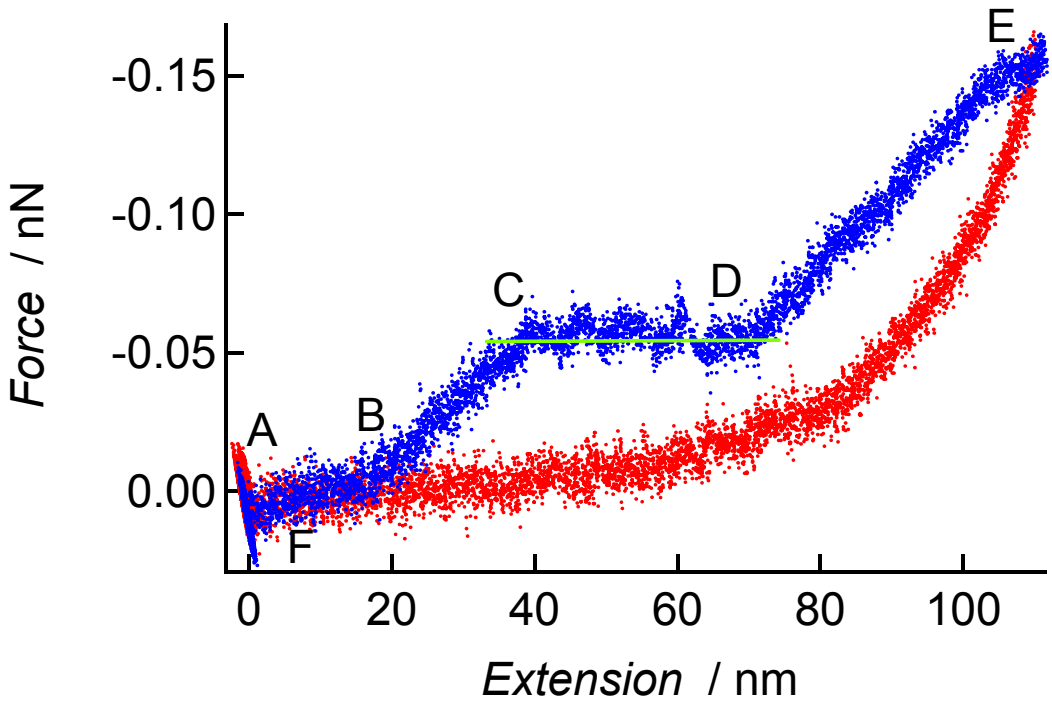

Figure 8-4 A typical stretch-relax cycle for the collapsed brush molecule in poor solvent poor solvent conditions. The detailed description is given in the text.

8.4 Scaling theory

The simplest assumption is that the side chains attract each other and overcome the stiffness of the main chain. The experiment suggests that the whole polymer forms a uniform globule induced by the side chain attraction along the entire polymer contour. This is most likely when the grafting density is very high, for example when practically each monomer contains a branch of side chain of M segments. Therefore the side chains cannot collapse inside themselves. Instead the chain forms a "super chain" with a certain diameter R_0, where R_0 is defined by the actual conformation of the side chains. The latter depends naturally on the nature of the solvent for the side chains. For densely grafted

chains in a good solvent, the diameter has been worked out using the Daoud – Cotton model, to be $R_0 \cong b\sigma^{1/4}M^{3/4}$, where b is the Kuhn step length and σ the grafting density (per unit length). This radius defines the effective thickness of the worm like chain, whose effective persistence length is given by $l_p \cong b\sigma^{17/8}M^{15/8}$. This thick chain forms in a good solvent now a semi-flexible chain, with the usual scaling in the long chain limit for a good solvents, i.e., $R_g \cong l_p\left(L/l_p\right)^{3/5}$, and $\left(L/l_p\right)>>1$, where $L = bN$ is the total length of the main chain, containing N segments. For shorter chains the overall radius of gyration is given by the result of the worm like chain. When the side chains collapse onto each other, the effective persistence length becomes reduced. Under the assumption of side chain collapse the new thickness of the chain can be estimated to $R_c \cong b\sigma^{1/4}M^{1/2}$, which yields a strongly reduced persistence length $l_p^c \cong b\sigma^{19/8}M^{5/4}$. Further we assume, according to the **Figure 8-2 (**AFM image of the collapsed brush molecule) that the chain collapses into a size $R_{coll} \cong l_p^c\left(L/l_p^c\right)^{1/3} \propto b\sigma^{19/12}M^{5/6}N^{1/3}$. Under external force this collapsed (wormlike) chain follows now a similar stress strain relation like the simple chain in a poor solvent. The force increases up to a certain value, then the chain becomes extended and reaches a plateau value of $f_{plateau} \approx kT/l_p^c$ before the main chain itself becomes extended, following for $f > f_{plateau}$ the WLC model.

The schematics of the stretching of the globule (A→E) can be understood as shown in **Figure 8-5**. The black parallel lines, shown in the schematics from (C→D) describe the segment-by-segment stretching out of the brush molecule. The coexistence of the stretched segments and the compact globule can be realized in this picture (C→D). This stretch-release cycle is entirely reproducible; **Figure 8-6** shows the superposition of 3 stretch-release cycles. In each case the energy expended in the deformation is greater than that recovered on relaxation.

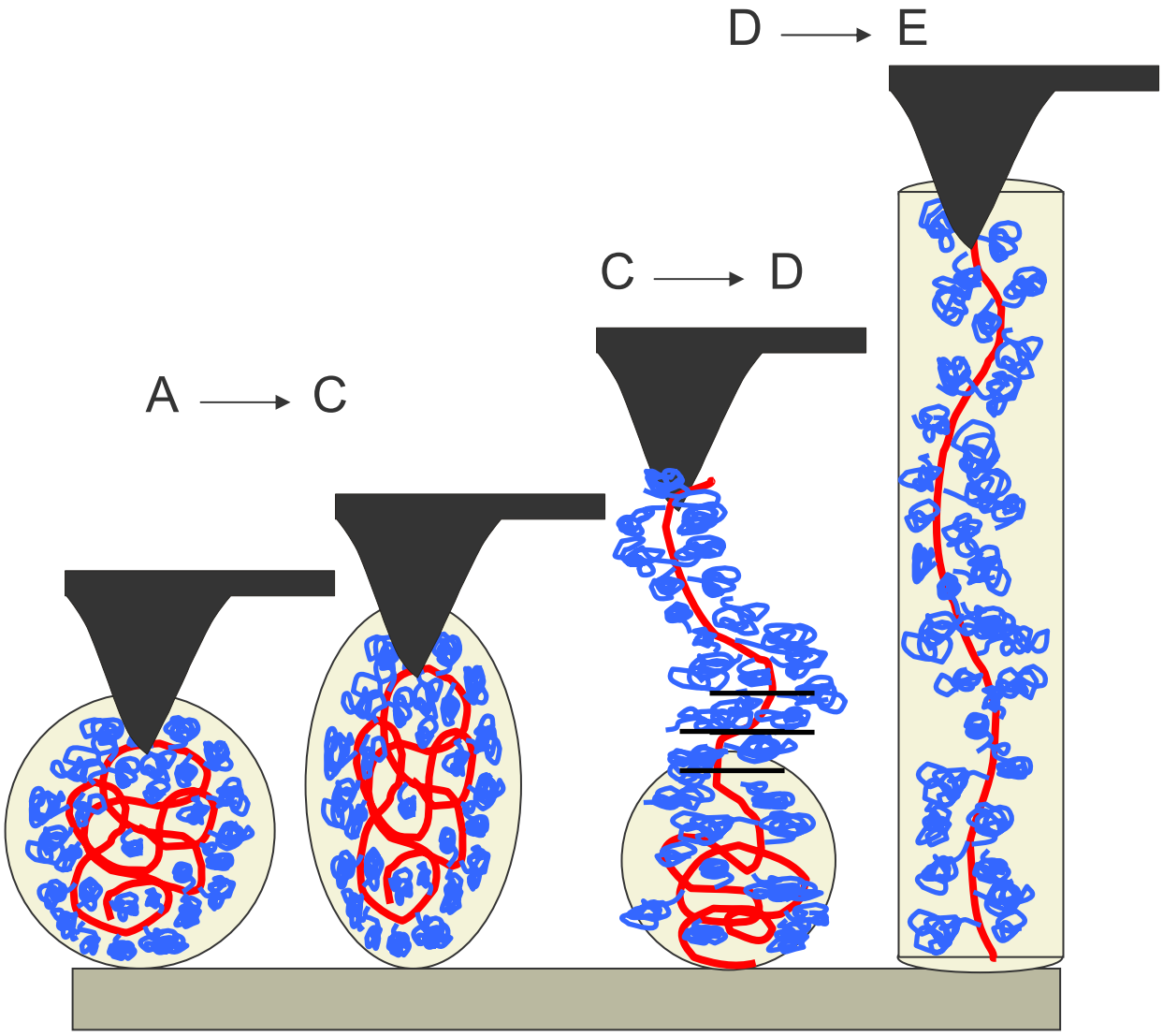

Figure 8-5 Schematics of the stretching of the globule.

8-6)

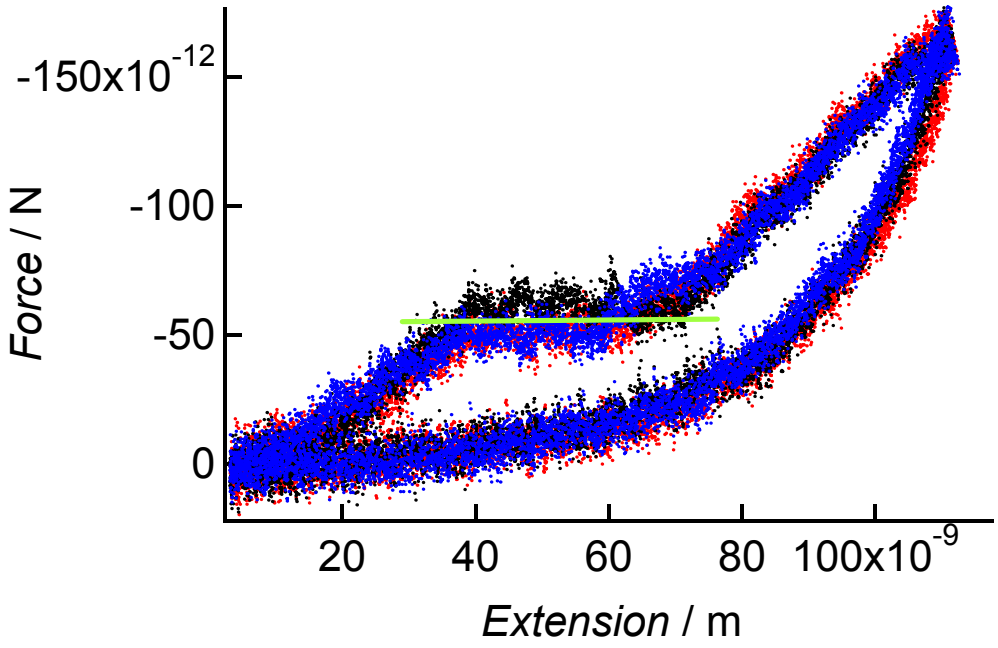

Figure 8-6 Superposition of three stretch-release cycles.

Stretch-relax curves were also obtained at pulling speeds merely of 5 nm/s. These curves not only demonstrated reduced plateau force ~ 20 pN but also a reduction in energy dissipation. From the scaling arguments $f_{plateau} \approx kT/l_p^c$, thus yieliding a persistence length of the collapsed brush molecule in the range 2-0.5 nm, results in a plateau force in the range of 2-8 pN in the quasi-static limit, i.e., zero pulling speed, which is in the range of the experimentally determined plateau force ~ 20 pN at 5 nm/s pulling speed. Most of the stretch-release cycles displayed no hysteresis at all as shown in **Figure 8-7**. This shows that the relaxing of the unwound globule depends on the pulling speed and that a pseudo-equilibrium is realized at low pulling speed.

8-7)

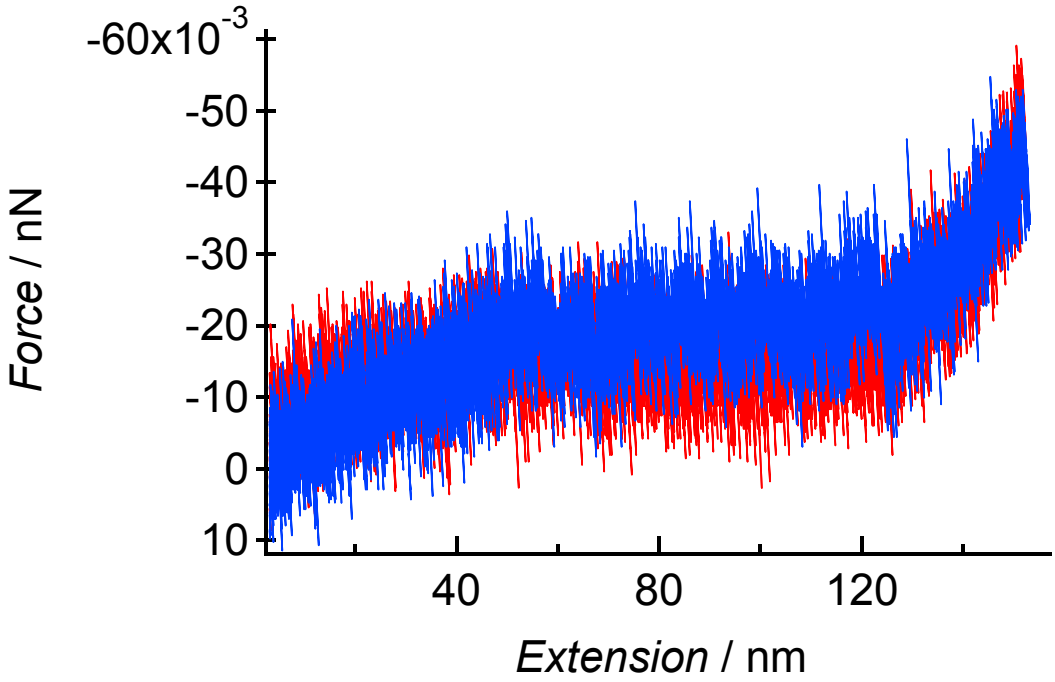

Figure 8-7 A stretch-release cycle measured at a pulling speed of 5 nm/s. No hysteresis between stretch release cycle is observed.

8.5 Conclusions

We have measured the stretch-release cycle of a single collapsed PNIPAM brush globule by force spectroscopy using the "fly-fishing" mode. We observe a force plateau in the stretch curve of a single collapsed PNIPAM brush globule, which is suggestive of a "ball-string" conformation. We also show that the unfolding-folding transitions of a collapsed PNIPAM brush molecule are dependent on the pulling speed. The plateau forces experimentally obtained at low pulling speeds (5 nm/s) are in the range as predicted by theory.

8.6 References

(1) Svoboda, K.; Block, S. M. *Annu. Rev. Biophys. Biomol. Struct.* **1994**, *23*, 247.

(2) Binnig, G.; Quate, C. F.; Gerber, C. *Phys. Rev. Lett.* **1986**, *56*, 930.

(3) Kishino, A.; Yanagida, T. *Nature* **1988**, *334*, 74.

(4) Janshoff, A.; Neitzert, M.; Oberdörfer, Y.; Fuchs, H. *Angew. Chem. Int. Ed.* **2000**, *39*, 3212.

(5) Hugel, T.; Seitz, M. *Macromol. Rapid Commun.* **2001**, *22*, 989.

(6) Rief, M.; Gautel, M.; Oesterhelt, F.; Fernandez, J. M.; Gaub, H. E. *Science* **1997**, *276*, 1109.

(7) Baumann, C. G.; Bloomfield, V. A.; Smith, S. B.; Bustamante, C.; Wang, M. D.; Block, S. M. *Biophys. J.* **2000**, *78*, 1965.

(8) Marszalek, P. E.; Oberdörfer, A. F.; Hongbin, L.; Fernandez, J. M. *Biophys. J.* **2003**, *85*, 2696.

(9) Wintermantel, M.; Schmidt, M.; Tsukahara, Y.; Kajiwara, K.; Kohjiya, S. *Macromol. Rapid Commun.* **1994**, *15*, 279.

(10) Wintermantel, M.; Fischer, K.; Gerle, M.; Ries, E.; Schmidt, M.; Kajiwara, K.; Urakawa, H.; Wataoka, I. *Angew. Chem. Int. Ed.* **1995**, *34*, 1472.

(11) Zhang, M.; Müller, A. X. E. *J.Polym. Sci. A: Polym. Chem* **2005**, *43*, 3461.

(12) Sheiko, S. S.; Moeller, M. *Chem. Rev.* **2001**, *101*, 4099.

(13) Li, C.; Gunari, N.; Fischer, K.; Janshoff, A.; Schmidt, M. *Angew. Chem. Int. Ed.* **2004**, *43*, 1101.

(14) Halperin, A.; Zhulina, E. B. *Eurphys. Lett.* **1991**, *15*, 417.

(15) Haupt, B. J.; Senden, T. J.; Sevick, E. M. *Langmuir* **2002**, *18*, 2174.

(16) Müller, D. J.; Kessler, M.; Oesterhelt, F.; Möller, C.; Gaub, H. E. *Biophys. J.* **2002**, *83*, 3578.

(17) Craig, A.; Terentjev, E. M. *J. Chem. Phys.* **2005**, *122*, 194901.

(18) Hutter, J. L.; Bechhoefer, J. *Rev. Sci. Instrum.* **1993**, *64*, 1868.

(19) Rief, M.; Oesterhelt, F.; Heymann, B.; Gaub, H. E. *Science* **1997**, *275*, 1295.

9 CONFORMATION AND ELASTICITY OF POLY - L - LYSINE CYLINDRICAL BRUSHES BY AFM

9.1 Introduction

Cylindrical polymer brushes or sometimes called bottle brushes, are long chain molecules consisting of a flexible backbone densely grafted with relatively long side chains provided that the main chain is much longer than the side chain.[1-4] In the presence of excluded volume interactions, the densely grafted side chains try to avoid strong overlapping, which induces an extremely high chain stiffness of the backbone. Cylindrical brushes with polyelectrolyte side chains are known as cylindrical polyelectrolyte brushes. Typical linear polyelectrolyte chains exhibit a charge density of one ionic charge per 0.25 nm contour distance or less, while the effective charge density of a cylindrical polyelectrolyte brush is much smaller than for linear polyions. However the charge density along the contour of the main chain is significantly higher than for a linear flexible chain.[5]

For any practical application of polyelectrolyte brushes the influence of multivalent ions, hydrophobic ions and the polyelectrolyte-surface interactions is of utmost importance. In particular the study of interactions of cylindrical polyelectrolyte brushes with charged biomolecules such as DNA, which might open a path for the understanding and the preparation of nonviral gene delivery systems and for optimizing the transfection efficiency.[6] Recently cylindrical brushes with polypeptide side chains were synthesized and were shown to exhibit a worm-like chain conformation. These molecules are of special interest because the effect of the helix-coil transition of the side chains on the main chain conformation can be studied.[7]

The adhesive behavior of polyelectrolytes is of central importance. Due to their unique adsorption properties at interfaces, synthetic polyelctrolytes are used in numerous industrial applications such as mineral separation, flocculation or as additives in paper production. The elasticity and desorption behavior of linear single polyelectrolyte chains

has been studied in detail, wherein linear polyvinylamine (PVA) chains physisorbed to an oppositely charged surface were probed.[8] The adsorption behavior of polyelectrolytes brushes is a complex issue and is often governed by electrostatic and hydrophobic interactions of the polyelectrolyte molecules with the charged surface. Since physisorbed polyelectrolyte cylindrical brushes exhibit a worm-like chain conformation, the desorption of these brushes could give insight into the effect of the polyelectrolyte topology on the adhesion forces on a solid support. The polylysine side chains strongly adsorb to the mica surface.

The development of new experimental tools, such as the atomic force microscope (AFM),[9] not only allows imaging but also mechanical interrogation of single molecules and macromolecular complexes under near-physiological conditions. It allows the measurement of intra- and intermolecular forces ranging from the pN-regime,[10,11] e.g. receptor-ligand systems to the nN-regime that is reached when single covalent bonds are ruptured. Polyelectrolyte desorption has already been monitored by single molecule force spectroscopy.[8] Recently the mechanical properties of single cylindrical polymer brushes with poly-isopropylarcylamide (PNIPAM) side chains were probed by AFM on mica surface. The imaging and stretching in aqueous solution clearly revealed the semiflexible nature of the cylindrical macromolecules exhibiting a "true" persistence length as high as 140 nm.[12]

Here we investigate the conformation of the polylysine cylindrical brushes under aqueous environment using AFM. The desoprtion of the physisorbed molecules on the mica surface is studied to obtain the adhesion forces and also to elucidate the entropic and enthalpic restoring forces as predicted by the extensible worm like chain model.

9.2 Experimental

Recently the synthesis of the poly-L-lysine cylindrical brushes using "grafting from" technique was reported by Zhang et. al.[7] **Scheme 8-1** shows the schematics of the cylindrical polymer brush with poly-L-lysine side chains. Tapping mode and contact mode imaging in aqueous solution was performed by placing the freshly cleaved mica in a homemade AFM PTFE fluid cell and introducing 100 μL droplet of MilliQ water.

While imaging the dilute polyelctrolyte solution was injected and the conformation of the molecules were observed without drying.

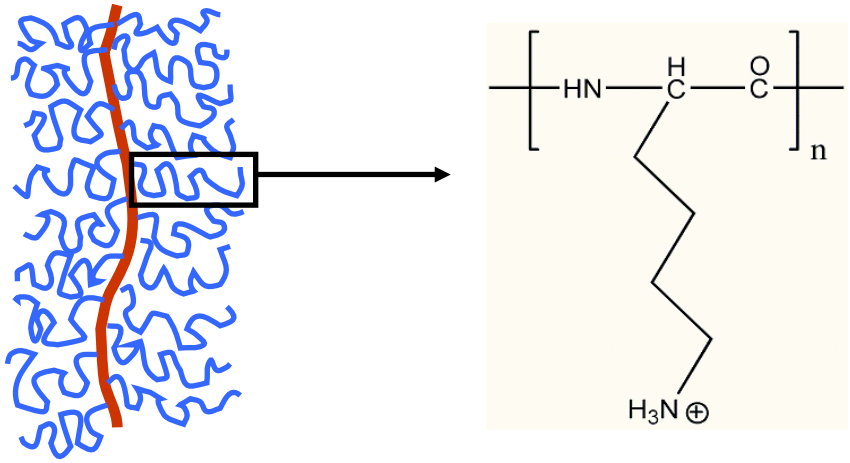

Scheme 9-1 Schematics of a cylindrical polyelectrolyte brush with poly-L-lysine side chains.

Force Spectroscopy experiments were carried out by dissolving the polyelectrolyte in MilliQ water at a concentration of ~ 0.1 mg/mL. 50 µL of the aqueous solution were placed on freshly cleaved mica mounted in a homemade AFM PTFE fluid cell and incubated for 1 h. Subsequently the surface was rinsed with water to remove excess of unbound polymer molecules. Force distance curves were recorded at 20 °C, in 1mM NaCl solution employing an MFP 3D microscope from Asylum Research, Santa Barbara, USA. V-shaped silicon nitride cantilevers purchased from Olympus exhibiting a nominal spring constant of 0.02 Nm^{-1} were used. Prior to use the spring constant was determined by the thermal noise method.[13]

9.3Results and Discussion

9.3.1 AFM imaging in solution

Figure 9-1a shows a height image of the cylindrical polylysine brushes imaged in MilliQ water using intermittent contact mode exhibiting an average height of 1.5 nm. The worm-like chain conformation is retained even under water. **Figure 9-1b** shows a phase image of the cylindrical polylysine brushes recorded in aqueous solution. wherein the **Figure 9-1c** shows a contact mode deflection image taken at higher scan rates (3hz) and a deflection set point of 0.1 V. **Figure 9-1d** shows a contact mode deflection image taken at lower scan rates (1hz) and a deflection set point of 0.5 V. The long cylindrical molecules are observed with a hint of a helical conformation in **Figure 9-1d**. This could be a tip-induced effect as no helicity was observed in light tapping mode. Finally the polylysine brushes were imaged under water using lateral force microscopy in presence of 1mM NaCl with low scan rates (0.8Hz) and a deflection set point of 1V. **Figures 9-1e-f** show the height and friction images in 1mM NaCl solution. The backbone and the side chain corona are clearly visible in the friction image. Even though the friction forces are damped under water it was possible to resolve the side chain corona.

9-1a)

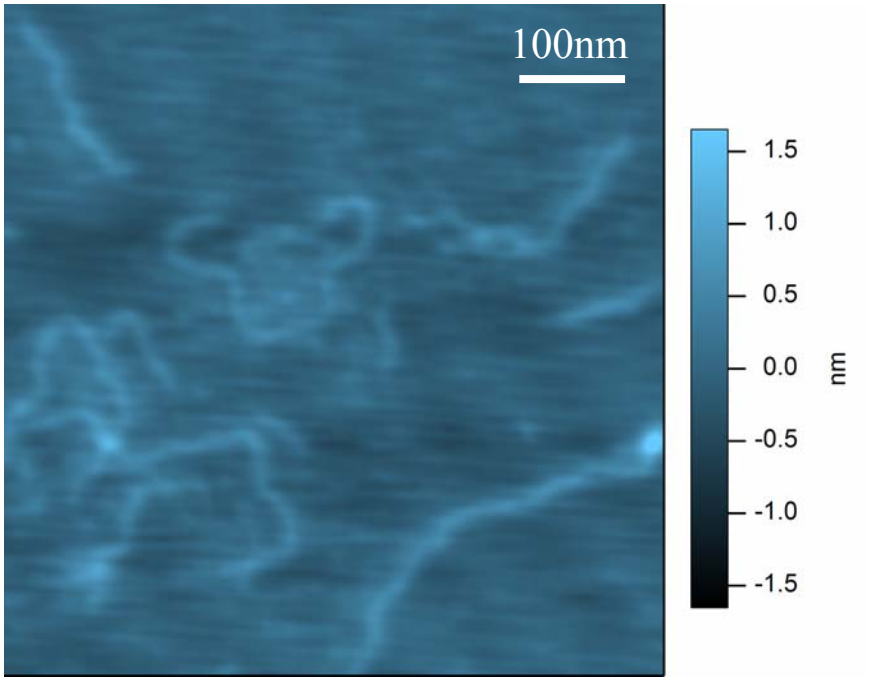

b)

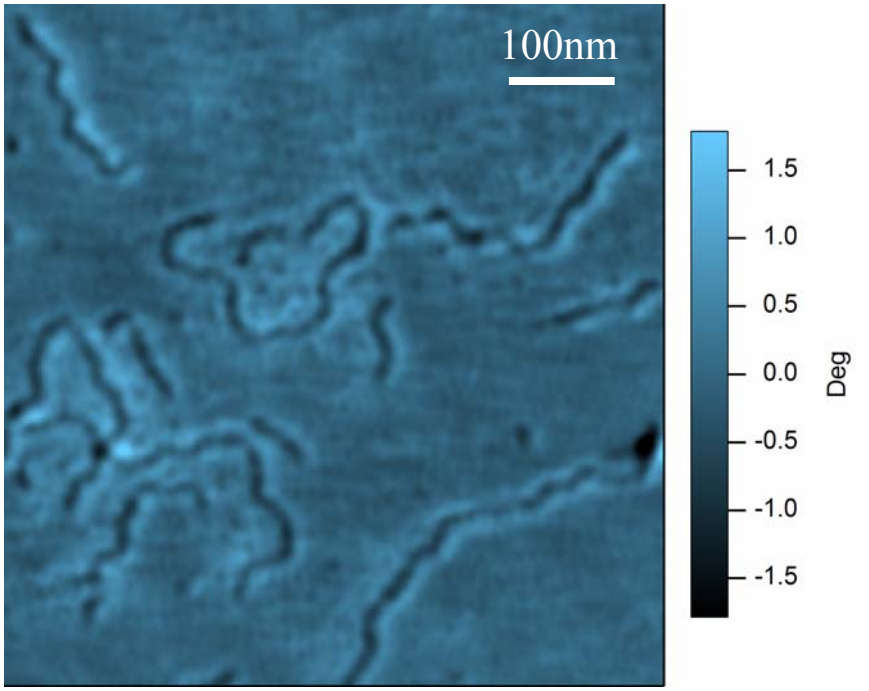

c)

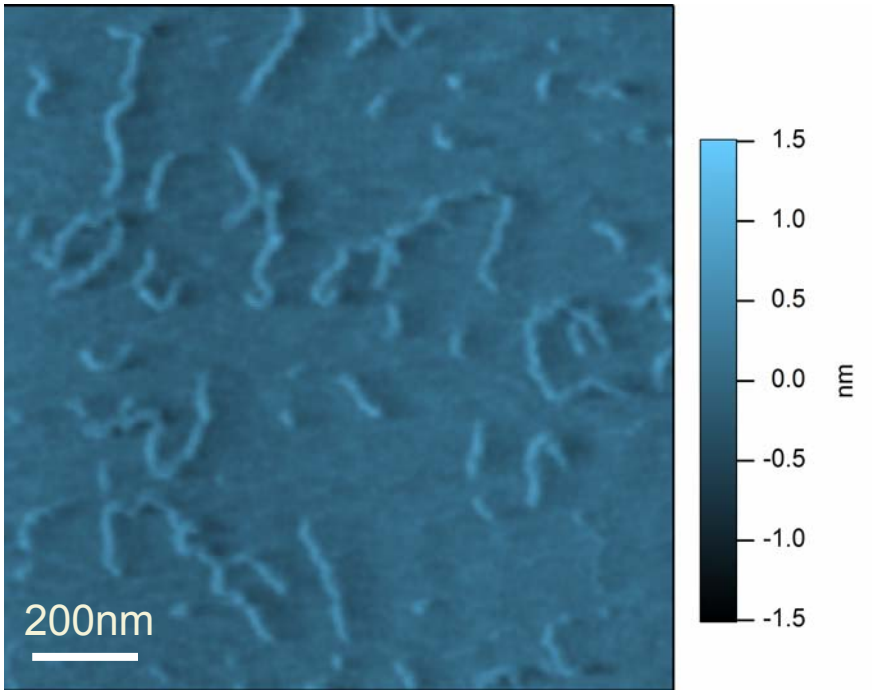

d)

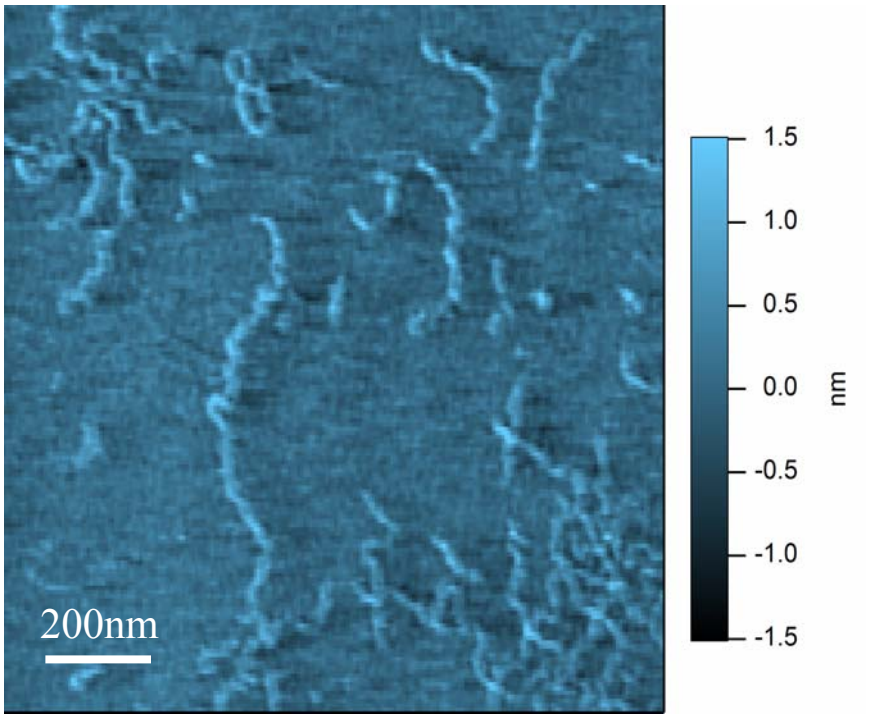

e)

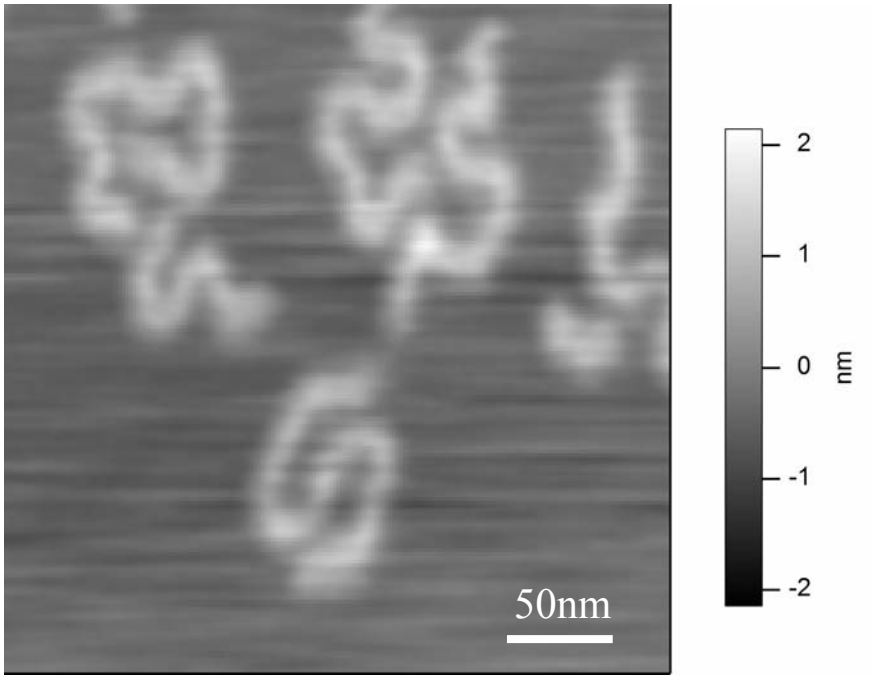

f)

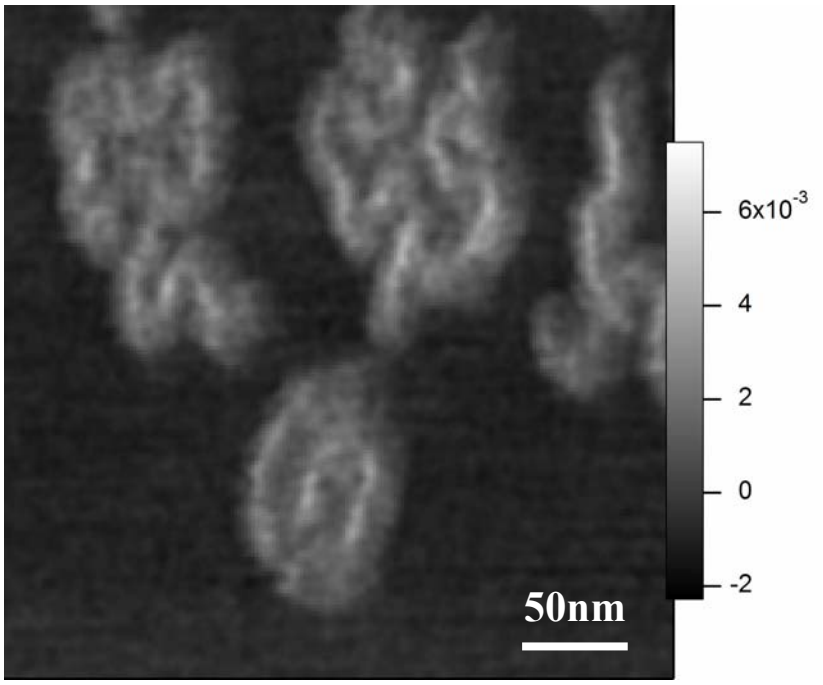

Figure 9-1a) AFM height image of height cylindrical poly-L-lysine brush molecules in aqueous solution. b) AFM phase image of phase cylindrical poly-L-lysine brush molecules in aqueous solution. c) Contact mode AFM deflection image taken with scan rate 3Hz. d) Contact mode AFM deflection image taken with scan rate 1 Hz. d) AFM height image of cylindrical poly-L-lysine brush molecules in 1mM NaCl solution. e) AFM lateral force image of the cylindrical poly-L-lysine brush molecules in 1mM NaCl solution showing the side chain corona.

9.3.2 Qualitative analysis of desorption of individual poly-L-lysine cylindrical brushes

Figures 92a-d show the different classes of events typically observed in desorption experiments of the cylindrical poly-L-lysine brushes in aqueous solution. A total of n = 1100 force curves are considered and trace and retrace curves are shown in the following graphs. **Figure 9-2a** shows a force extension curve in which no desorption event was observed that is there was no interaction of the tip with the molecule. The

absence of stretching events is found in only 25% of all curves. 10 % of these curves showed a large nonspecific adhesion which is observed between 0-120 nm extension length with adhesion forces up to ~ 1 nN. **Figure 9-2b** shows the discontinuous desorption of the polylysine cylindrical brush from the surface. The force curve basically reflects a plateau like shape originating from the rupture of several bonds. 20% of all the force extension curves exhibited such a discontinuous desorption process. The plateau with a constant force can be interpreted as continuous desorption,[8] wherein the consecutive rupturing of very many bonds is monitored. Such a typical plateau is shown in **Figure 9-2c**. The height of the desorption plateau reflects the equilibrium desorption force required to peel the polymer off the surface segment by segment. 30 % of the curves showed such a behavior. Desorption of multiple molecules is unavoidable and is shown in **Figure 9-2d.** The figure shows the desorption of two molecules of different length. Around 10 % of the force extension curves showed multiple desorption events. Finally it was also possible to stretch individual polylysine molecules. **Figure 9-2e** shows a stretch event in which a polymer bridge is formed between the tip and the substrate. 15 % of all the curves showed such stretch events.

9-2a)

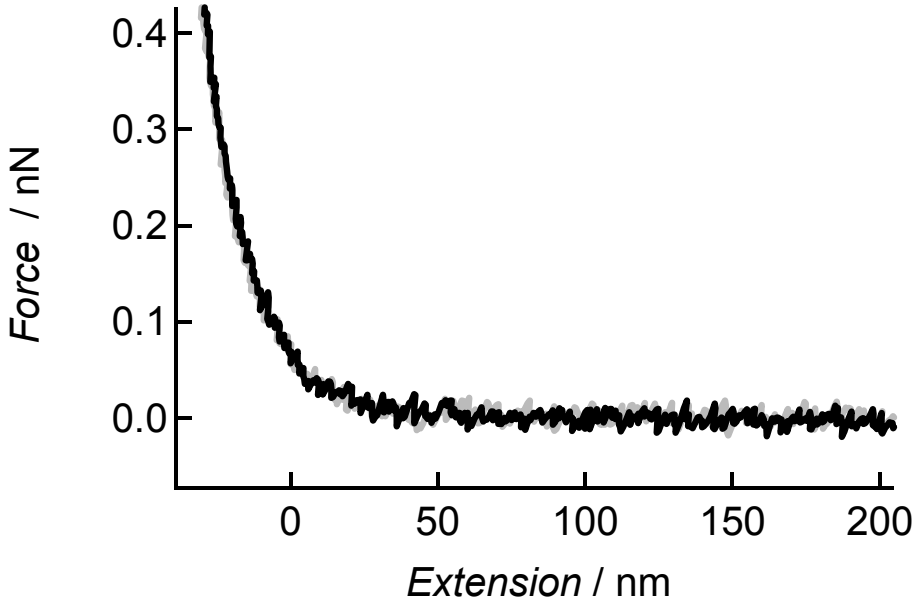

b)

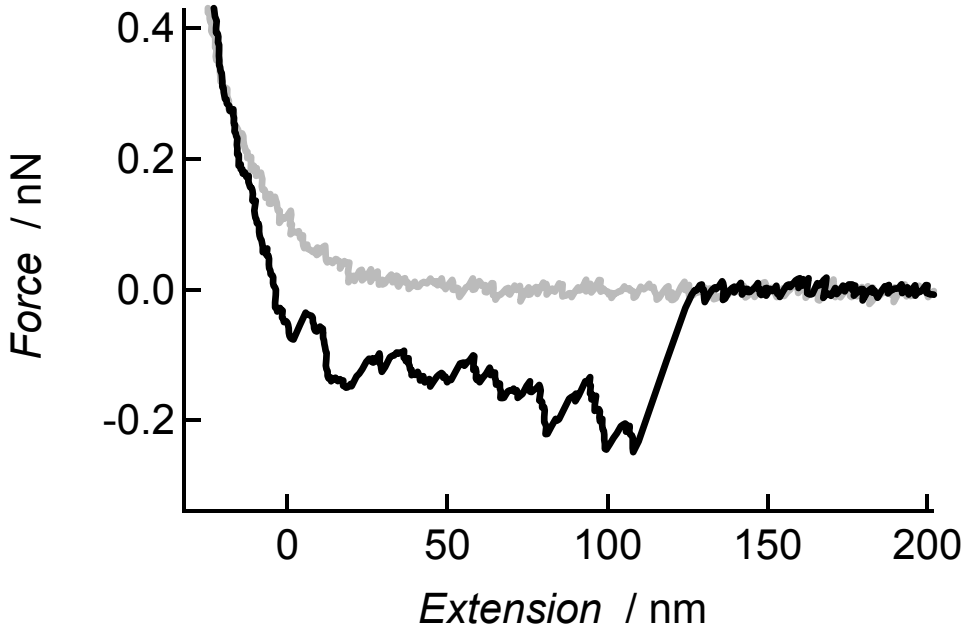
0.4
0.2
0.0
-0.2
Force / nN
0
50
100
150
200
Extension / nm

c)

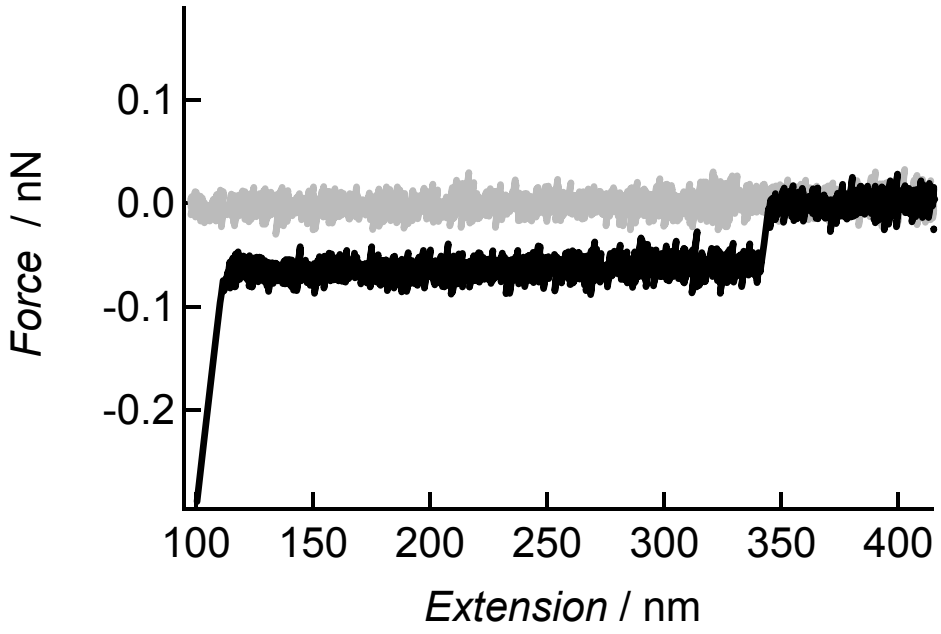
0.1
0.0
-0.1
-0.2
Force / nN
100
150
200
250
300
350
400
Extension / nm

d)

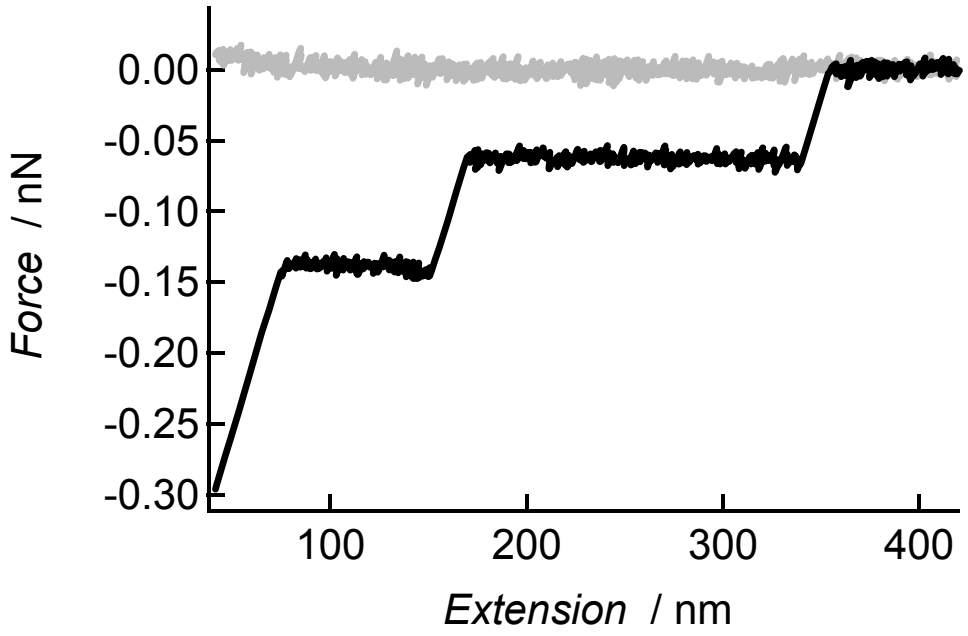
0.00
-0.05
-0.10
-0.15
-0.20
-0.25
-0.30
Force / nN
100
200
300
400
Extension / nm

e)

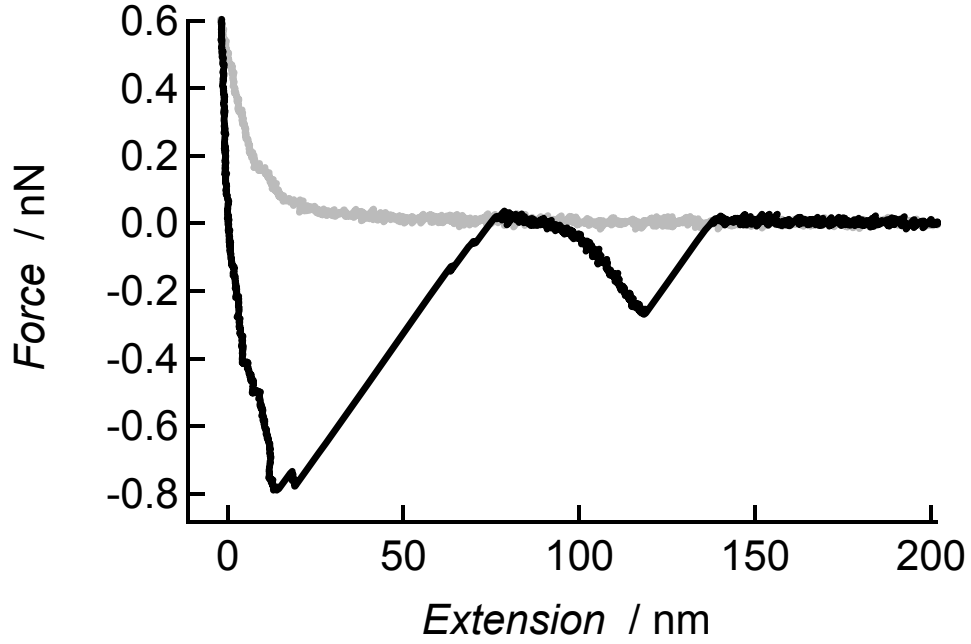
0.6
0.4
0.2
0.0
-0.2
-0.4
-0.6
-0.8
Force / nN
0
50
100
150
200
Extension / nm

Figure 9-2: a) Force extension curve representing 25 % of all curves (*n* = 1100) showing no desorption or stretching event. b) Discontinuous desorption of an individual cylindrical poly-L-lysine brush molecule (20 % of the force spectroscopy experiments). c) Plateau event with constant force interpreted as continuous desorption (30 % of all force curves). d) 14 % of all force curves display multiple desorption events in which two molecules are involved. e) Shows a stretch event in which a polymer bridge is formed between the tip and the sample. (15% of all curves show stretch events)

The desorption forces were observed to lie in between 50-150 pN. The average desorption force obtained by SMFS experiments was 70 pN. A pH dependence on the desorption forces was however not studied. Also a systematic desorption length analysis was performed. **Figure 9-3a** shows the histogram of desorption lengths with an average desorption length L^* = (167.4 ± 9.5) nm. In order to compare the desorption length with the actual contour length of the molecule derived from the AFM images under water a systematic contour length analysis was carried out on the images. The image size used for the analysis was 1×1 μm^2 with 512×512 pixels. Bends in the range below 2 nm can thus not be resolved. **Figure 9-3b** shows the histogram of the contour lengths measured from the images taken in air, yielding a weight average contour length L_w^{AFM} = (292.5 ± 14) nm and a polydispersity of $L_w L_n^{-1}$ = 1.16 (assuming a normal distribution). It can be observed that the average desorption lengths are much smaller the average contour lengths of the molecule, as expected.

9.3.3 Molecule Specific Force Spectroscopy

In order to study the desorption process in more detail, a controlled desorption experiment was carried out. An imaging-stretch-imaging experiment, which combines the two techniques of AFM and SMFS was performed to observe the desorption process *in situ*. **Figure 9-4a** shows an intermittent contact mode AFM height image of the

polylysine cylindrical brushes. The worm-like chain conformation is clearly observed. The contour length of the molecule of interest is ~100 nm.

9-3 a)

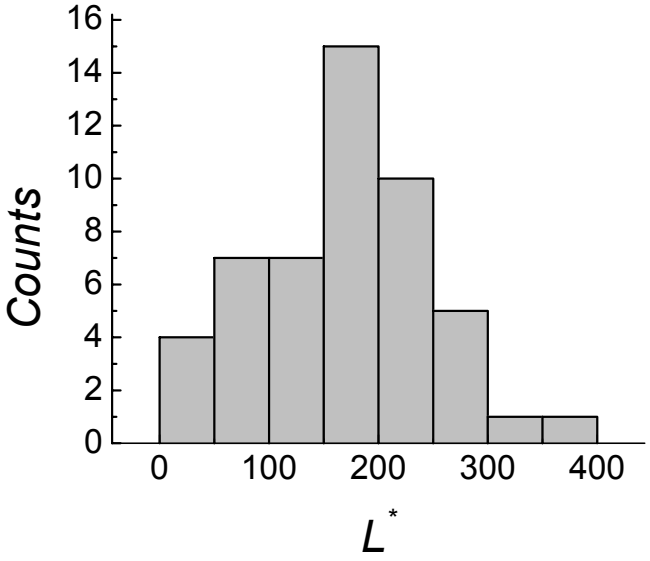

b)

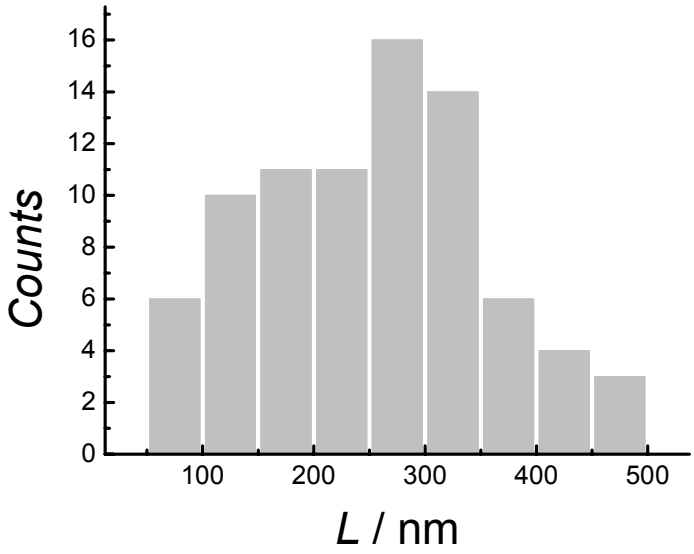

Figure 9-3 a) Histogram of desorption lengths, with average desorption length L^* = 167.4 ± 9.5 nm. b) Histogram of contour lengths from AFM images with average contour length L = (292.5 ± 14) nm.

After imaging, the AFM stylus was positioned over this cylindrical brush molecule and pressed onto the molecule as indicated by the arrow in the image with a force of ~ 1nN for about 1s after which the tip was retracted. **Figure 9-4b** shows the discontinuous desorption event on retracting the tip from the surface. The desorption length from the force extension curve is ~ 50 nm. Now the instrument is switched back to intermittent contact mode and the image is taken of the same molecule at exactly the same position. **Figure 9-4c** shows the AFM height image after manipulation. It is observed that only 50 % of the molecule was desorbed while the rest of the contour remains unaffected.

It is possible to evaluate the persistence length l_p of the molecules from the AFM images in the framework of the WLC model. The method relies on the equation of Kratky-Porod, which relates the end-to-end distance $\langle R^2 \rangle$, the contour length L and the persistence length in two dimensions (equation (2)):[14]

$$\langle R^2 \rangle_{2D} = 4 l_p L \left(1 - \frac{2 l_p}{L} \left(1 - e^{-\frac{L}{2 l_p}} \right) \right) \qquad (1)$$

The wormlike nature of the polymer is clearly visible in the AFM images and the persistence length was analyzed by means of equation (1). **Figure 9-5** shows a graph of end-to-end distance $\langle R^2 \rangle$ as a function of contour length as well as the corresponding fit of equation (1). The persistence length obtained from the fit was l_p = (24.7 ± 5) nm.

However, determination of the persistence length using AFM images has a serious drawback related to the interaction of the molecules with the substrate.[12] As a consequence, it is appropriate to measure force extension curves of the molecule by employing single molecule force spectroscopy (SMFS) enabling one not only to determine the persistence of the molecule in a more direct manner but also to explore the

4a)

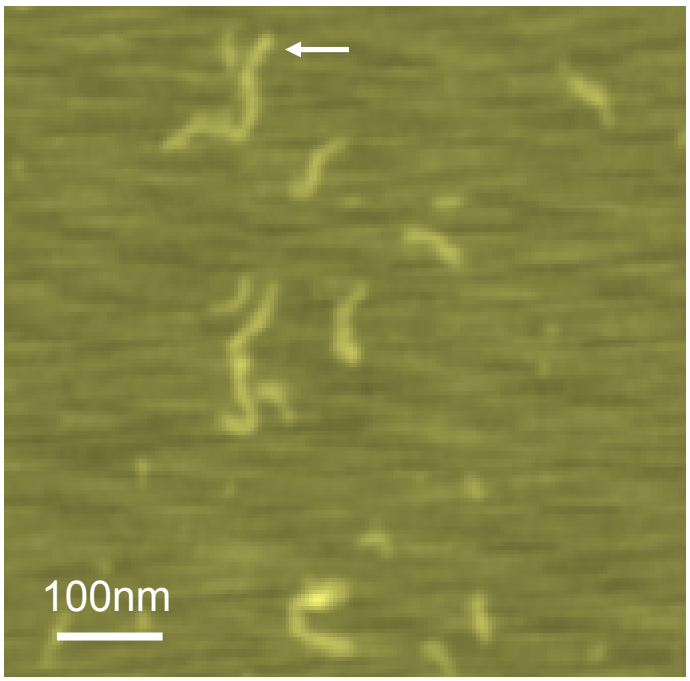

b)

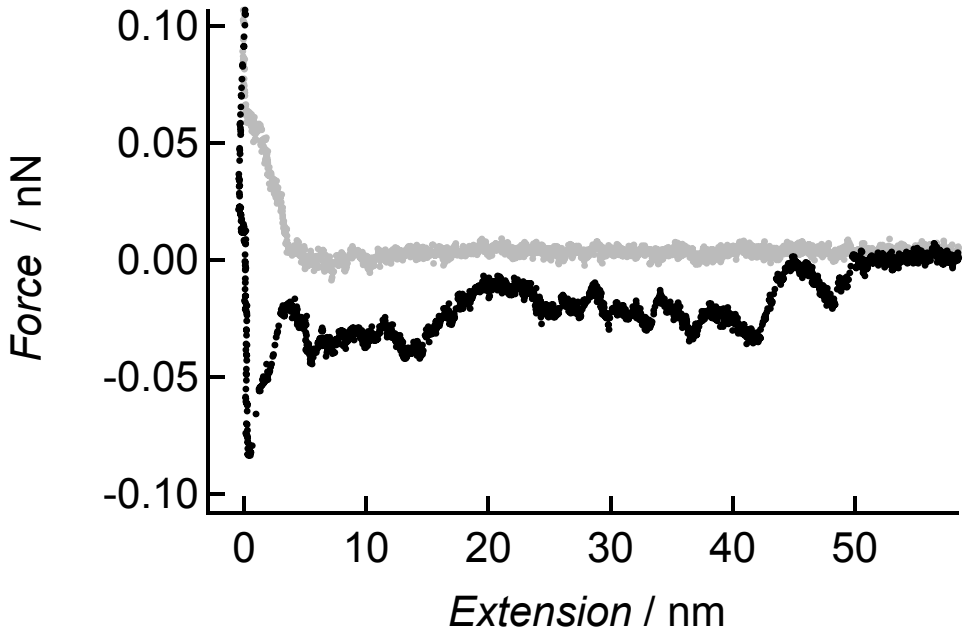

c)

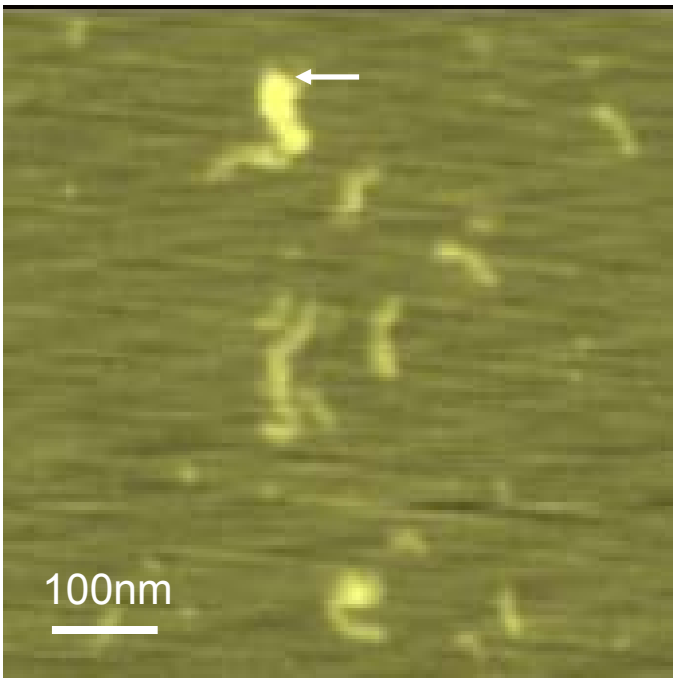

Figure 9-4a) AFM height image of the poly-L-lysine cylindrical brush molecules under aqueous solution. The arrow indicates the molecule chosen for manipulation. b) Force-extension curve showing discontinuous desorption event. c) AFM height image after manipulation. The arrow indicates the molecule manipulated.

mechanical properties of the cylindrical polylysine brushes also in a force regime beyond the pure entropic restoring forces.

9.3.4 Elasticity of single polylysine cylindrical brushes

The elastic properties of the polylysine were probed by stretching individual molecules. It should be noted that the force extension profiles recorded were rather complex consisting of contributions from the substrate and /or tip, from bond rupture of short strands, as well as from entanglements.

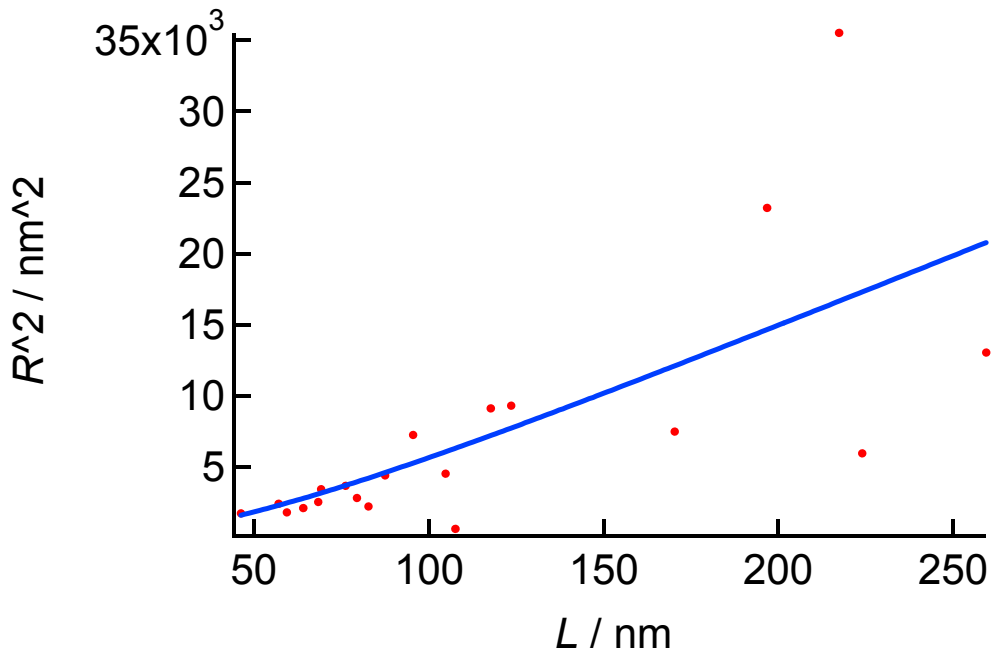

Figure 9-5 Mean-square end-to-end distance $\langle R^2 \rangle$ as a function of brush contour length *L*. The continuous blue line is the corresponding fit of equation (1) yielding a persistence length of l_p = (24.7 ± 5) nm.

Therefore the elastic properties of the cylindrical brushes were studied using the "fly-fishing" mode.[15] In this mode the tip was allowed to approach and retract step by step without indenting into the sample film until a binding event was registered. Thus it is possible to repeatedly stretch and relax a single molecule before reaching its rupture limit. The "fly-fishing" mode was used in order to minimize multiple attachments to the tip.

In the "fly-fishing" mode two types of force extension curves were observed. **Figure 9-6a** shows the force-extension curves on stretching and subsequently on relaxing the same cylindrical brush molecule at a pulling speed of 100 nms^{-1}. The two curves are superimposable showing that the stretching of the cylindrical polylysine brush molecules is completely reversible. The black curve is the stretch curve while the grey is that of the

relaxing curve. The second type shown in **Figure 9-6b** was observed when the molecule was stretched beyond

9-6 a)

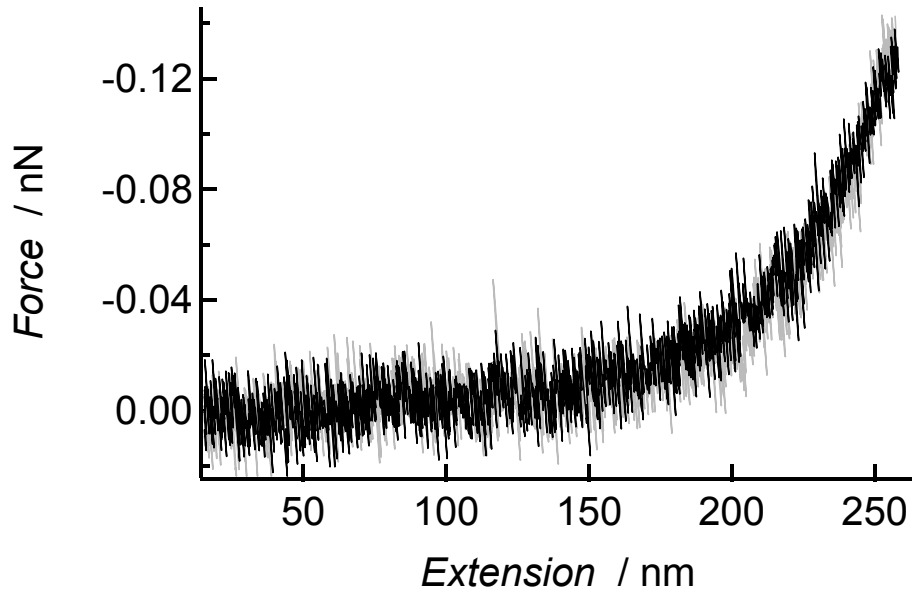

b)

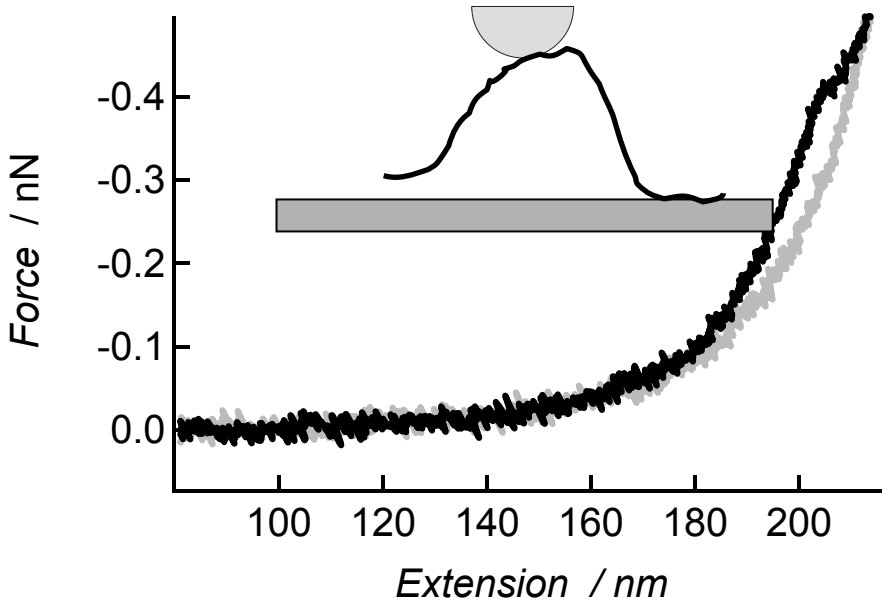

Figure 9-6 a) Force-extension curve of a single poly-L-lysine brush molecule measured in the "Fly-Fishing" mode showing complete reversibility. b) Fishing

curve showing a marked hysteresis probably due to stretching of a loop as depicted in the inset.

300 pN. 50 % of the fishing curves when stretched beyond 300 pN exhibited force extension curves as depicted in **Figure 9-6b**. Such a kink occurred in between 300-400 pN. The deviations from perfect reversibility could have several origins. It could be that the backbone might adopt a helical conformation, which could explain the kink between 300-400 pN. It is well known that a helix-coil transition occurs at these forces. However high resolution AFM imaging of these molecules does not show any hint of helicity. Another reason could be that two molecules of almost similar contour length being stretched and relaxed simultaneously, which however is highly improbable. Another explanation could be the stretching of a loop as depicted in the scenario in **Figure 9-6b**. The molecule detaches from one end and then the molecule is relaxed. Such a scenario could lead to a kink in the fishing curve. However, it is quite unlikely that one end of a loop consistently detaches from the surface at a force of 300-400 pN. Therefore the true origin of this kink could not be identified.

9.3.5 Persistence length determination:

The fishing curves were fitted by the Odjik model model that includes linear elastic contributions arising from the stretching of bond angles and covalent bonds: [16]

$$\frac{x}{L} = 1 - \frac{1}{2}\left(\frac{k_b T}{F l_p}\right)^{\frac{1}{2}} + \frac{F}{\Phi} \qquad (2)$$

F is the force and L is the contour length of the stretched brush molecule. The characteristic length scale expressing the cylindrical brush's bending rigidity is the persistence length, l_p, which is defined as the decay length of the directional correlation along the polymer chain. Finally the chain's extensibility upon stretching is described by the segment elasticity, Φ.

Figure 9-7 shows a fishing curve. The black curve is the stretch and the grey is that of the relax curve. The red continuous line is a nonlinear curve fit employing the

Odjik model, providing a persistence length of (21 ± 2 nm) and a segment elasticity of (0.6 ± 0.05) nN. 10 fish curves were fitted using the Odjik model giving persistence length between 7-23 nm. The scatter of persistence length could be due to the anchoring angles of the molecule to the tip and surface as explained in chapter 6. The relatively small persistence length could be due to short grafted side chains. Short side chains would allow the backbone to remain more flexible. This has been studied in detail using neutron scattering on polystyrene cylindrical brush molecules, where a pronounced persistence length dependence on the side chain length was observed.[17]

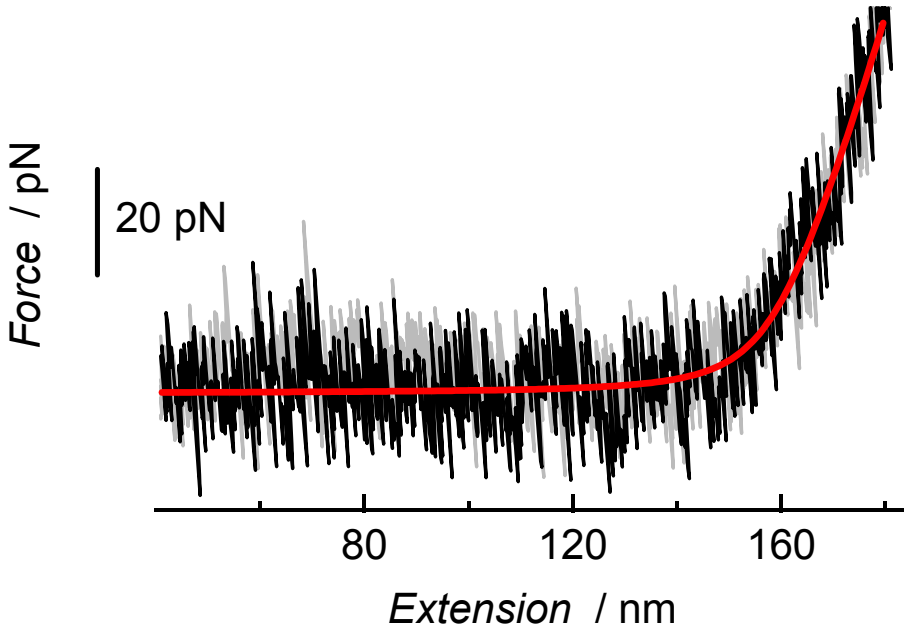

Figure 9-7) Force-extension curve of a single poly-L-lysine brush molecule measured in "Fly-Fishing" mode showing complete reversibility. The continuous red line is the corresponding fit of equation (2) yielding a persistence length of l_p = (21 ± 2) nm and a segment elasticity Φ = (0.6 ± 0.05) nN.

9.4 Conclusions and Outlook

The desorption behavior of poly-L-lysine cylindrical brush molecules was studied. The plateau events observed in the force-extension curves are interpreted as continuous desorption of the polyelectrolyte cylindrical brush molecule. We have also shown that "molecule specific force spectroscopy" would help to resolve whether the desorption events originate from single or multiple molecules and could have the potential to resolve the statistical uncertainties usually encountered in SMFS experiments. We have directly measured the force versus separation profiles of individual cylindrical poly-L-lysine brushes as they are extended between an AFM tip and the substrate. The fly-fishing curves are best described by the extensible Odjik model accounting for the deformation of bond angles as well as stretching of the bonds. From the images of bottlebrush molecules on mica we inferred an average persistence length of 24 nm assuming that the molecules are in their equilibrium state on the surface. The persistence lengths derived from the fly-fishing curves varied from 7-23 nm which is in good accordance with the imaging results.

In the future it would be very interesting to study in detail the desorption behavior of the polyelectrolyte brush molecules in different electrolyte solutions in order understand the electrostatic interaction of the polymer with the surface. Also many more stretching experiments could be carried out in order to obtain the "true" persistence length as in the case of PNIPAM cylindrical brush molecules.

9.5 References

(1) Sheiko, S. S.; Moeller, M. *Chem. Rev.* **2001**, *101*, 4099.

(2) Li, C.; Gunari, N.; Fischer, K.; Janshoff, A.; Schmidt, M. *Angew. Chem. Int. Ed.* **2004**, *43*, 1101.

(3) Zhang, A.; Shu, L.; Bo, Z.; Schlüter, A. D. *Macromol. Chem. Phys.* **2003**, *204*, 328.

(4) Schlüter, A. D.; Rabe, J. P. *Angew. Chem. Int. Ed.* **2000**, *39*, 864.

(5) Jürgen, R.; Gröhn, F.; Stamm, M. *Polyelctrolyte Brushes*; Springer, 2004; Vol. 265.

(6) Gössel, I.; Shu, L.; Schlüter, A. D.; Rabe, J. P. *J. Am. Chem. Soc.* **2002**, *124*, 6860.

(7) Zhang, B.; Fischer, K.; Schmidt, M. *Macromol. Chem. Phys.* **2005**, *206*, 157.

(8) Hugel, T.; Grosholz, M.; Clausen-Schaumann, H.; Pfau, A.; Gaub, H. E.; Seitz, M. *Macromolecules* **2001**, *34*, 1039.

(9) Binnig, G.; Quate, C. F.; Gerber, C. *Phys. Rev. Lett.* **1986**, *56*, 930.

(10) Janshoff, A.; Neitzert, M.; Oberdörfer, Y.; Fuchs, H. *Angew. Chem. Int. Ed.* **2000**, *39*, 3212.

(11) Hugel, T.; Seitz, M. *Macromol. Rapid Commun.* **2001**, *22*, 989.

(12) Gunari, N.; Schmidt, M.; Janshoff, A. *Macromolecules* **under revision**.

(13) Hutter, J. L.; Bechhoefer, J. *Rev. Sci. Instrum.* **1993**, *64*, 1868.

(14) Rivetti, C.; Walker, C.; Bustamante, C. *J. Mol. Biol.* **1998**, *280*, 41.

(15) Rief, M.; Oesterhelt, F.; Heymann, B.; Gaub, H. E. *Science* **1997**, *275*, 1295.

(16) Odijk, T. *Macromolecules* **1995**, *28*, 7016.

(17) Zhang, B.; Johannes Gutenberg Universität, Mainz, Germany, 2004.

10 SODIUM DODECYL SULFATE INDUCED CYLINDER-GLOBULE TRANSITION IN POLY-L-LYSINE BRUSH MOLECULES

10.1 Introduction

Cylindrical polymer brushes or sometimes called bottle brushes, are long chain molecules consisting of a flexible backbone densely grafted with relatively long side chains provided that the main chain is much longer than the side chain.[1-4] Due to steric overcrowding and excluded volume interactions, the densely grafted side chains try to avoid strong overlapping, which induces an extremely high stiffness of the backbone. In chapter 6 the mechanical properties of single cylindrical polymer brushes with poly-isopropylarcylamide (PNIPAM) side chains were probed by AFM on mica surface. The imaging and stretching in aqueous solution clearly revealed the semiflexible nature of the cylindrical macromolecules exhibiting a "true" persistence length as high as 140 nm.[5]

Cylindrical brushes with polyelectrolyte side chains exhibit distinct properties and are in prime focus in polymer research. The properties and synthetic strategies has been reviewed recently.[6]

By interaction of two oppositely charged polyelectrolytes, polyelectrolyte-polyelectrolyte complexes (PECs, or so-called symplexes) are formed. These PECs can form loose aggregates or well-defined nanoparticles. In a similar way polyelectrolytes form complexes with oppositely charged surfactants and polyelectrolyte-surfactant complexes (PSCs) are obtained. The key factors, which determine the cooperativity of the binding of an ionic surfactant to oppositely charged polyelectrolytes are not clearly understood yet, and depend on the chemical nature, rigidity, charge density and molecular architecture of the polymer and also on the chemical nature of the surfactant.[7]

While linear polyelectrolyte/surfactant systems were extensively investigated,[8-11] only a limited amount of studies for hyperbranched polymers (star polymers, dendrimers) are found. The crucial role of the molecular architecture was clearly demonstrated by the studies on dendrimer/surfactant systems.[12-14] Depending on the number of the consecutive generations, supramolecular surfactant/macromolecule structures, including interpolymer

and intrapolymer structures, were reported. So far no studies of cylindrical polyelectrolyte brush/surfactant complexes are reported.

An interesting feature of the cylindrical polyelectrolyte brush/surfactant interactions is the change in polymer conformation as a consequence of surfactant binding, which deserves closer investigation. Recently cylindrical brushes with poly-L-lysine side chains were synthesized and were shown to exhibit a worm-like chain conformation.[15] The AFM characterization, desorption behavior and mechanical properties were studied in detail as explained in the previous chapter. Here, we investigate the formation of well-defined supramolecular complexes formed by cylindrical poly-L-lysine brush molecules and sodium dodecylsulfate (SDS).

10.2 Experimental

The poly-L-lyine brush molecules were immobilized on a freshly cleaved mica surface by first placing a 15 μl droplet of the dilute polymer solution (c = 0.012 g/l) on the mica surface and after 5 sec the spin caster was turned on. The molecular architecture of the polymer was studied in air with a Multimode AFM instrument (Nanoscope IIIa controller, Digital Instruments, Santa Barbara, CA) operating with amplitude feedback in the intermittent contact mode. Silicon tips with a nominal tip radius of ~ 15 nm, spring constant of 42 N/m and a resonance frequency of 250-300 kHz were used.

The cylindrical polyelectrolyte brush-SDS complex was prepared by adding the surfactant (1 mM) dropwise to the aqueous poly-L-lysine brush solution (c = 0.012 g/L), at constant stirring. The chemical structure of the poly-L-lysine cylindrical brush molecule was described in chapter 8. The chemical structure of SDS is shown in **Scheme10-1**. polymer solution. The conformations of the complex were studied at a molar SDS / lysine residue ratio of < 1. Further additions were made in 100 μl increments. The conformations were studied in a range of molar SDS / lysine residue ratio 1-2. After two minutes of addition, the polymer-surfactant complex molecules were spin cast as described above on a freshly cleaved mica surface in the same way as for the poly-L-lysine brush molecules. Direct spin casting was not used in order to avoid spin casting artifacts such as orientation of the molecules.

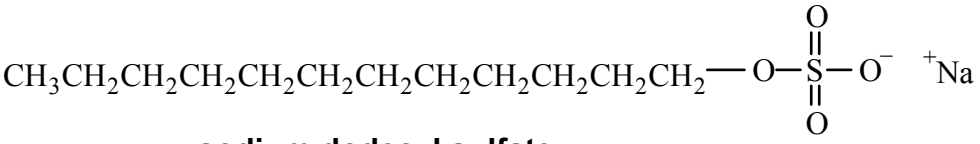

sodium dodecyl sulfate

Scheme 1: Chemical structure of sodium dodecyl sulfate.

For measurements in solution, 50 µL of the polymer/complex solution were placed on a freshly cleaved mica surface, mounted in a homemade AFM PTFE fluid cell and incubated for 5 min. Subsequently the surface was rinsed with water and measured in Milli Q water without drying. A MFP 3D microscope from Asylum Research, Santa Barbara, USA was used for imaging in contact mode.

10.3 Results and Discussion

Figure 10-1a shows a height image of the cylindrical poly-L-lysine brushes in the absence of surfactant imaged in air using intermittent contact mode. **Figure 10-1b** shows a height profile of a single brush molecule (average height of 0.8 ± 0.2 nm). The semiflexible nature of the molecules can be inferred from the image.

For imaging of brush-surfactant complexes in air, 100 µl of 1mM SDS was then added dropwise to the poly-L-lysine brush solution with constant stirring. After two min. of stirring 15 µl of the poly-L-lysine brush-surfactant complex solution was placed on a freshly cleaved 1×1 cm mica surface and after 5 sec. the spin caster was turned on.

Figure 10-2a shows the AFM height image of the complex molecules. The shrinking of the molecules is substantial as compared to the image shown in **Figure 10-1a**. Both the images are shown with the same scale. **Figure 10-2b** shows the height profile of a single complex. The increase in height is clearly visible. The complex has an average height of (1.4 ± 0.2) nm as compared to (0.8 ± 0.2) nm of the uncomplexed brush molecules.

10-1a)

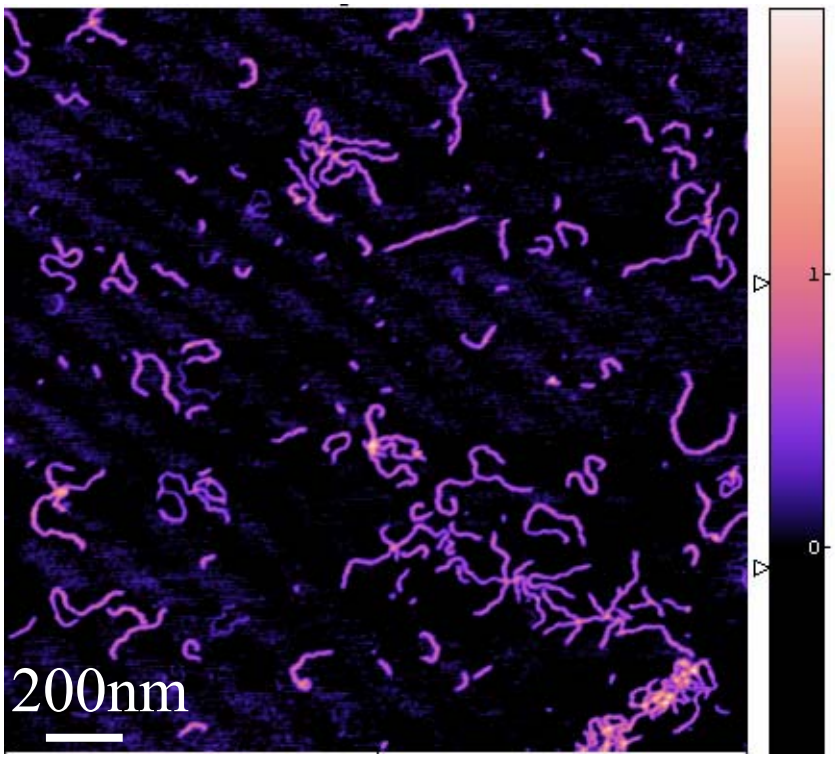

b)

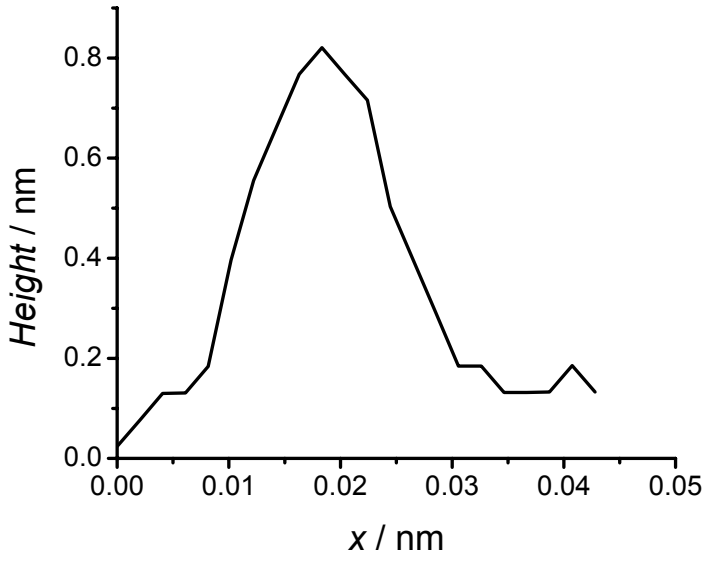

Figure 10-1 a) AFM height image of the cylindrical poly-L-lysine brush molecules adsorbed from a dilute (c = 0.012g/l) aqueous solution. b) Height profile of a single brush molecule.

Figures 10-3a and **b** show AFM height images taken at different areas of the mica surface to show that almost every molecule undergoes a conformational change. The conformation depicted in these images can be interpreted as either meander-like or helical. **Figures 10-4a** and **b** show the 3-dimensional images, which resemble more a helical conformation. **Figure 10-5** shows a phase image of an individual poly-L-lysine brush –SDS complex molecule exhibiting a marked helical conformation.

The speculated reason for the formation of helical conformations could be that the surfactant binds to the polylysine side chains and induces a hydrophobic shrinking thus causing the molecule to wind up as depicted in the scenario in **Figure 10-6**. Since the lysine-surfactant complexes become insoluble in water they most likely assemble within the core of the helix, which is stabilized by the uncomplexed side chains at the periphery of the complex.

As observed in the AFM images almost all the molecules show helix-like conformations and a detailed analysis of individual complexes reveals an average helical pitch of (16 ± 5) nm. **Figure 10-7a** shows an AFM height image of an individual complex molecule exhibiting two helical pitches of 17 and 21 nm. The turns 1-3 show a periodicity of 17 nm while 4 and 5 show a helical pitch of 21 nm. Some complexes only partially form a helix. The lack of helicity in parts of one complex is clearly shown in **Figure 10-7b**. There could be two reasons for such behavior, one being adsorption artifacts leading to the spreading of the helix on the surface. The second scenario could be envisioned as the cooperative binding of the surfactant to the poly-L-lysine side chains leading to ordered structures in parts of the molecule and unordered in the other part as shown in the **Figure10-7b**, i.e. the surfactant is unevenly distributed along the brush polymer.

With further addition of surfactant, all the side chains are eventually complexed with the surfactant and hence the charges are entirely neutralized. This causes the side chains to collapse and hence the complex forms a compact globule similar to the PNIPAM cylindrical brush molecules in a poor solvent[2] as sketched in **Figure 10-6**. **Figure 10-8a** shows a typical AFM height image of single collapsed complex molecules in air. The diameters of the collapsed globules range from 50-150 nm with an average height of (3 ± 0.4) nm. **Figure 10-8b** displays the height profile of a most likely single

chain complex. Also collapsed molecules with larger diameters are observed, which probably consist of aggregated complexes. In **Figure 10-9** the AFM height image resolves several brush molecules within the collapsed aggregate. With further addition of SDS the complex precipitate.

10-2 a)

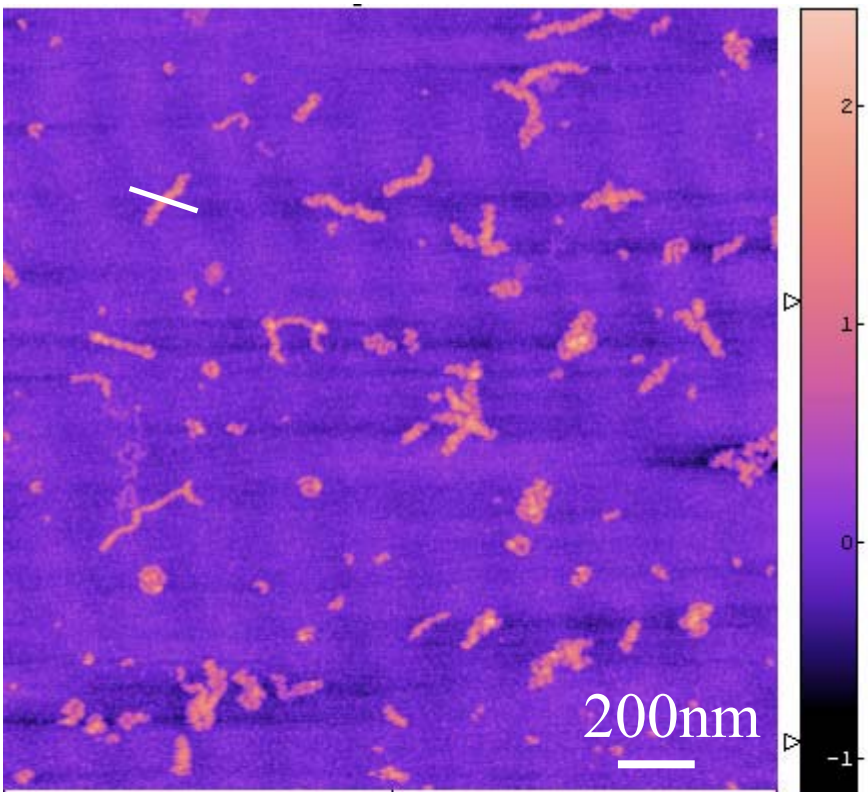

b)

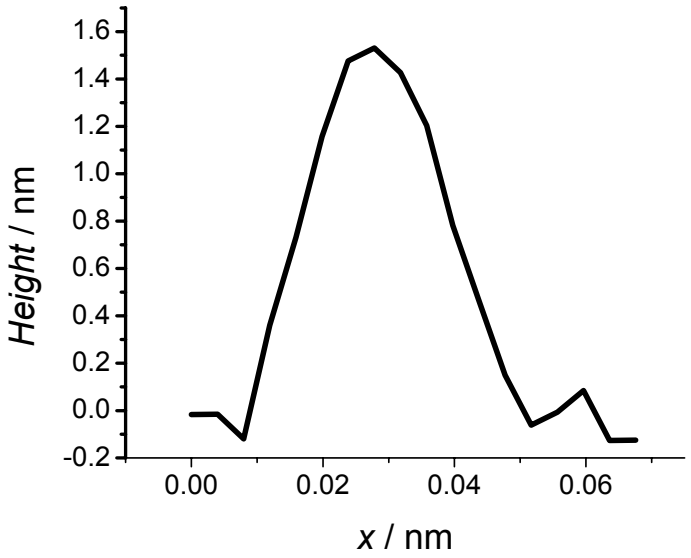

Figure 10-2a) AFM height image in air of the poly-L-lysine brush-SDS complexes, at a molar SDS/lysine residue ratio of < 1. b) Height profile of a single complex molecule.

10-3a)

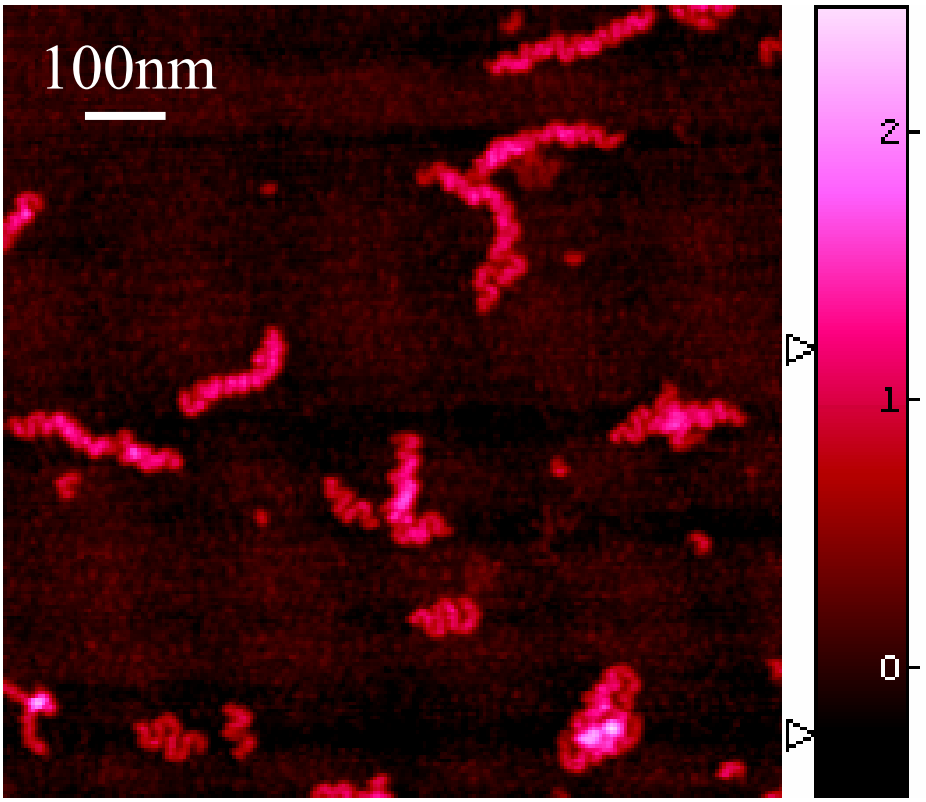

b)

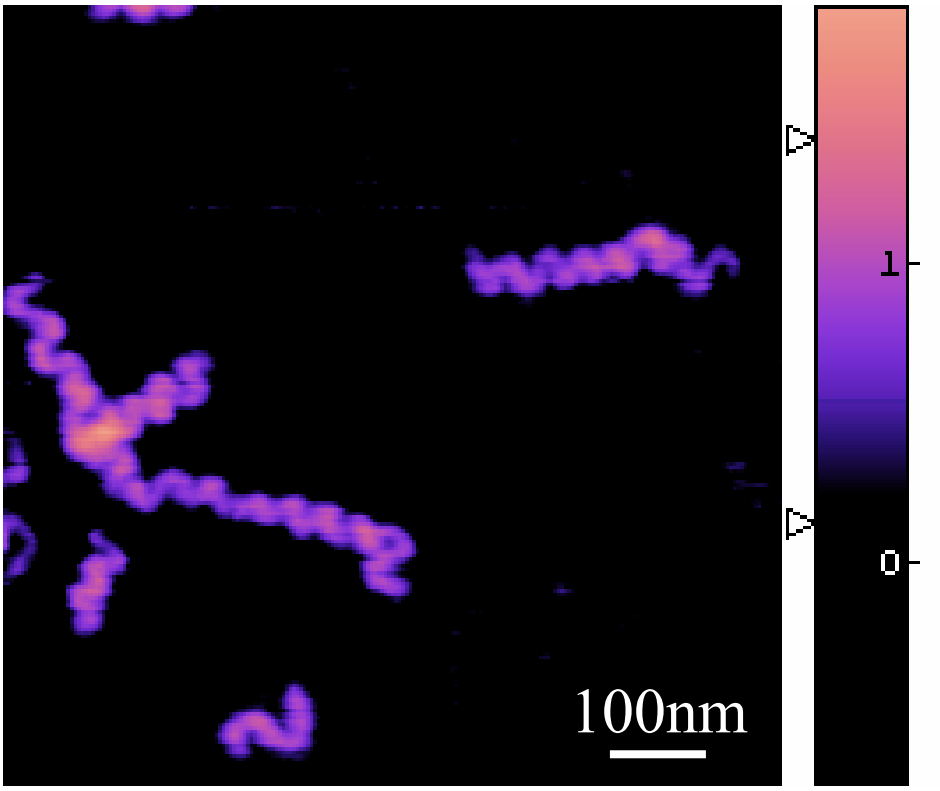

Figure 10-3 a) and b) AFM height images of the poly-L-lysine brush-SDS complexes.

10-4a)

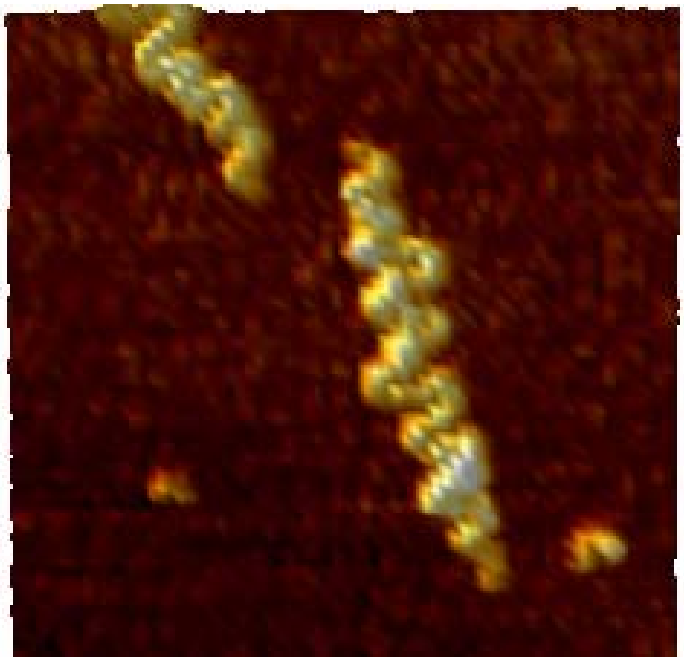

b)

Figure 10-4 a) and b) 3-dimensional height images of the poly-L-lysine brush-SDS complexes revealing the helical conformation.

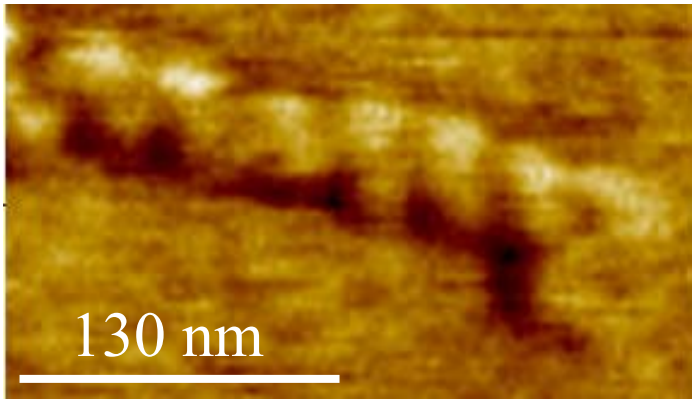

Figure 10-5 AFM phase image of an individual poly-L-lysine brush-SDS complex.

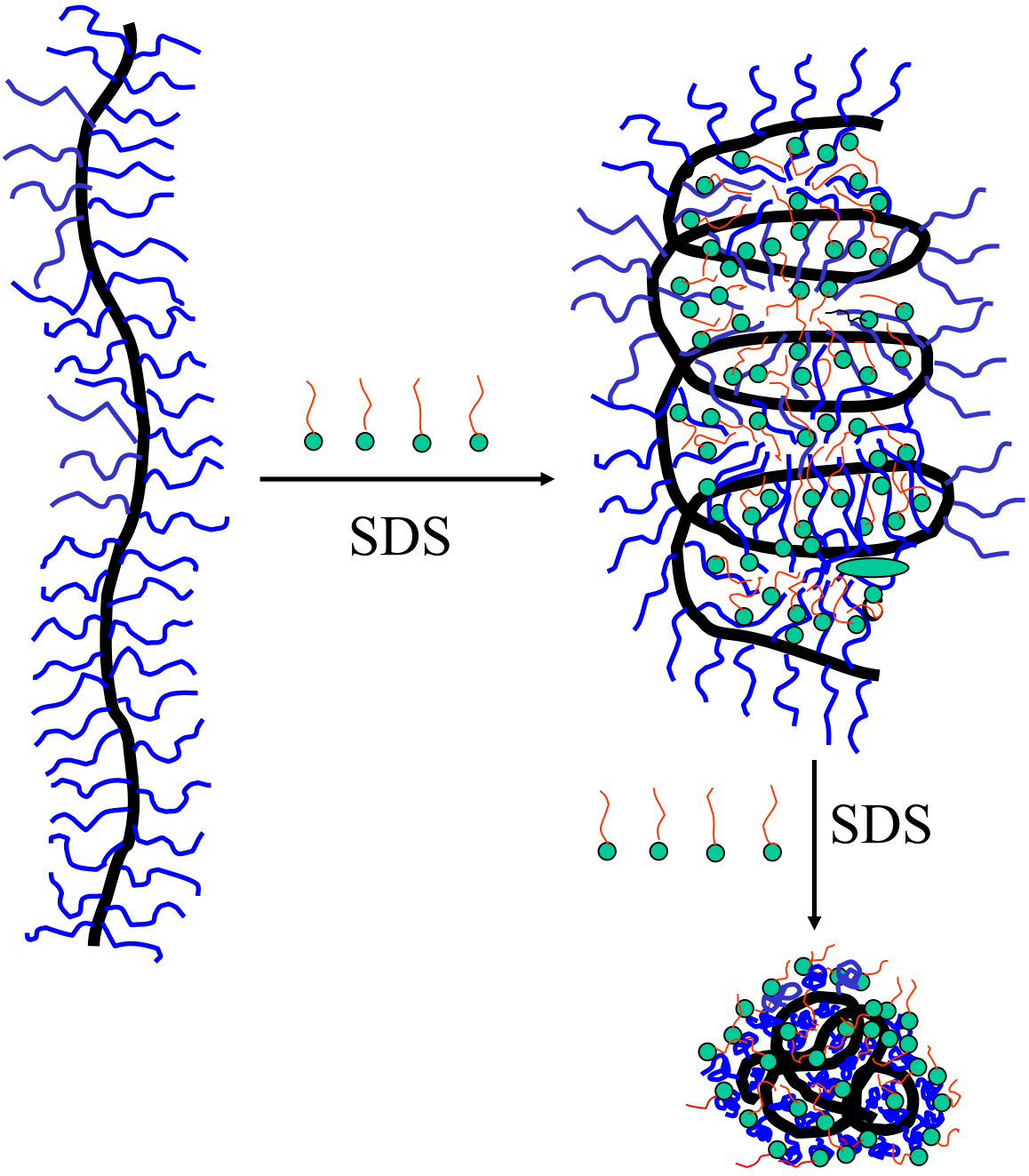

Figure 10-6 Speculated scenario to explain the surfactant induced collapse of the poly-L-lysine cylindrical brush molecules.

10-7a)

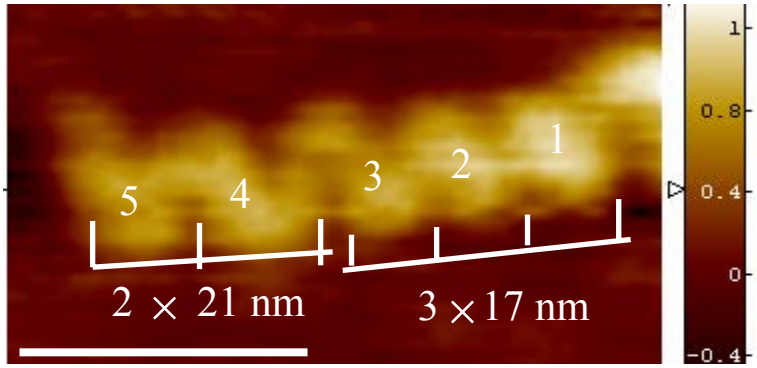

b)

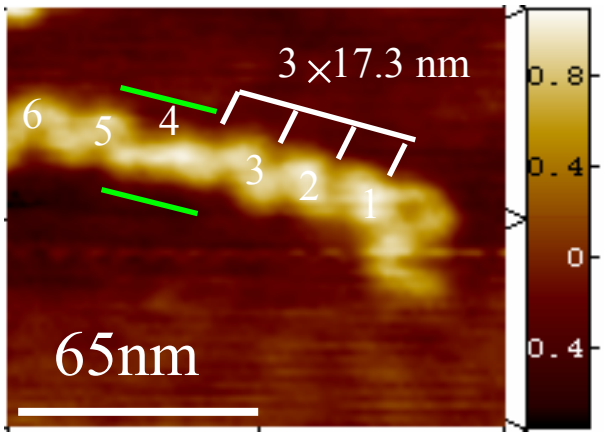

Figure 10-7 a) AFM topography image of an individual poly-L-lysine brush-complex exhibiting a helical pitch of 17 nm (turns 1-3) and 21 nm (turns 4-5). b) AFM topography image of an individual poly-L-lysine brush-complex exhibiting a lack of helicity (shown by the green parallel line).

10-8a)

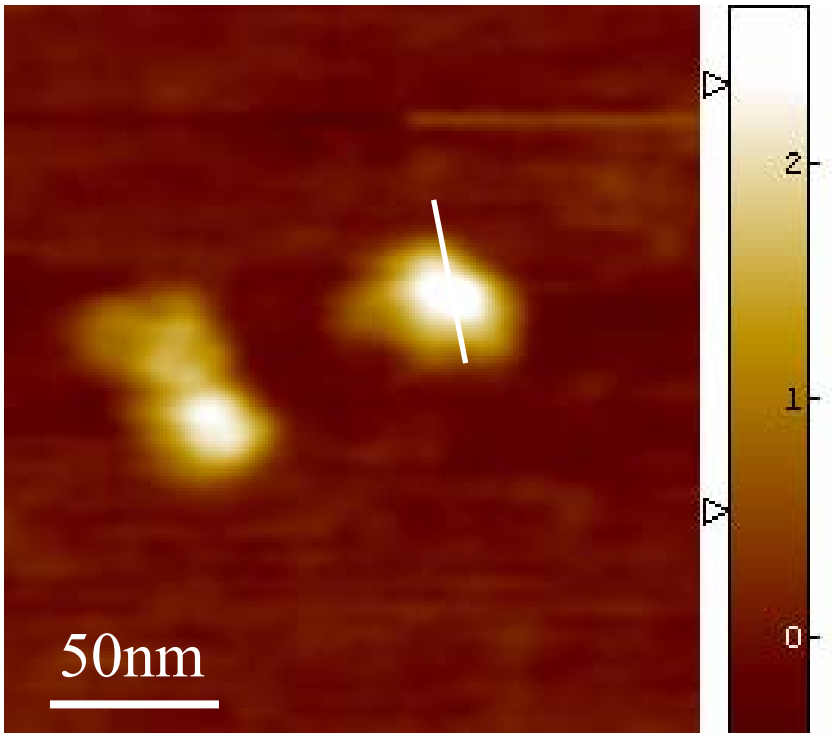

b)

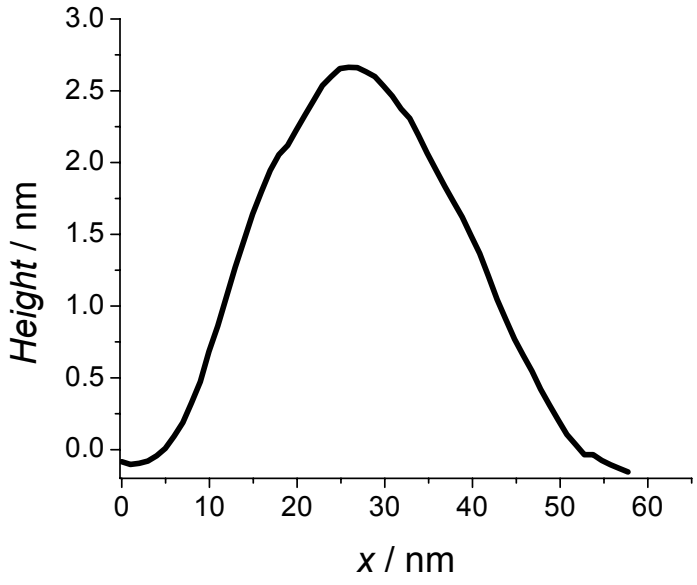

Figure 10-8a) AFM topography image in air of the collapsed poly-L-lysine brush-SDS complex molecules, at a molar SDS/lysine residue ratio of ≈ 2. b) Height profile of a single collapsed complex.

10-9)

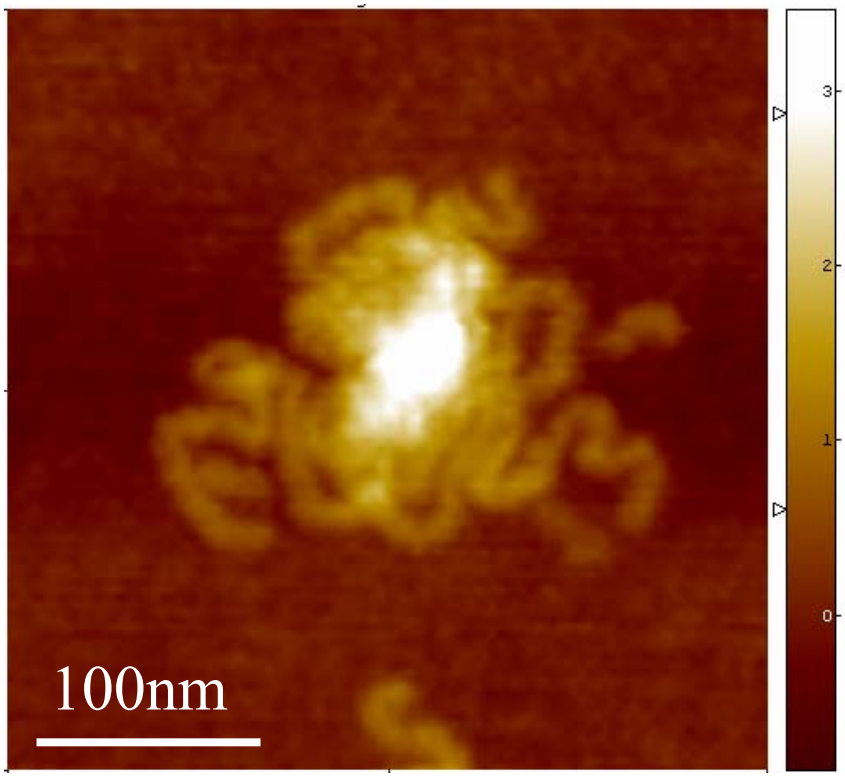

Figure 10-9) AFM height image of aggregated poly-L-lysine brush-SDS complexes in air, at a molar SDS/lysine residue ratio of ≈ 2.

The poly-L-lysine brush-SDS complex molecules were also measured under aqueous solution. AFM imaging under aqueous solution was described in chapter 8. **Figure 10-10** shows an AFM deflection image of the poly-L-lysine brush-SDS complex, at a molar SDS/lysine residue ratio of ≈ 1. The arrows indicate the most prominent molecules exhibiting the helix-like conformation, observed in the dry state. The globular conformations were also observed under aqueous solution. **Figure 10-11** shows an AFM height image of the poly-L-lysine brush-SDS complexes. The globules could be interpreted as single brush-SDS complex or as complex aggregates. In **Figure 10-12a** and **b** the AFM height and the deflection image is presented for the same collapsed complex. It might be inferred from the image that the structure is formed from a single collapsed complex.

10-10)

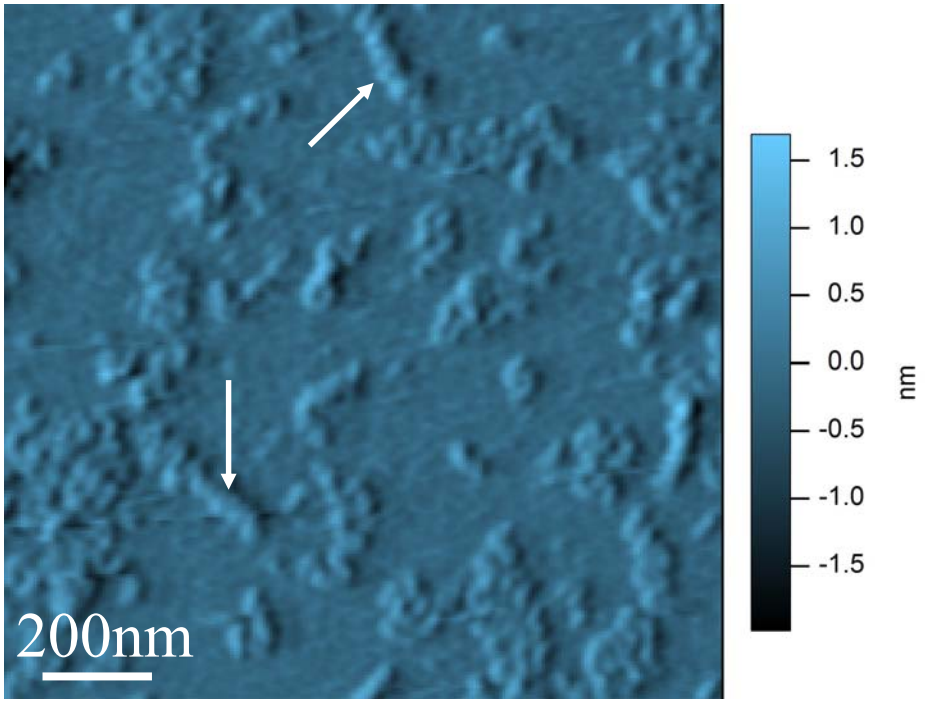

Figure 10-10) Under water AFM deflection image of poly-L-lysine brush-SDS complexes, at a molar SDS/lysine residue ratio of ≈ 1. Arrows indicate the pronounced helix-like conformations.

10-11)

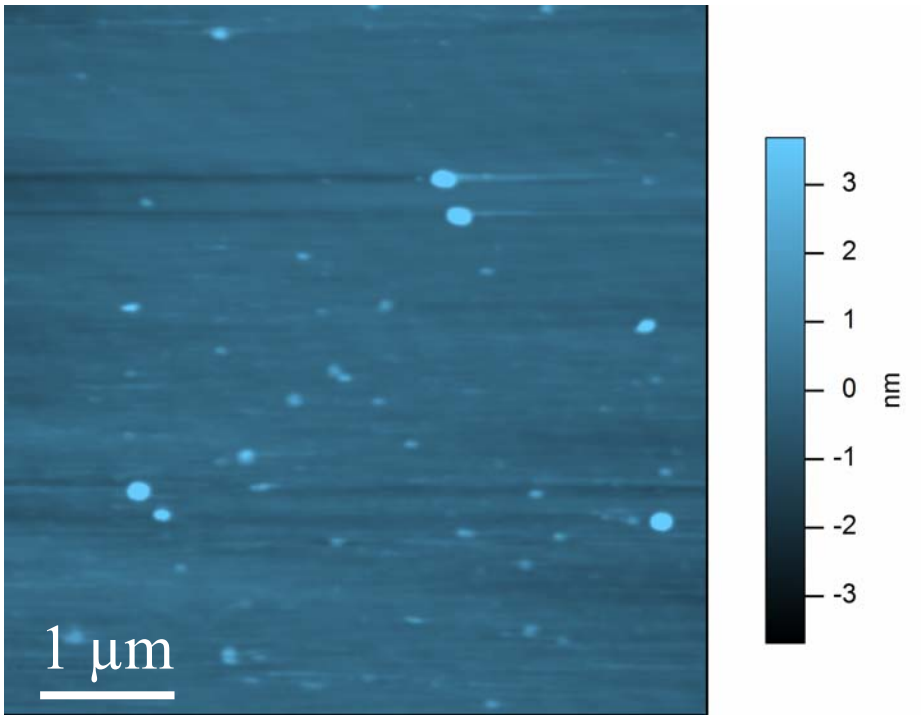

Figure 10-11) Under water AFM height image of Poly-L-lysine brush-SDS complex molecules, at a molar SDS/lysine residue ratio of ≈ 2

10-12a)

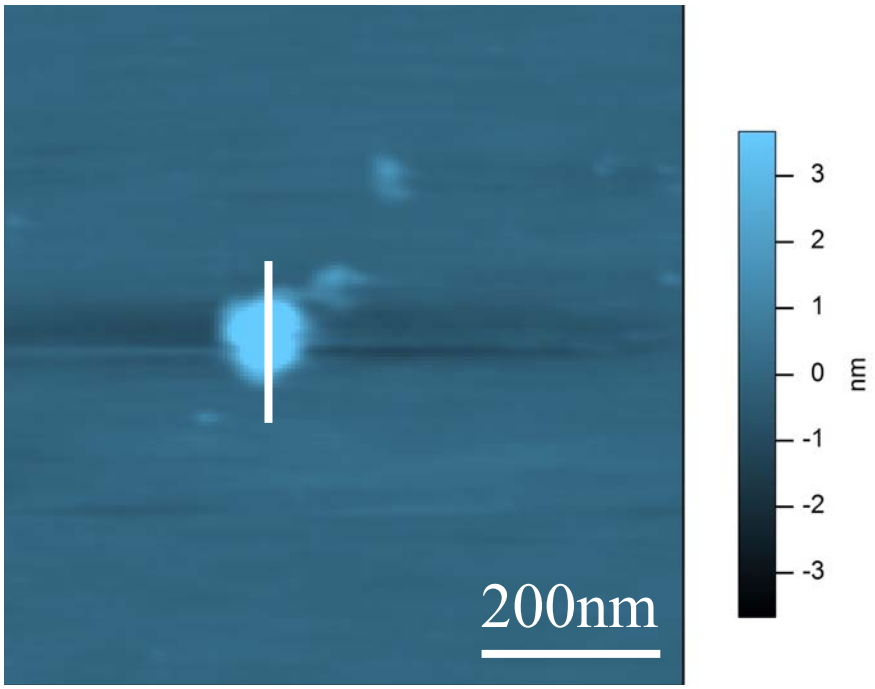

b)

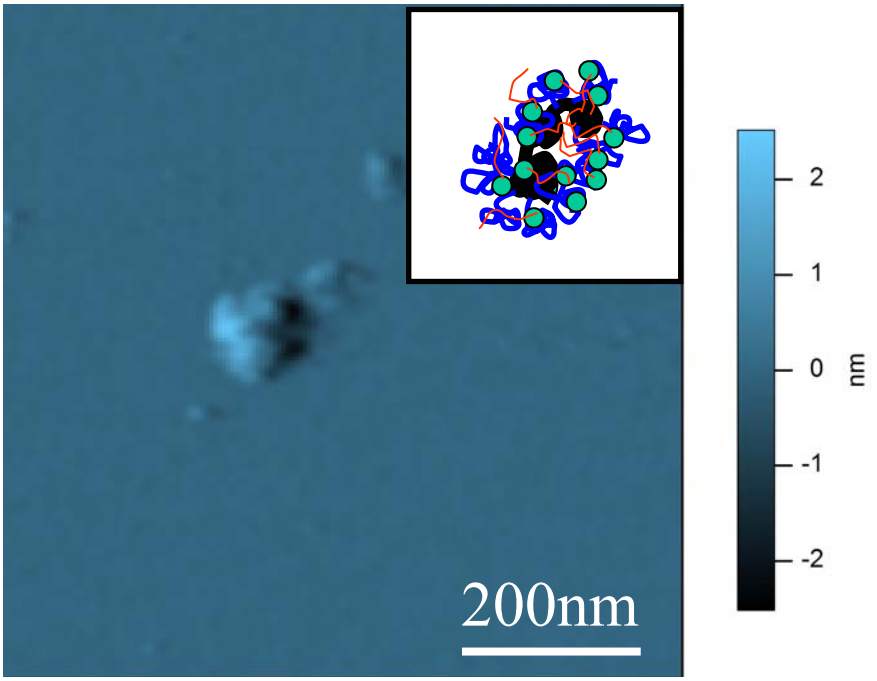

Figure 10-12 a) Under water AFM height image of single poly-L-lysine brush-SDS complex molecule, at a molar SDS/lysine residue ratio of ≈ 2 b) Deflection image.

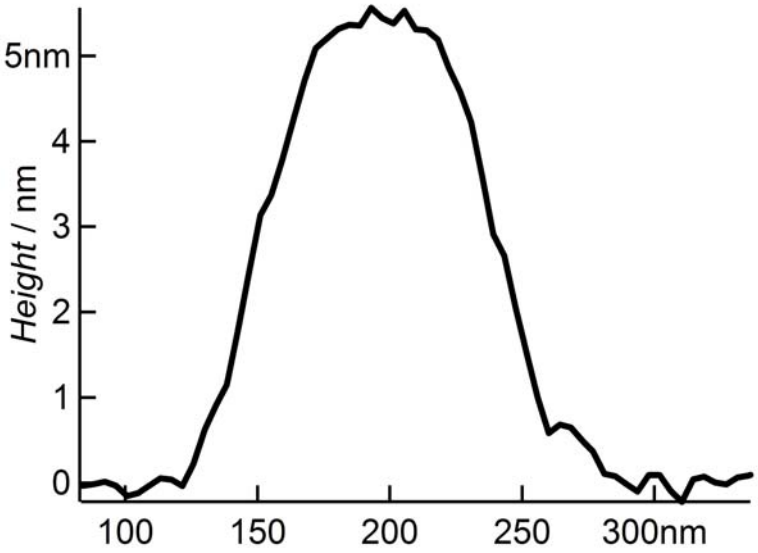

Figure 10-13) Height profile of a single complex molecule shown in figure 13 a.

The inset of the deflection image shows a possible conformation of the complex molecule. The average height of the complexes was 7 nm and varies from 4-12 nm. **Figure 10-13** shows a height profile of a most likely single collapsed complex shown in **Figure 10-12 a**.

10.4 Conclusions

Conformational transitions in poly-L-lysine cylindrical brush molecules due to binding of sodium dodecyl sulfate were observed by AFM imaging. With increasing SDS the molecules shrink and show undulations on the mica surface. The conformation resembles that of a helix which may be formed due to the surfactant binding to the side chains causing the molecule to wind up (hydrophobic shrinking), while the uncomplexed

side chains remain extended at the periphery of the complex and provide solubility. Further increase in SDS concentration leads to a collapse of the complex.

10.5 References

(1) Sheiko, S. S.; Moeller, M. *Chem. Rev.* **2001**, *101*, 4099.

(2) Li, C.; Gunari, N.; Fischer, K.; Janshoff, A.; Schmidt, M. *Angew. Chem. Int. Ed.* **2004**, *43*, 1101.

(3) Zhang, A.; Shu, L.; Bo, Z.; Schlüter, A. D. *Macromol. Chem. Phys.* **2003**, *204*, 328.

(4) Schlüter, A. D.; Rabe, J. P. *Angew. Chem. Int. Ed.* **2000**, *39*, 864.

(5) Gunari, N.; Schmidt, M.; Janshoff, A. *Macromolecules* **under revision**.

(6) Jürgen, R.; Gröhn, F.; Stamm, M. *Polyelctrolyte Brushes*; Springer, 2004; Vol. 265.

(7) Goddard, E. D.; Ananthapadmanabhan, K. P. *Interaction of Surfactants with Polymers and Proteins*; Eds.: CRC Press: Boca Raton, Fl., 1993.

(8) Meszaros, R.; Thompson, L.; Bos, M.; Varga, I.; Gilanyi, T. *Langmuir* **2003**, *19*, 609.

(9) Chandar, P.; Somasundaran, P.; Turro, N. J. *Macromolecules* **1988**, *21*, 950.

(10) Chu, D. Y.; Thomas, J. K. *J. Am. Chem. Soc.* **1986**, *108*, 6270.

(11) Xia, J.; Zhang, H.; Rigsbee, D. R.; Dubin, P. L.; Shaikh, T. *Macromolecules* **1993**, *26*, 2759.

(12) Caminati, G.; Turro, N. J.; Tomalia, D. A. *J. Am. Chem. Soc.* **1990**, *112*, 8515.

(13) Gopidas, K. R.; Leheny, A. R.; Caminati, G.; Turro, N. J.; Tomalia, D. A. *J. Am. Chem. Soc.* **1991**, *113*, 7335.

(14) Li, Y.; Msmillan, C. A.; Bloor, D. M.; Penfold, J.; Warr, J.; Holzwarth, J. F.; Wyn-Jones, E. *Langmuir* **2000**, *16*, 7999.

(15) Zhang, B.; Fischer, K.; Schmidt, M. *Macromol. Chem. Phys.* **2005**, *206*, 157.

SUMMARY

The Ph.D. thesis deals with the conformational study of individual cylindrical polymer brush molecules using atomic force microscopy (AFM). Imaging combined with single molecule manipulation has been used to unravel questions concerning conformational changes, desorption behavior and mechanical properties of individual macromolecules and supramolecular structures.

In the first part of the thesis (**chapter 5**) molecular conformations of cylindrical polymer brushes with poly-(N-isopropylacrylamide) (PNIPAM) side chains were studied in various environmental conditions. Also micelle formation of cylindrical brush-coil blockcopolymers with polyacrylic acid side chains and polystyrene coil have been visualized.

In **chapter 6** the mechanical properties of single cylindrical polymer brushes with (PNIPAM) side chains were investigated. Assuming that the brushes adopt equilibrium conformation on the surface, an average persistence length of l_p=(29 ± 3) nm was determined by the *end-to-end distance* vs. *contour length* analysis in terms of the wormlike chain (WLC) model. Stretching experiments suggest that an exact determination of the persistence length using force extension curves is impeded by the contribution of the side chains. Modeling the stretching of the bottle brush molecule as extension of a dual spring (side chain and main chain) explains the frequently observed very low persistence length arising from a dominant contribution of the side chain elasticity at small overall contour lengths. We show that it is possible to estimate the "true" persistence length of the bottle brush molecule from the intercept of a linear extrapolation of the inverse square root of the apparent persistence length ($\left(l_{\mathrm{p}}^{\mathrm{app}}\right)^{-\frac{1}{2}}$) vs. the inverse contour length (L^{-1}) plot. By virtue of this procedure a "true" persistence length of 140 nm for the PNIPAM brush molecules is predicted.

Chapter 7 and **8** deal with the force-extension behavior of PNIPAM cylindrical brushes studied in poor solvent conditions. The behavior is shown to be qualitatively different from that in a good solvent. Force induced globule-cylinder conformational changes are monitored using "molecule specific force spectroscopy" which is a combined

AFM imaging and SMFS technique. An interesting behavior of the unfolding-folding transitions of single collapsed PNIPAM brush molecules has been observed by force spectroscopy using the so called “fly-fishing” mode. A plateau force is observed upon unfolding the collapsed molecule which is attributed to a phase transition from a collapsed brush to a stretched conformation.

Chapter 9 describes the desorption behavior of single cylindrical polyelectrolyte brushes with poly-L-lysine side chains deposited on a mica surface using the “molecule specific force spectroscopy” technique to resolve statistical discrepancies usually observed in SMFS experiments. Imaging of the brushes and inferring the persistence length from a *end-to-end distance* vs. *contour length* plot results in an average persistence length of $l_p = (25 \pm 5)$ nm assuming that the chains adopt their equilibrium conformation on the surface. Stretching experiments carried out on individual poly-L-lysine brush molecules by force spectroscopy using the “fly-fishing” mode provide a persistence length in the range of 7-23 nm in reasonable accordance with the imaging results.

In **chapter 10** the conformational behavior of cylindrical poly-L-lysine brush-sodium dodecyl sulfate complexes was studied using AFM imaging. Surfactant induced cylinder to helix-like to globule conformational transitions were observed.

OUTLOOK

Cylindrical polymer brushes with thermally sensitive side chains may be utililized as nano actuation devices. It may be anticipated that the force induced unfolding of a collapsed globule to a cylinder might lead to a better understanding of the collapse forces itself. Another interesting aspect would be the direct observation of the *in-situ* collapse of a single brush molecule.